

# UNIVERSITY OF JOENSUU DEPARTMENT OF PHYSICS VÄISÄLÄ LABORATORY

# **DISSERTATIONS 12**

STUDIES ON DIFFRACTIVE OPTICS AND PARTIAL COHERENCE

PASI VAHIMAA

# Contents

1	Intr	oduction		1				
2	Maxwell's equations and boundary conditions							
	2.1	Maxwell's equations		6				
		2.1.1 Two-dimensional fields						
	2.2	Boundary conditions						
	2.3	Energy density and Poynting vector	٠.	8				
3	War	e propagation in homogeneous media		10				
	3.1	Angular spectrum representation		10				
		3.1.1 Rigorous solution						
		3.1.2 Paraxial approximations						
	3.2	Rayleigh-Sommerfeld diffraction formula		12				
4	Coh	erence theory		14				
_	4.1	Complex analytic signal						
	4.2	Cross-correlation function						
	4.3	Cross-spectral density function						
	4.4	Propagation of cross-spectral density						
	4.5	Coherent mode representation	• •	17				
	4.6	Model fields	• •	17 18				
			•					
5		ing diffraction		20				
	5.1	Geometry of the problem						
	5.2	Rayleigh expansions						
		5.2.1 Detour-phase principle						
	5.3	About the solution of grating-diffraction problems						
	5.4	Modal expansion methods						
		5.4.1 Exact eigenmode method						
		5.4.2 Legendre polynomial expansion method		26				
		5.4.3 Fourier-expansion method		27				
		5.4.4 Boundary conditions		28				
		5.4.5 Comparison of modal methods		30				
	5.5	Rigorous coupled-wave analysis		30				
	5.6	Space-domain methods						

vi			C	01	tent	<u>s</u>
6	n:a	fraction analysis: continuous signals			9.6	•
U	6.1				33	
		Introduction				_
	6.2	Eigenmode method for modulated apertures				
		6.2.1 Exact eigenmodes	٠	٠	. 33	
		6.2.2 Polynomial expansion of the modes		•	. 3	
		6.2.3 Boundary conditions		•	. 3	į
	6.3	Periodic elements with finite incident beam				7
	6.4	Diffraction of spatially partially coherent fields			. 38	3
7	Apr	proximate methods			39	)
	$7.1^{-}$	Thin element approximation			. 39	)
	7.2	First-order two-wave coupled-wave theory				
8	Das					
0		ign of diffractive elements			42	
	8.1	Design freedoms				•
	8.2	Upper bound of the diffraction efficiency				
	8.3	Design methods	٠		. 43	}
	8.4	IFTA for spatially partially coherent light				Į
	8.5	Non-paraxial Gaussian to flat-top beam shaping			. 47	7
9	Coh	nerence and diffraction			50	)
	9.1	Grating vibrator				
	9.2	Bragg selective gratings				
	<b>U</b>	9.2.1 Coherence analysis				
		9.2.2 Examples				
		9.2.2 Examples	•	•	. 08	)
10		pagation invariance and self-imaging			57	7
	10.1	Talbot effect			. 57	7
		10.1.1 Examples			. 59	}
	10.2	Lau effect			. 59	)
		10.2.1 Examples				ļ
	10.3	Propagation-invariant fields				
		10.3.1 Quasi-rigorous analysis of diffractive axicons				-
		10.3.2 Examples				
1 1	7	oth-order diffractive elements			74	
11						_
		Introduction				_
	11.2	Zeroth-order complex amplitude modulation				_
		11.2.1 Examples	•		. 75	)
12		veguide analysis with diffractive optics			81	
	12.1	Waveguide modes			. 81	L
	12.2	Beam coupling into a planar waveguide			. 83	
	12.3	Waveguide discontinuities			. 86	

# Chapter 1

# Introduction

Optics is a rapidly advancing branch of technology. During the past decade optical elements and systems have become an important part of our daily life. Some examples of this development are optical fibers in telecommunication, CD players, and security elements in credit cards and bank notes. The latter are good examples of diffractive optical elements. This thesis will introduce some theoretical calculations concerning diffractive optical elements, optical fields, and optical waveguides.

Let us first briefly consider different approaches to the analysis of optical fields and systems, illustrated in Fig. 1.1. The simplest approach is known as ray optics: the optical field is described as a bundle of rays, which propagate in free space along straight lines and refract at smooth surfaces according to Snell's law. Although this picture of light propagation is highly simplified, it is often sufficiently accurate; it is widely employed in the analysis and design of macroscopic optical systems. However, this ray optical approach ignores the wave nature of light.

In scalar wave optics, the light field is described by a single scalar wave function, which satisfies the wave equation. The most important consequences of the wave nature of light are the phenomena known as diffraction and interference. The diffraction of light will possess a central role in this thesis, while the interference of light is simply an effect that occurs when several wave functions are summed. In the limit  $\lambda \to 0$ , where  $\lambda$  is the wavelength of light, the results of wave optics often reduce to those of ray optics.

In electromagnetic theory the light field is no longer understood as a single scalar wave function; it is described by a pair of three-dimensional vector fields. These fields are called the electric and the magnetic field and they are coupled according to the classical Maxwell's equations. In quantum optics, the electric and magnetic fields are quantized.

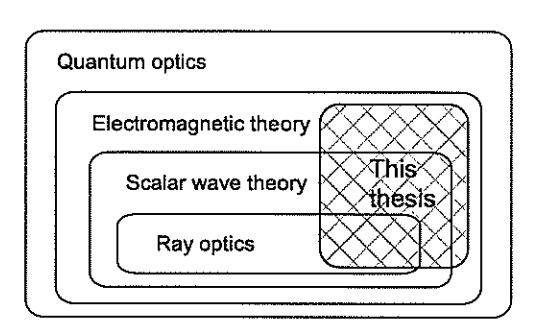


Fig. 1.1: Different approaches to the description of optical phenomena.

As a result, one deals with operators rather that wave functions. Quantum optical effects become important when the optical field contains only few photons. We will not be concerned with quantum effects in this thesis. Real optical fields are never completely deterministic. Such fluctuating fields are described using optical coherence theory, which can be formulated in the framework of scalar wave optics, electromagnetic theory, or quantum optics, and which is used also in this thesis.

In this thesis we employ mostly scalar wave optics and electromagnetic theory of optics. As mentioned earlier, the wave nature of light implies the phenomenon of diffraction. But what is diffractive optics? There is no generally agreed definition, but one can classify under diffractive optics all optical phenomena that are originated by microstructures and can not been explained using refractive or reflective optics. Optical components that employ diffraction are known as diffractive elements.

The first diffractive element that gained wide applicability is the diffraction grating [1], a periodic microstructure with period d. Many other diffractive elements can be described as gratings at least locally. In grating theory the choice of analysis and design method depends critically on the grating period [2], and a similar division is applicable to more complex elements (at least locally) if d is replaced by the concept of characteristic feature size of the microstructure. Independently of the feature size, one can in principle solve Maxwell's equations exactly and thus obtain the rigorous solution of the diffraction problem. However, this is usually a very demanding task; the memory size and the finite speed of computers limit the maximum period or size of the elements that one can analyze rigorously. Thus one is often forced to look for approximative methods.

Let us assume that the grating period d (or the size of each feature of the element) is much shorter than the wavelength  $\lambda$ . Then light does not resolve the individual features, but rather experiences a locally averaged refractive index distribution. In this case the element can be described as a homogeneous "effective" medium whose effective refractive index depends on the details of the microstructure and also on the polarization state of the incident field. On the other hand, if all features of the element are very large compared to the wavelength, the diffracted field is paraxial and independent on the polarization state of the (paraxial) incident field. Thus the diffracted field can be described by a single scalar function and the element can be modelled by means of a complex-amplitude transmission function that can be determined by optical path calculations [3]. This method is called the complex-amplitude transmittance method. In the intermediate region  $d \approx \lambda$ , the field must be described as an electromagnetic vector field and the diffraction pattern can depend strongly on the polarization state of the incident field. This region is called the resonance domain of diffractive optics [2].

For a long time diffraction was seen purely as a limitation in optical systems. For example, the resolution of an imaging system is limited by diffraction. As already mentioned, the first real application of diffractive optics was the use gratings in spectroscopy [1]. Here diffractive elements are superior to prisms, because their greater dispersion provides a larger angular separation between different wavelengths. Furthermore, the sign of grating dispersion is opposite to that of a prism, which enables one to correct the chromatic aberration by means of a hybrid lens, which is a combination of refractive and diffractive lenses [4–6].

The most significant step in diffractive optics after the invention of the diffraction grat-

ing was the invention of holography [7–10]. This made it possible to fabricate complicated diffractive elements by optical interference. Using this technology, amazingly realistic 3D pictures can be recorded. However, one must have an object which to reproduce, which may be impossible or impractical in some situations.

If the signal to be generated by the diffractive optical element is sufficiently simple, it may be possible to calculate the required diffractive structure. A simple example is a diffractive element that acts like a conventional lens. Such diffractive lenses are often called micro Fresnel lenses [11]. The original Fresnel zone plate modulated the amplitude of the field, but one can also make so-called phase Fresnel lenses that modulate only the phase and thereby focus a larger fraction of incident light [12–14].

The development of computers has made it possible to calculate more complicated diffractive elements. Originally these were binary amplitude elements, known as computer-generated holograms [15–17]. However, the problem with amplitude elements is that the diffraction efficiency is poor, usually at most a few per cent. The solution is again the use of microstructures that modulate only the phase of the field [18–24]. In fact, it is known that the control of phase is far more important than the control of amplitude [25].

With the expansion of diffractive optics it has become apparent that this flexible technology can be seen as a generalization of conventional optics [26,27]. A large number of different applications have been proposed and demonstrated. One rapidly growing branch of applications is optical document security. Conventional holograms are used as security features in, e.g., credit cards, but they are rather easy to copy [28]. One must therefore employ more sophisticated microstructures, which are extremely hard to copy, or to produce with sufficient quality without access to expensive equipment, such as electron beam lithography [29–34].

Diffractive optics also has a large number of industrial applications. For example, one can shape a Gaussian laser beam to produce a desired intensity distribution, such as a flat-top profile, across some other plane [35, 36]. Furthermore, one can divide a single laser beam into many separate beams, which can be coupled simultaneously into, e.g., optical fibers [37]. Such multiple beam splitters are useful, for example, in high-power laser material processing [38]. Other industrial applications include solar cells [39] and precision alignment [40]; even applications in space technology have been proposed [41,42]. In information processing it is possible to use diffractive optical elements in different ways: Apart from classical applications in spatial filtering [3] one can, e.g., use acousto-optic diffractive elements in signal processing [43,44] or realize Haar wavelets [45]. Furthermore, diffractive optics is a central technology in optical interconnections [46-49].

It seems likely that the importance of diffractive optics will continue its rapid increase also in the future. To reduce the size of optical systems, the packaging and integration of diffractive elements will gain importance [49–52]. Also, there will be more interest in dynamic optical elements, which will require investigation of new optical materials. For example, photorefractive [53], liquid-crystal [48, 54, 55] and bio-organic materials are interesting in this context. In modern physics, the boundaries between different fields of science have smoothed. The influence of chemistry, communication theory and information processing in the development of optics has become ever more important.

This thesis can be divided into two parts. In the first part, comprising Chapters 1–7, all the theory needed later is introduced to make the discussion reasonably self-contained.

1 Introduction

In the second part, several different diffractive optical elements and systems are analyzed. In Chapter 2, the basis for the entire thesis is laid: Maxwell's equations and the electromagnetic boundary conditions are presented, and measures for the energy properties of the field are introduced. In Chapter 3, Maxwell's equations are solved in homogeneous media. This provides a rigorous method to calculate the electromagnetic field in any plane  $z=z_1$  if the field is known across a reference plane  $z=z_0$ . Some important approximations are also derived. Chapter 4 provides a brief overview of optical coherence theory: it is well known that completely coherent fields can not exist and therefore the understanding of coherence theory is relevant also in diffractive optics. Indeed, spatially and temporally partially coherent fields will be considered rather frequently in this thesis.

In Chapter 5 we discuss perhaps the most fundamental theoretical problem in diffractive optics, i.e., plane wave diffraction from an infinite grating. Solution methods to be employed later in this thesis are derived rigorously by solving Maxwell's equations together with the appropriate boundary conditions for a periodically modulated medium. Some other frequently used methods are also reviewed, and comments on the usefulness of the different analysis methods in various geometries are given. In reality, neither the illumination wave nor the diffractive element is infinite. Thus, in Chapter 6, rigorous analysis methods of both non-periodic elements and finite incident beams are introduced. Also a method to solve diffraction problem with partially coherent incident field is described. In Chapter 7, some useful approximative methods to solve diffraction problems are introduced. Typically, these methods are much easier to apply than the rigorous methods, which motivates one to apply them whenever possible. However, there exist so many approximative methods that only those employed in this thesis are introduced.

In Chapter 8, the basic theory of designing diffractive elements is discussed. Some design methods based on geometrical optics, paraxial wave optics, and rigorous theory are reviewed. This Chapter also contains some original material: an iterative Fourier-transform algorithm for spatially partially coherent light is presented. Furthermore, the design and analysis of a beam shaping element in the non-paraxial domain of diffractive optics is introduced. The main results have been published in Ref. [56].

The remaining chapters contain results obtained by the author. In Chapter 9, some methods to modify the coherence properties of light by diffractive elements are investigated. A new method to reduce spatial coherence by means of a vibrating grating is introduced. Then the use of Bragg selectivity of a thick grating to extract a coherent component from a partially coherent field is described [57].

Chapter 10 deals with the phenomena of self-imaging and propagation invariance of optical fields. The effect of spatial partial coherence of the incident field in a non-paraxial Talbot imaging system is analyzed. It is shown that the intensity fluctuations that appear in non-paraxial analysis decrease when the degree of spatial coherence of the field is suitably reduced. Further, the validity of the paraxial approximation in the case of Lau effect [58] is analyzed. As reported in Ref. [59], serious intensity fluctuations appear even when the length of the grating period is several hundreds of wavelengths. Finally, a new analysis method of locally one-dimensional periodic elements is introduced and applied to the analysis of finite-aperture Bessel beams generated by diffractive axicons.

Chapter 11 deals with zeroth-order diffractive elements. A new method for encoding an arbitrary amplitude and phase modulated field into an on-axis zeroth-order structure

is introduced with some examples [60,61]. The final Chapter 12 is concerned with the application of rigorous grating theory to waveguide analysis. This method is applied to calculate beam coupling into planar waveguides, the analysis of discontinuities in waveguides, and phase modulation by ion-exchanged slab waveguides.

The work presented in this thesis is of theoretical and numerical nature. All theoretical developments are presented in detail, but only a limited number of numerical examples are included to illustrate the main features of the theoretical results. A part of this work has already been published or accepted for publication:

- 1. P. Vahimaa and J. Turunen, "Lau effect: non-paraxial analysis," Journal of Modern Optics 43, 1361–1369 (1996).
- J. Turunen, P. Vahimaa, M. Honkanen, O. Salminen, and E. Noponen, "Zeroth-order complex-amplitude modulation with dielectric Fourier-type diffractive elements," Journal of Modern Optics 43, 1389-1398 (1996).
- 3. M. Kuittinen, P. Vahimaa, M. Honkanen, and J. Turunen, "Beam shaping in non-paraxial domain of diffractive optics," Applied Optics (in press).
- 4. P. Vahimaa and J. Turunen, "Bragg diffraction of spatially partially coherent fields," Journal of Optical Society of America A (in press).
- V. Kettunen, P. Vahimaa, J. Turunen, and E. Noponen, "Zeroth-order coding of complex-amplitude in two dimensions," Journal of Optical Society of America A (in press).

These publications contain some experimental verifications of the author's theoretical and numerical results. Several other publications based on the work presented in this thesis have either been submitted or are under preparation.

# Chapter 2

# Maxwell's equations and boundary conditions

### 2.1 Maxwell's equations

Let us consider a time-harmonic electromagnetic field of frequency  $\omega$ . It is characterized by three-dimensional electric and magnetic fields of the form

$$E(r,t) = \Re\{E(r)\exp(-\mathrm{i}\omega t)\},\tag{2.1}$$

$$H(\mathbf{r},t) = \Re\{E(\mathbf{r})\exp(-\mathrm{i}\omega t)\},\tag{2.2}$$

where r = (x, y, z) is the three-dimensional position vector and  $\Re$  means the real part. In a continuous medium, these time-harmonic fields satisfy Maxwell's equations

$$\nabla \times \boldsymbol{E}(\boldsymbol{r}) = \mathrm{i}\omega \boldsymbol{B}(\boldsymbol{r}),\tag{2.3}$$

$$\nabla \times \boldsymbol{H}(\boldsymbol{r}) = \boldsymbol{J}(\boldsymbol{r}) - \mathrm{i}\omega \boldsymbol{D}(\boldsymbol{r}), \tag{2.4}$$

$$\nabla \cdot \boldsymbol{D}(\boldsymbol{r}) = \rho(\boldsymbol{r}),\tag{2.5}$$

$$\nabla \cdot \boldsymbol{B}(\boldsymbol{r}) = 0, \tag{2.6}$$

where D(r), B(r), J(r), and  $\rho(r)$  are the electric displacement, the magnetic induction, the electric current density and the electric charge density, respectively. In linear isotropic media we have constitutive relations

$$D(r) = \epsilon(r)E(r), \tag{2.7}$$

$$B(r) = \mu(r)H(r), \tag{2.8}$$

$$J(r) = \sigma(r)E(r), \tag{2.9}$$

where  $\epsilon(r)$ ,  $\mu(r)$ , and  $\sigma(r)$  are known as the permittivity, the magnetic permeability, and the conductivity, respectively. The permittivity  $\epsilon$  is written as  $\epsilon(r) = \epsilon_r(r)\epsilon_0$ , where  $\epsilon_0$  is the permittivity in vacuum and  $\epsilon_r$  is the relative permittivity. The refractive index of the medium is defined as  $n(r) = \sqrt{\epsilon_r(r)}$ .

In the case of nonlinear materials,  $\epsilon$ ,  $\mu$  and  $\sigma$  are also functions of the electromagnetic field itself. Furthermore, if the medium is anisotropic, they are not scalar functions but tensors. However, in this thesis we always assume that the medium is linear and isotropic.

#### 2.1.1 Two-dimensional fields

In the general three-dimensional case, one has to solve four scalar field components simultaneously; one can eliminate, e.g.,  $E_z$  and  $H_z$  from Eqs. (2.3) and (2.4) using Eqs. (2.5) and (2.6). If the field and the medium are both invariant in y direction, all partial y-derivatives vanish in Maxwell's equations (2.3)–(2.6), which consequently reduce to the following set of partial differential equations:

$$i\omega B_x(x,z) = -\frac{\partial}{\partial z} E_y(x,z),$$
 (2.10)

$$i\omega B_z(x,z) = \frac{\partial}{\partial x} E_y(x,z),$$
 (2.11)

$$\frac{\partial}{\partial z}H_x(x,z) - \frac{\partial}{\partial x}H_z(x,z) = J_y(x,z) - i\omega D_y(x,z), \qquad (2.12)$$

$$J_x(x,z) - i\omega D_x(x,z) = -\frac{\partial}{\partial z} H_y(x,z), \qquad (2.13)$$

$$J_z(x,z) - i\omega D_z(x,z) = \frac{\partial}{\partial x} H_y(x,z), \qquad (2.14)$$

$$\frac{\partial}{\partial z}E_x(x,z) - \frac{\partial}{\partial x}E_z(x,z) = i\omega B_y(x,z). \tag{2.15}$$

On the other hand, it follows from the constitutive relations (2.7)–(2.9) that E||D||J and B||H in an isotropic medium. Thus Eqs. (2.10)–(2.15) form two independent sets.

In the first three equations, Eqs. (2.10)–(2.12), the only nonvanishing component of the electric field is  $E_y(x,z)$ . This component completely specifies the electromagnetic field, since the non-vanishing components of the magnetic field,  $H_x$  and  $H_z$ , are obtained directly from Eqs. (2.10) and (2.11), provided that  $E_y$  is known:

$$\boldsymbol{H}(x,z) = \frac{1}{i\omega\mu(x,z)} \left[ -\hat{\boldsymbol{x}}\frac{\partial}{\partial z} E_y(x,z) + \hat{\boldsymbol{z}}\frac{\partial}{\partial x} E_y(x,z) \right]. \tag{2.16}$$

Here  $\hat{x}$  and  $\hat{z}$  represent the unit coordinate vectors. One can obtain a differential equation for  $E_y$  alone by substituting Eqs. (2.10) and (2.11) into Eq. (2.12) and using constitutive equations (2.7)–(2.9):

$$\frac{\partial}{\partial x} \left[ \frac{1}{\mu(x,z)} \frac{\partial}{\partial x} E_y(x,z) \right] + \frac{\partial}{\partial z} \left[ \frac{1}{\mu(x,z)} \frac{\partial}{\partial z} E_y(x,z) \right] + \omega^2 \left[ \epsilon(x,z) + i\sigma(x,z)/\omega \right] E_y(x,z) = 0.$$
(2.17)

This is called TE polarization.

In diffractive optics, one is usually interested in non-magnetic materials, with  $\mu = \mu_0 =$  constant. Moreover, we define the complex relative permittivity  $\hat{\epsilon}_r(x,z)$  and the complex refractive index  $\hat{n}(x,z)$  by

$$\hat{\epsilon}_r(x,z) = [\hat{n}(x,z)]^2 = \epsilon_r(x,z) + i\sigma(x,z)/\omega\epsilon_0. \tag{2.18}$$

These quantities reduce to the corresponding real functions  $\epsilon_r$  and n when the conductivity  $\sigma$  vanishes. The wave number of the field is defined as

$$k = 2\pi/\lambda = \omega/c = \omega(\epsilon_0 \mu_0)^{1/2},$$
 (2.19)

where  $\lambda$  and c are the wavelength of the field and the speed of light in vacuum, respectively. Using this notation, Eq. (2.17) reduces to the Helmholtz equation

$$\frac{\partial^2}{\partial x^2} E_y(x,z) + \frac{\partial^2}{\partial z^2} E_y(x,z) + k^2 \hat{\epsilon}_r(x,z) E_y(x,z) = 0.$$
 (2.20)

On the other hand, in Eqs. (2.13)–(2.15) the only nonvanishing component of the magnetic field is  $H_y(x,z)$ . This is called TM polarization. Substitution of Eqs. (2.13) and (2.14) into Eq. (2.15), with constitutive equations (2.7)–(2.9), yields

$$\frac{\partial}{\partial x} \left[ \frac{1}{\hat{\epsilon}_r(x,z)} \frac{\partial}{\partial x} H_y(x,z) \right] + \frac{\partial}{\partial z} \left[ \frac{1}{\hat{\epsilon}_r(x,z)} \frac{\partial}{\partial z} H_y(x,z) \right] + k^2 H_y(x,z) = 0. \tag{2.21}$$

Again, once  $H_y$  is known, one can use Eqs. (2.13) and (2.14) to solve the electric field.

#### 2.2 Boundary conditions

Maxwell's equations hold when the material parameters  $\epsilon$ ,  $\mu$  and  $\sigma$  are continuous. If a discontinuous boundary separates two continuous media 1 and 2, one can transform the field vectors across it using the electromagnetic boundary condition. We denote by  $n_{12}$  a unit vector of the boundary, which points from medium 1 to medium 2, and write the boundary conditions as

$$n_{12} \cdot (B_2 - B_1) = 0, (2.22)$$

$$n_{12} \cdot (D_2 - D_1) = \rho_S,$$
 (2.23)

$$n_{12} \times (E_2 - E_1) = 0, \tag{2.24}$$

$$n_{12} \times (H_2 - H_1) = J_S, \tag{2.25}$$

where  $\rho_S$  and  $J_S$  denote the surface charge density and surface current density, respectively. If medium 2 is perfectly conducting  $(\sigma = \infty)$ , the field inside it must vanish, i.e.,  $B_2 = H_2 = D_2 = E_2 = 0$ . If the conductivity is finite or both materials are dielectric, the surface charge and current densities vanish.

### 2.3 Energy density and Poynting vector

Most often we are interested in the energy properties of the electromagnetic field. The electromagnetic energy density is defined as

$$w(\mathbf{r},t) = w_e(\mathbf{r},t) + w_h(\mathbf{r},t), \tag{2.26}$$

where

$$w_e(\mathbf{r},t) = \frac{1}{2}\mathbf{E}(\mathbf{r},t) \cdot \mathbf{D}(\mathbf{r},t)$$
 (2.27)

is the electric energy density and

$$w_h(r,t) = \frac{1}{2} \boldsymbol{H}(r,t) \cdot \boldsymbol{B}(r,t)$$
 (2.28)

is the magnetic energy density. Since the frequency  $\omega$  of the field is large in the optical region, one can not usually measure the instantaneous values of these energy densities but rather their time averages [62]

$$\langle w_e(\mathbf{r},t)\rangle = \frac{1}{4}\epsilon(\mathbf{r})|\mathbf{E}(\mathbf{r})|^2$$
 (2.29)

and

$$\langle w_h(\mathbf{r},t)\rangle = \frac{1}{4}\mu(\mathbf{r})|\mathbf{H}(\mathbf{r})|^2. \tag{2.30}$$

The time average of the electromagnetic energy density is then

$$\langle w(\mathbf{r},t)\rangle = \langle w_e(\mathbf{r},t)\rangle + \langle w_h(\mathbf{r},t)\rangle.$$
 (2.31)

The Poynting vector  $S = E \times H$  is a measure of energy flow in the field. Again, one is interested in the time average

$$\langle S(r,t)\rangle = \frac{1}{2}\Re\{E(r)\times H^*(r)\}.$$
 (2.32)

To obtain the magnitude of the energy flow in some specific direction, one simply takes a scalar product of the Poynting vector and the unit vector in that direction.

# Chapter 3

# Wave propagation in homogeneous media

In this Chapter we will solve Maxwell's equations in a homogeneous medium. The geometry of the problem is illustrated in Fig. 3.1. The electromagnetic field is supposed to be known across some plane  $z=z_0$  and one is interesting in the field at the plane  $z=z_0+\Delta z$ . The medium between these planes is assumed to be homogeneous and, for simplicity, also dielectric with refractive index n. The field at the plane  $z_0$  can either be infinite or limited by some aperture  $\mathcal{A}$ .

### 3.1 Angular spectrum representation

#### 3.1.1 Rigorous solution

The simplest solution of Maxwell's equations is a plane electromagnetic wave. A linear combination of these plane waves is, of course, also a solution. In fact, an arbitrary electromagnetic field in a homogeneous medium can be represented as a linear combination of plane waves [63,64]. This is not the only possible representation of the electromagnetic field, but it is simple and elegant.

It follows from Eqs. (2.3) and (2.4) that

$$\nabla^2 \mathbf{E}(\mathbf{r}) + k^2 n^2 \mathbf{E}(\mathbf{r}) = 0. \tag{3.1}$$

In what follows we derive the propagation laws for E(r) in Eq. (3.1). Since a similar equation holds for all components of the electric field, one can separately solve  $E_x$ . The third component  $E_z$  is then obtained from Eq. (2.5), and finally one can compute all components of H from Eqs. (2.3) and (2.8). The exact solution of Eq (3.1) for a single

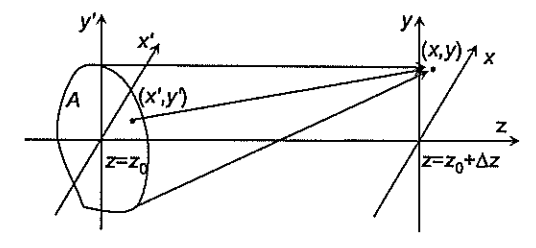


Fig. 3.1: Geometry of field propagation in a homogeneous medium.

scalar field component U may be expressed in the form

$$U(x, y, z) = \iint_{-\infty}^{\infty} T(\alpha, \beta) \exp\{i2\pi[\alpha x + \beta y + w(z - z_0)]\} d\alpha d\beta$$
$$+ \iint_{-\infty}^{\infty} R(\alpha, \beta) \exp\{i2\pi[\alpha x + \beta y - w(z - z_0)]\} d\alpha d\beta, \tag{3.2}$$

where w can be either real or imaginary:

$$w = \begin{cases} [(n/\lambda)^2 - (\alpha^2 + \beta^2)]^{1/2} & \text{when } \alpha^2 + \beta^2 \le (n/\lambda)^2 \\ i[(\alpha^2 + \beta^2) - (n/\lambda)^2]^{1/2} & \text{otherwise.} \end{cases}$$
(3.3)

With w real, the solution (3.2) represents plane waves that propagate in directions  $k = 2\pi(\alpha, \beta, w)$  or  $k = 2\pi(\alpha, \beta, -w)$ . When w is imaginary, the waves either decay or grow exponentially.

It follows from the radiation condition [2] that, in the far-zone, the field must assume the form of an outgoing spherical wave. Thus, in Eq. (3.2),  $R(\alpha, \beta) = 0$  and the solution reduces to

$$U(x, y, z) = \iint_{-\infty}^{\infty} T(\alpha, \beta, z_0) \exp\left\{i2\pi \left[\alpha x + \beta y + w(z - z_0)\right]\right\} d\alpha d\beta, \tag{3.4}$$

where

$$T(\alpha, \beta, z_0) = \iint_{-\infty}^{\infty} U(x, y, z_0) \exp[-i2\pi(\alpha x + \beta y)] dxdy$$
 (3.5)

is known as the angular spectrum of the field at  $z=z_0$ . Note that if U initially contains high spatial frequencies with  $\alpha^2 + \beta^2 > (n/\lambda)^2$ , the corresponding waves decay exponentially in positive z-direction. Such waves are called evanescent fields. They appear whenever there exist discontinuities in the medium. Although evanescent fields do not carry energy away from the discontinuity boundary, they can be useful. For example, in atom optics one can use evanescent electric fields as mirrors or gratings [65].

#### 3.1.2 Paraxial approximations

Angular spectra of many wave fields are of significant amplitude only when the angle between the wave vector k and the z-axis is small, in other words, when the function  $T(\alpha, \beta, z_0)$  is appreciably non-zero only when  $\alpha^2 + \beta^2 \ll (n/\lambda)^2$ . In such circumstances we can employ the paraxial approximation in the spatial frequency domain,

$$2\pi w = kn \left[ 1 - \frac{\lambda^2}{n^2} (\alpha^2 + \beta^2) \right]^{1/2} \approx kn - \frac{\pi \lambda}{n} (\alpha^2 + \beta^2)$$
 (3.6)

in Eq. (3.4) to obtain the Fresnel propagation formula

$$U(x,y,z) = \frac{n \exp(ikn\Delta z)}{i\lambda\Delta z} \exp\left[\frac{i\pi n}{\lambda\Delta z}(x^2 + y^2)\right] \times \iint_{-\infty}^{\infty} U(x',y',z_0) \exp\left[\frac{i\pi n}{\lambda\Delta z}(x'^2 + y'^2)\right] \exp\left[-\frac{i2\pi n}{\lambda\Delta z}(xx' + yy')\right] dx'dy'.$$
(3.7)

If, in addition, the phase factor  $(\pi n/\lambda \Delta z)(x'^2 + y'^2)$  in Eq. (3.7) is small, we obtain the Fraunhofer propagation formula

$$U(x, y, z) = \frac{n \exp(ikn\Delta z)}{i\lambda\Delta z} \exp\left[\frac{i\pi n}{\lambda\Delta z}(x^2 + y^2)\right] \times \iint_{-\infty}^{\infty} U(x', y', z_0) \exp\left[-\frac{i2\pi n}{\lambda\Delta z}(xx' + yy')\right] dx'dy', \tag{3.8}$$

which is applicable in the far zone. The Fraunhofer approximation is certainly valid if the field vanishes outside some aperture A and  $\lambda \Delta z$  is much larger than the size of the aperture. However, it can be accurate even if the distance  $\Delta z$  fails to satisfy this condition.

The strength of the angular spectrum representation is that the field can be propagated from one plane to another by Fourier transforms, which can be evaluated efficiently using the Fast Fourier-Transform (FFT) algorithm. Owing to the inherent periodicity of the FFT algorithm, non-periodic fields must be zero-padded, i.e., one must add a frame of zeros around the aperture. The amount of zero-padding depends on the angular spectrum and the distance between the planes.

### 3.2 Rayleigh-Sommerfeld diffraction formula

The angular spectrum representation is a rigorous method to propagate the electromagnetic field in the spatial frequency domain, whereas the approximate Fresnel and Fraunhofer integrals are purely space-domain representations of field propagation. Rigorous versions of space-domain methods also exist. For example, the Weyl representation of a spherical wave (see, e.g., Ref. [63], page 126) transforms the angular spectrum representation into the Rayleigh-Sommerfeld diffraction integral of the first kind:

$$U(x, y, z) = \iint_{-\infty}^{\infty} U(x', y', z_0) \left( \frac{1}{nkr_{12}} - i \right) \frac{nz}{\lambda r_{12}^2} \exp(inkr_{12}) dx' dy', \tag{3.9}$$

where

$$r_{12} = \sqrt{\Delta z^2 + (x - x')^2 + (y - y')^2}.$$
 (3.10)

We will apply the Rayleigh-Sommerfeld formula in the cylindrical coordinate system

$$\begin{cases} x = r\cos\phi \\ y = r\sin\phi \end{cases} \begin{cases} x' = \rho\cos\varphi \\ y' = \rho\sin\varphi \end{cases}$$
(3.11)

i.e., in the form

$$U(r, \phi, z) = \int_0^\infty \int_0^{2\pi} \rho U(\rho, \varphi, z_0) \left( \frac{1}{nkr_{12}} - i \right) \frac{nz}{\lambda r_{12}^2} \exp(inkr_{12}) d\rho d\varphi, \tag{3.12}$$

where now

$$r_{12} = \sqrt{\Delta z^2 + r^2 + \rho^2 - 2r\rho\cos(\varphi - \phi)}.$$
 (3.13)

In Eq. (3.12) one can make a paraxial approximation in the space-domain, i.e.,

$$r_{12} \approx \Delta z + (r^2 + \rho^2)/2 - r\rho\cos(\varphi - \phi),$$
 (3.14)

which leads to the Fresnel and Fraunhofer approximations [3].

Clearly, with the Rayleigh-Sommerfeld diffraction formula, the field at the plane  $z=z_0+\Delta z$  can be calculated by two integrations, whilst the angular spectrum representation requires four integrations. Thus if one is not able to use FFT-algorithms or analytical solutions, the Rayleigh-Sommerfeld diffraction integral may be faster to evaluate numerically. This happens, e.g., when the aperture of the element is much larger than the signal window. There exist efficient methods to solve the Rayleigh-Sommerfeld diffraction formula numerically, especially in the analysis of waves in focal regions of lenses [66].

# Chapter 4

# Coherence theory

Thus far, the electric and the magnetic fields have been assumed time-harmonic and therefore deterministic, or coherent. However, fully coherent fields do not exist in nature. We next provide a short introduction to optical coherence theory. We assume throughout this Chapter that the field propagates in a homogeneous medium with refractive index n. A comprehensive analysis of partially coherent fields can be found in Ref. [63].

### 4.1 Complex analytic signal

Let  $V^{(r)}(\mathbf{r},t)$  denote the real classical scalar wave function (a single scalar component of the electromagnetic field) at point  $\mathbf{r}$  and time t. If the function  $V^{(r)}(\mathbf{r},t)$  is square-integrable, i.e., if

$$\int_{-\infty}^{\infty} \left[ V^{(r)}(\boldsymbol{r}, t) \right]^2 dt < \infty, \tag{4.1}$$

it can be represented as a Fourier-integral

$$V^{(r)}(\mathbf{r},t) = \int_{-\infty}^{\infty} v(\mathbf{r},\omega) \exp(-\mathrm{i}\omega t) d\omega. \tag{4.2}$$

Since  $V^{(r)}(r,t)$  is real function, it follows that  $v(r,-\omega)=v^*(r,\omega)$ . Thus all the information about the wave function is contained in the positive part of the function  $v(r,\omega)$ . It is convenient to define a complex analytic wave function as

$$V(\mathbf{r},t) = \int_0^\infty v(\mathbf{r},\omega) \exp(\mathrm{i}\omega t) \mathrm{d}\omega. \tag{4.3}$$

This complex analytic signal is a natural extension of the complex representations of the monochromatic fields in Eqs. (2.1) and (2.2) (see, e.g., [63], Chapter 6).

#### 4.2 Cross-correlation function

Because of the high frequencies (of order 10<sup>15</sup> Hz) of optical fields, one is usually not able to measure the field itself but rather its time averaged values, as already mentioned in Chapter 2. Usually the fields of interest are stationary, which means that the values of the statistical properties of the field are independent of the origin of time. Physically realizable fields are typically ergodic, which implies that the ensemble average over different realizations of the field is the same as a time average of a single realization.

Let us define the cross-correlation function of the field as

$$\Gamma(r_1, r_2, t_1, t_2) = \langle V^*(r_1, t_1) V(r_2, t_2) \rangle_e, \tag{4.4}$$

where  $\langle \cdot \rangle_e$  means averaging over an ensemble of different field realizations. This is called the second order mutual coherence function. If the field is both stationary and ergodic, the ensemble average may be replaced by the time average

$$\Gamma(\boldsymbol{r}_{1}, \boldsymbol{r}_{2}, \tau) = \langle V^{*}(\boldsymbol{r}_{1}, t)V(\boldsymbol{r}_{2}, t + \tau)\rangle_{T}$$

$$= \lim_{T \to \infty} \frac{1}{2T} \int_{-T}^{T} V^{*}(\boldsymbol{r}_{1}, t)V(\boldsymbol{r}_{2}, t + \tau)dt. \tag{4.5}$$

In this thesis all fields are supposed to be both ergodic and stationary. Thus we may suppress the index T and interprete all averages as either time or ensemble averages.

The instantaneous intensity of the field is defined as  $I(\mathbf{r},t) = V^*(\mathbf{r},t)V(\mathbf{r},t)$  and its time average is

$$\langle I(\mathbf{r},t)\rangle = \langle V^*(\mathbf{r},t)V(\mathbf{r},t)\rangle = \Gamma(\mathbf{r},\mathbf{r},t).$$
 (4.6)

The definition of the cross-correlation function, Eq. (4.5), implies that

$$\Gamma(r_2, r_1, \tau) = \Gamma^*(r_1, r_2, -\tau).$$
 (4.7)

It is convenient to normalize the mutual coherence function as

$$\gamma(\mathbf{r}_1, \mathbf{r}_2, \tau) = \frac{\Gamma(\mathbf{r}_1, \mathbf{r}_2, \tau)}{[\langle I(\mathbf{r}_1, 0) \rangle \langle I(\mathbf{r}_2, 0) \rangle]^{1/2}}.$$
(4.8)

It follows from the Schwarz's inequality that the quantity  $\gamma(r_1, r_2, \tau)$ , known as the complex degree of coherence, satisfies

$$0 \le |\gamma(r_1, r_2, \tau)| \le 1. \tag{4.9}$$

If  $|\gamma(\mathbf{r}_1, \mathbf{r}_2, \tau)| = 1$ , the field is said to be fully coherent in the space-time domain. If, on the other hand,  $|\gamma(\mathbf{r}_1, \mathbf{r}_2, \tau)| = 0$ , the field is said to be completely incoherent.

One can similarly define higher-order coherence functions [63], but for our purposes it suffices to consider these second-order coherence functions.

# 4.3 Cross-spectral density function

The cross-spectral density function  $W(r_1, r_2, \omega)$  is defined as the Fourier-transform of the mutual coherence function:

$$W(\mathbf{r}_1, \mathbf{r}_2, \omega) = \frac{1}{2\pi} \int_{-\infty}^{\infty} \Gamma(\mathbf{r}_1, \mathbf{r}_2, \tau) \exp(i\omega\tau) d\tau.$$
 (4.10)

When  $r_1 = r_2$ , one usually denotes by

$$S(\mathbf{r},\omega) = W(\mathbf{r},\mathbf{r},\omega) \tag{4.11}$$

the spectral density (or the power spectrum) of the field. Conversely,

$$\Gamma(\mathbf{r}_1, \mathbf{r}_2, \tau) = \int_0^\infty W(\mathbf{r}_1, \mathbf{r}_2, \omega) \exp(-i\omega\tau) d\omega$$
 (4.12)

and

$$\Gamma(\mathbf{r}, \mathbf{r}, \tau) = \int_0^\infty S(\mathbf{r}, \omega) \exp(-i\omega\tau) d\omega. \tag{4.13}$$

Equations. (4.10) and (4.12) constitute the so-called generalized Wiener-Khintchine theorem.

From Eq. (4.7) and the definition of the cross-spectral density function it follows that

$$W(\boldsymbol{r}_2, \boldsymbol{r}_1, \omega) = W^*(\boldsymbol{r}_1, \boldsymbol{r}_2, \omega). \tag{4.14}$$

Using the Fourier-integral representation of the complex analytic signal, it also follows that

$$\langle v^*(\mathbf{r}_1, \omega)v(\mathbf{r}_2, \omega')\rangle = W(\mathbf{r}_1, \mathbf{r}_2, \omega)\delta(\omega - \omega'), \tag{4.15}$$

where  $\delta(\omega)$  is the Dirac delta function. Thus different frequency components of the field are completely uncorrelated. The cross-spectral density function  $W(r_1, r_2, \omega)$  measures the correlation between points  $r_1$  and  $r_2$  at frequency  $\omega$ .

It can be shown (see [63], page 171) that the cross-spectral density is a non-negative definite Hermitian kernel: for any n points  $r_1, r_2, \ldots, r_n$ , for any n complex numbers  $a_1, a_2, \ldots, a_n$ , and for any frequency  $\omega$ ,

$$\sum_{j=1}^{n} \sum_{k=1}^{n} a_{j}^{*} a_{k} W(\mathbf{r}_{j}, \mathbf{r}_{k}, \omega) \ge 0.$$
 (4.16)

With the choice n=1, it follows that the spectral density function is a non-negative function, which is a very desirable property for a spectrum. Similarly, the choice n=2 implies that

$$|W(r_1, r_2, \omega)| \le [W(r_1, r_1, \omega)]^{1/2} [W(r_2, r_2, \omega)]^{1/2}.$$
 (4.17)

Thus it is possible to normalize the cross-spectral density function as

$$\mu(\mathbf{r}_1, \mathbf{r}_2, \omega) = \frac{W(\mathbf{r}_1, \mathbf{r}_2, \omega)}{[S(\mathbf{r}_1, \omega)S(\mathbf{r}_2, \omega)]^{1/2}},$$
(4.18)

where the normalized function  $\mu(\mathbf{r}_1, \mathbf{r}_2, \omega)$  is called the spectral degree of coherence. It follows from Eq. (4.17) that

$$0 \le |\mu(\mathbf{r}_1, \mathbf{r}_2, \omega)| \le 1. \tag{4.19}$$

It should be noted that, in general,  $\gamma(r_1, r_2, \tau)$  and  $\mu(r_1, r_2, \omega)$  are not Fourier-transforms of each other [67].

### 4.4 Propagation of cross-spectral density

Let us suppose that the cross-spectral density function of the field is known across the plane  $z=z_0$ . It was shown above that different frequency components are non-correlated and may therefore be handled separately. For this reason, the explicit frequency dependence is suppressed in this Section to simplify notation. One is interested in the cross-spectral density function  $W(x_1, y_1, z_1, x_2, y_2, z_2)$ , with  $W(x_1', y_1', z_0, x_2', y_2', z_0)$  assumed to be known. Similarly as in Chapter 3, one obtains

$$W(x_{1}, y_{1}, z_{1}, x_{2}, y_{2}, z_{2})$$

$$= \iiint_{-\infty}^{\infty} A(\alpha_{1}, \beta_{1}, z_{0}, \alpha_{2}, \beta_{2}, z_{0}) \exp[-i2\pi(x_{1}\alpha_{1} - x_{2}\alpha_{2} + y_{1}\beta_{1} - y_{2}\beta_{2})]$$

$$\times \exp\{-i2\pi[w^{*}(\alpha_{1}, \beta_{1})\Delta z_{1} - w(\alpha_{2}, \beta_{2})\Delta z_{2}]\} d\alpha_{1}d\alpha_{2}d\beta_{1}d\beta_{2}, \qquad (4.20)$$

where  $w(\alpha, \beta)$  is given by Eq. (3.3),  $\Delta z_j = z_j - z_0$ , j = 1, 2, and the function

$$A(\alpha_{1}, \beta_{1}, z_{0}, \alpha_{2}, \beta_{2}, z_{0}) = \iiint_{-\infty}^{\infty} W(x_{1}, y_{1}, z_{0}, x_{2}, y_{2}, z_{0})$$

$$\times \exp[i2\pi(\alpha_{1}x_{1} - \alpha_{2}x_{2} + \beta_{1}y_{1} - \beta_{2}y_{2}]dx_{1}dx_{2}dy_{1}dy_{2}$$

$$(4.21)$$

is known as the angular correlation function [68].

Very often one is interested in the cross-spectral density in the far-zone. Let us denote by  $r = r\hat{s}$  the position vector of the point P, where  $\hat{s}$  is a unit vector. Using the stationary phase method (see e.g. [63], pages 128–144), the cross-spectral density is found to be

$$W(r_1\hat{s}_1, r_2\hat{s}_2) = \frac{n^2 \cos \theta_1 \cos \theta_2}{\lambda^2} A(n\hat{s}_{1x}/\lambda, n\hat{s}_{1y}/\lambda, z_0, n\hat{s}_{2x}/\lambda, n\hat{s}_{2y}/\lambda, z_0) \frac{\exp\left[ikn(r_1 - r_2)\right]}{r_1 r_2},$$
(4.22)

where  $\theta$  is the angle between the unit position vector  $\hat{s}$  and z-axis. The radiant intensity of the field, which appears to be the only quantity in physical radiometry that can be defined without ambiguity [69], is defined as

$$J(\hat{s}) = r^2 W(r\hat{s}, r\hat{s}) \text{ when } r \to \infty,$$
 (4.23)

and thus

$$J(\hat{\mathbf{s}}) = \left(\frac{n\cos\theta}{\lambda}\right)^2 A(n\hat{s}_{1x}/\lambda, n\hat{s}_{1y}/\lambda, z_0, n\hat{s}_{2x}/\lambda, n\hat{s}_{2y}/\lambda, z_0). \tag{4.24}$$

The radiant intensity determines how much energy propagates in the direction  $\hat{s}$ . If the field is completely spatially coherent in the plane  $z=z_0$ , it follows that

$$J(\hat{\mathbf{s}}) = \left(\frac{n\cos\theta}{\lambda}\right)^2 \left| T\left(\frac{ns_x}{\lambda}, \frac{ns_y}{\lambda}\right) \right|^2. \tag{4.25}$$

# 4.5 Coherent mode representation

It follow from Mercer's theorem (Ref. [63], page 68) that the cross-spectral density function can be represented as

$$W(\mathbf{r}_1, \mathbf{r}_2, \omega) = \sum_{n=0}^{\infty} c_n(\omega) \psi_n^*(\mathbf{r}_1, \omega) \psi_n(\mathbf{r}_2, \omega), \tag{4.26}$$

where  $\psi_n(r,\omega)$  are the eigenfunctions and  $c_n(\omega)$  are the eigenvalues of the Fredholm integral equation

$$\int_{\mathcal{A}} W(\mathbf{r}_1, \mathbf{r}_2, \omega) \psi_n(\mathbf{r}, \omega) \mathrm{d}^3 \mathbf{r}_1 = c_n(\omega) \psi_n(\mathbf{r}_2, \omega). \tag{4.27}$$

A closer examination of the components

$$W_n(\mathbf{r}_1, \mathbf{r}, \omega) = c_n(\omega)\psi_n^*(\mathbf{r}_1, \omega)\psi_n(\mathbf{r}_2, \omega)$$
(4.28)

shows that

$$|\mu_n(\mathbf{r}_1, \mathbf{r}_2, \omega)| = 1$$
 (4.29)

for all n. Thus all the field components  $\psi_n(r,\omega)$ , which satisfy the standard Helmholtz equation, are completely spatially coherent. The decomposition (4.26) is therefore called a coherent mode representation of the field. It allows one to treat a spatially partially coherent field as a sum of completely coherent fields. Thus one can, for example, solve any diffraction problem for a spatially partially coherent field by solving the problem separately for each coherent mode and thereafter sum the resulting modal fields to obtain the complete cross-spectral density function of the diffracted partially coherent field.

#### 4.6 Model fields

Let us consider some examples of partially coherent fields. If the spectral degree of coherence  $\mu(r_1, r_2, \omega)$  depends on  $r_1$  and  $r_2$  only through the difference  $r' = r_2 - r_1$ , one speaks of a Schell-model field. The cross-spectral density function is then of the form

$$W(r_1, r_2, \omega) = [S(r_1, \omega)S(r_2, \omega)]^{1/2} \mu(r_2 - r_1, \omega).$$
(4.30)

Furthermore, if both the spectral degree of coherence and the spectral density are Gaussian functions, i.e.,

$$S(\mathbf{r},\omega) = A^{2}(\omega) \exp\left[-\mathbf{r}^{2}/2w^{2}(\omega)\right], \qquad (4.31)$$

$$\mu(\mathbf{r},\omega) = \exp\left[-\mathbf{r}^2/2\sigma_g^2(\omega)\right], \tag{4.32}$$

the field is called a Gaussian Schell-model field. Here w and  $\sigma_g$  are positive quantities that describe the width of the intensity distribution and the correlation length of the field, respectively, and  $A(\omega)$  is a measure of the weights of different frequency components. If  $\sigma_g \gg w$ , the field is essentially spatially coherent and it behaves much like a completely coherent Gaussian field (e.g., a fundamental-mode laser beam). If, in contrary,  $\sigma_g \ll w$ , the field is globally incoherent and it is called quasi-homogeneous. The field can nevertheless propagate in a beamlike fashion [70–72].

Let us consider a two-dimensional Gaussian Schell-model field, which has its waist located at  $z=z_0$  and is invariant in y direction. Then the cross-spectral density function at the waist is

$$W(x_1, z_0, x_2, z_0) = W_0 \exp\left[-(x_1^2 + x_2^2)/w^2\right] \exp\left[-(x_1 - x_2)^2/2\sigma_g^2\right],\tag{4.33}$$

where  $W_0$  is a constant. Its coherent modes are Hermite-Gaussian functions [72,73]

$$\phi_n(x) = \frac{1}{\sqrt{2^n n!}} \left( \frac{2}{\pi w^2 \beta} \right)^{1/4} H_n\left( \frac{x\sqrt{2}}{w\sqrt{\beta}} \right) \exp\left( -\frac{x^2}{w^2 \beta} \right), \tag{4.34}$$

where

$$\beta = [1 + (w/\sigma_q)^2]^{-1/2}. (4.35)$$

The corresponding modal coefficients are found to be

$$c_n = W_0 \sqrt{2\pi} \frac{w\beta}{1+\beta} \left(\frac{1-\beta}{1+\beta}\right)^n, \tag{4.36}$$

i.e., the number of modes with significant amplitudes increases rapidly when the state of coherence of the field is reduced.

# Chapter 5

# Grating diffraction

### 5.1 Geometry of the problem

Consider the geometry of Fig. 5.1. Between the planes z=0 and z=h there exists an element with a periodically modulated refractive index distribution. Outside this region the media are supposed to be homogeneous. The element is illuminated by a plane wave arriving from the negative z-direction. The problem is to solve the complex amplitudes of all plane wave components of the field scattered by the modulated region. If the modulation of the refractive index distribution or the surface relief profile is slow compared to the optical wavelength  $\lambda$ , the problem can usually be solved using the traditional theories of refraction and reflection at discontinuous interfaces or graded-index media. If, however, the details in the modulated region are comparable to  $\lambda$ , rigorous diffraction theory must be applied.

The media in regions 1 (z < 0) and 3 (z > h) are supposed to be homogeneous with permittivities  $\epsilon_r = \epsilon_1 = n_1^2$  and  $\epsilon_r = \epsilon_3 = n_3^2$ , respectively. In general, the medium in region 2  $(0 \le z \le h)$  can be arbitrarily modulated in x, y, and z directions. This region is illuminated by a plane wave incident at some angle  $\theta$  between the wave vector k and the z-axis.

In this thesis only y-invariant configurations of the type illustrated in Fig. 5.1are needed. Therefore the TE/TM decomposition of the field (see Section 2.1.1) is valid. Rigorous diffraction analysis of gratings in conical incidence (the incident wave does not

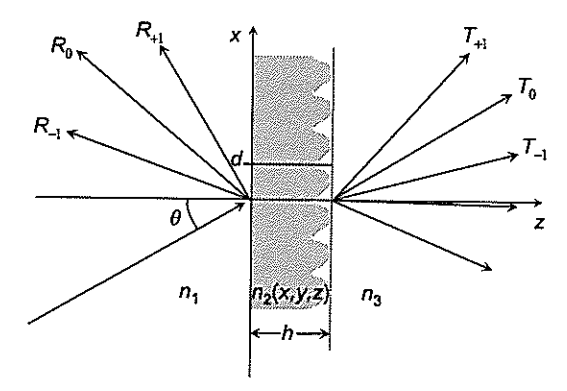


Fig. 5.1: Geometry of the grating diffraction problem.

propagate in the xz plane) is also possible [74–77], as is the analysis of 3D modulated gratings [78–82].

### 5.2 Rayleigh expansions

Since the refractive index distribution is supposed to be periodic in the region 2, i.e.,  $\hat{\epsilon}_r(x+d,z) = \hat{\epsilon}_r(x,z)$ , it follows from the Bloch theorem that all the field components in region 2 must be pseudoperiodic [2]:

$$U(x+d,z) = U(x,z) \exp(iu_0 d),$$
 (5.1)

where  $u_0 = kn_1 \sin \theta$  and  $\theta$  is the angle of incidence. As it was seen in Chapter 3, in region 3 all components of the forward-propagating part of the diffracted electromagnetic field at z = h can be expressed as a linear combination of plane waves

$$U_d(x,h) = \int_{-\infty}^{\infty} T(\alpha,h) \exp(i2\pi\alpha x) d\alpha.$$
 (5.2)

Because the diffracted field must be pseudoperiodic, it follows that

$$T(\alpha, h) = \sum_{m=-\infty}^{\infty} T_m \delta(\alpha - u_m/2\pi), \tag{5.3}$$

where  $u_m = u_0 + 2\pi m/d$  and  $\delta(\alpha)$  is the Dirac delta function. Writing  $u_m = kn_3 \sin \theta_m$  and recalling that  $u_0 = kn_1 \sin \theta$  one obtains the familiar grating equation

$$n_3 \sin \theta_m = n_1 \sin \theta + m\lambda/d. \tag{5.4}$$

In region 1 one obtains a similar expression for the backward-diffracted orders:

$$n_1 \sin \theta_m = n_1 \sin \theta + m\lambda/d. \tag{5.5}$$

Substitution of Eq. (5.3) in the two-dimensional form of Eq. (3.4) yields the so-called Rayleigh expansion

$$U_d(x, z \ge h) = \sum_{m=-\infty}^{\infty} T_m \exp\{i[u_m x + t_m(z - h)]\},$$
 (5.6)

where

$$t_m = \begin{cases} [(kn_3)^2 - u_m^2]^{1/2} & \text{if } |u_m| \le kn_3\\ i[u_m^2 - (kn_3)^2]^{1/2} & \text{otherwise.} \end{cases}$$
 (5.7)

The Fourier coefficients  $T_m$  can be calculated from

$$T_m = \frac{1}{d} \int_0^d U_d(x, h) \exp(-\mathrm{i}u_m x) \mathrm{d}x \tag{5.8}$$

if the field at the plane z = h is known.

Using similar reasoning, it follows that the outgoing field in the region  $z \leq 0$  can be written as

$$U_d(x, z \le 0) = \sum_{m = -\infty}^{\infty} R_m \exp\left[i(u_m x - r_m z)\right], \tag{5.9}$$

where

$$r_m = \begin{cases} [(kn_1)^2 - u_m^2]^{1/2} & \text{if } |u_m| \le kn_1\\ i[u_m^2 - (kn_1)^2]^{1/2} & \text{otherwise} \end{cases}$$
 (5.10)

and

$$R_m = \frac{1}{d} \int_0^d U_d(x, 0) \exp(-iu_m x) dx.$$
 (5.11)

Expressions (5.6) and (5.9), known as Rayleigh expansions, can be generalized to a three dimensional case, where the grating is periodic in both x and y directions with periods  $d_x$  and  $d_y$ , respectively.

### 5.2.1 Detour-phase principle

We just showed that, outside the grating area, the diffracted field can be expressed in the form of Rayleigh expansions. Let us suppose now that the angle of incidence is  $\theta=0$ . Then any diffracted field component at the grating surface z=h may be expressed as

$$U_d(x,h) = \sum_{m=-\infty}^{\infty} T_m \exp(i2\pi mx/d), \qquad (5.12)$$

where

$$T_m = \frac{1}{d} \int_0^d U_d(x, h) \exp(-i2\pi mx/d) dx.$$
 (5.13)

If the grating is now shifted in x direction by an amount  $\Delta x$ , as illustrated in Fig. 5.2, the diffracted field becomes

$$U'_d(x + \Delta x, h) = U_d(x, h).$$
 (5.14)

Thus

$$T'_{m} = \frac{1}{d} \int_{0}^{d} U'_{d}(x, h) \exp(-i2\pi mx/d) dx$$

$$= \frac{1}{d} \exp(-i2\pi m\Delta x/d) \int_{-\Delta x}^{d-\Delta x} U_{d}(x', h) \exp(-i2\pi mx'/d) dx'.$$
 (5.15)

Since  $U_d$  is a periodic function, integration over one period does not depend on the initial point. Thus one obtains

$$T'_{m} = T_{m} \exp(-i2\pi m\Delta x/d). \tag{5.16}$$

This result is the general form of Lohmann's famous detour-phase principle [15, 16].

Equation (5.16) implies that if we shift the grating in the x direction by an amount  $\Delta x$ , then the phase of the *m*th diffracted order changes from  $\phi_m$  to

$$\phi_m' = \phi_m - 2\pi m \Delta x/d. \tag{5.17}$$

This principle permits the control of the phase of any diffracted order, except the zeroth order. The result is fully rigorous and it holds equally for diffracted orders in region 1.

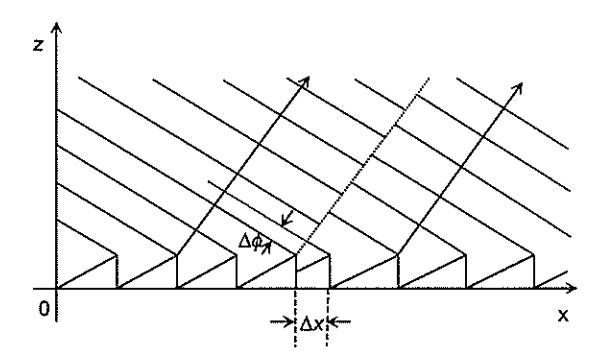


Fig. 5.2: Lohmann's detour-phase principle.

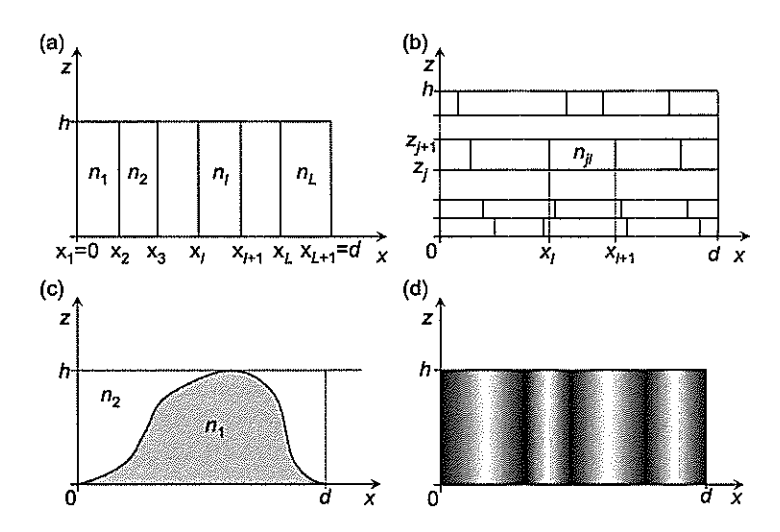


Fig. 5.3: Different types of gratings: (a) binary lamellar grating, (b) multilevel lamellar grating, (c) continuous surface profile grating, (d) index modulated grating.

### 5.3 About the solution of grating-diffraction problems

There exist plenty of methods to solve grating-diffraction problems numerically. For the purposes of this thesis, it is not necessary to describe the details of each method since several excellent reviews exist [2,83,84].

In Fig. 5.3 some different types of gratings are illustrated. In Fig. 5.3a the refractive index in region 2 is constant between some values  $x_l$  and  $x_{l+1}$  and uniform in z direction through the entire region 0 < z < h. The refractive index values  $n_l$  can be arbitrary, but often only two different values, usually  $n_1$  and  $n_3$ , with one of them equal to unity, are preferred for fabrication reasons. In Fig. 5.3b the grating contains several layers similar to Fig. 5.3a. This kind of grating is called a multilevel lamellar grating. These two types of lamellar grating can be fabricated, e.g., by etching into glass [85–87], with direct laser beam [88, 89] or electron beam [90–92] writing of the mask structure. In Fig. 5.3c the

boundaries between areas with different refractive index are no longer assumed to be vertical. This type of profiles can be made by variable-exposure laser [1,93] or electron electron lithography [94–97]. The refractive index can also vary continuously inside the grating area. In Fig. 5.3d this kind of index-modulated grating is represented; it can be realized, e.g., by optical holography [98–100].

Basically, solution methods of the grating-diffraction problem can be divided into two different categories: space-domain methods and modal methods. In space-domain methods, one solves the entire diffracted field (a sum of all diffracted orders) simultaneously all over the space and thereafter projects the diffracted field into the base formed by the diffraction orders. The best-known example of these methods is the integral method [83, 101]. The weakness of space-domain methods is that the field is represented using points in x-axis as a base. Thus the base is uncountable and the number of sampling points one must include into the analysis may be very large. However, these methods must be used when one wants to analyze continuous surface profile gratings rigorously.

In modal methods, one expresses the diffracted field as a sum of pseudoperiodic wave-guide modes inside the grating and effectively transforms the calculations into the spatial frequency domain. The base in which the field is represented is now countable and the number of base functions that must be included in the calculations is usually smaller than in space-domain methods. Modal methods can be used directly when the grating is invariant in the z direction. Thus these methods can be applied in the cases of lamellar and index-modulated gratings. However, one can also analyze continuous profile gratings by dividing the grating area into several layers (as illustrated in Fig. 5.3b), which are approximately lamellar gratings [102], if the field representation in various slabs are matched at the boundaries inside modulated region.

# 5.4 Modal expansion methods

We next suppose that the diffractive element is divided into J layers that can be either binary lamellar or index-modulated, but y invariant. We solve the field inside each layer and thereafter use the boundary conditions at each surface  $z=z_j$  to match the fields in different layers. Thus the solution of the diffraction problem is divided into two distinct problems: (1) solving the modes in each layer and (2) matching the boundary conditions. The calculations in part (1) depend greatly on the chosen approach, while part (2) is always simply a solution of a set of linear equations.

Let us first consider a single layer located between boundaries  $z_j \geq 0$  and  $z_{j+1} \leq h$ . The refractive index distribution inside this layer is supposed to be  $\hat{\epsilon}_r(x)$ . We make the separation of variables, U(x,z) = X(x)Z(z), where  $U = E_y$  and  $U = H_y$  in TE and TM polarizations, respectively. In TE polarization, this yields the equations

$$\frac{\mathrm{d}^2}{\mathrm{d}x^2}X(x) + \left[k^2\hat{\epsilon}_r(x) - \gamma^2\right]X(x) = 0 \tag{5.18}$$

and

$$\frac{d^2}{dz^2}Z(z) + \gamma^2 Z(z) = 0,$$
(5.19)

where  $\gamma$  is the separation constant. In TM polarization, the Eq. (5.19) remains unchanged, but Eq. (5.18) must be replaced by

$$\hat{\epsilon}_r(x)\frac{\mathrm{d}}{\mathrm{d}x}\left[\frac{1}{\hat{\epsilon}_r(x)}\frac{\mathrm{d}}{\mathrm{d}x}X(x)\right] + \left[k^2\hat{\epsilon}_r(x) - \gamma^2\right]X(x) = 0.$$
 (5.20)

The solution of Eq. (5.19) is easily found to be

$$Z(z) = a \exp[i\gamma(z - z_j)] + b \exp[-i\gamma(z - z_{j+1})].$$
 (5.21)

We will see that in the case of periodic elements, there exists a discrete set of solutions  $X_m(x)$ , which will be called modes. There exist different methods for solving these modes and some of them will be introduced in the next subsections. We will consider only one of the layers and omit the index j for the sake of notational simplicity.

#### 5.4.1 Exact eigenmode method

The exact eigenmode method was introduced by Maystre and Petit [103] in the case of a rectangular array of grooves in perfectly conducting material. Later this method was extended to finitely conducting [104, 105], dielectric [106], multilevel [76], and multiply grooved lamellar gratings [107]. Also it is possible to analyze conically mounted gratings with the exact eigenmode method [75,76]. Here we will assume non-conical mounting but the grating may have an arbitrary lamellar structure.

In exact modal methods the refractive-index profile in the x direction must be such that one can solve the mode functions  $X_m(x)$  analytically. This is possible if the refractive index is piecewise constant in x direction. We assume TE polarization (TM polarization can be analyzed with slight modifications), a refractive index profile of the form  $\hat{n}(x) = \hat{n}_l$  when  $x_l < x < x_{l+1}$ , with  $x_1 = 0$  and  $x_{L+1} = d$  (d = grating period). The solution  $X_l(x)$  is then easily found in the lth block:

$$X_{l}(x) = A_{l} \exp[i\beta_{l}(x - x_{l})] + B_{l} \exp[-i\beta_{l}(x - x_{l+1})], \tag{5.22}$$

where

$$\beta_l = \begin{cases} \sqrt{(k\hat{n}_l)^2 - \gamma^2} & \text{if } |\gamma| \le k\hat{n}_l \\ i\sqrt{\gamma^2 - (k\hat{n}_l)^2} & \text{otherwise} \end{cases}$$
 (5.23)

One can determine the separation constant  $\gamma$  by requiring that both X(x) and its derivative are continuous at each boundary  $x = x_l$ , and that the modes are pseudoperiodic (see Section 5.2). Using these continuity conditions one obtains a matrix equation that connects the amplitudes  $A_l$  and  $B_l$  in two adjacent blocks:

$$\begin{bmatrix} 1 & \exp(\mathrm{i}\beta_{l}d_{l}) \\ \beta_{l} & -\beta_{l}\exp(\mathrm{i}\beta_{l}d_{l}) \end{bmatrix} \begin{bmatrix} A_{l} \\ B_{l} \end{bmatrix} = \begin{bmatrix} \exp(\mathrm{i}\beta_{l-1}d_{l-1}) & 1 \\ \beta_{l-1}\exp(\mathrm{i}\beta_{l-1}d_{l-1}) & -\beta_{l-1} \end{bmatrix} \begin{bmatrix} A_{l-1} \\ B_{l-1} \end{bmatrix}, \quad (5.24)$$

where  $d_l = x_{l+1} - x_l$  is the width of the lth block. Due to the pseudoperiodicity, one also requires that

$$\begin{bmatrix} 1 & \exp(\mathrm{i}\beta_1 d_1) \\ \beta_1 & -\beta_1 \exp(\mathrm{i}\beta_1 d_1) \end{bmatrix} \begin{bmatrix} A_1 \\ B_1 \end{bmatrix} = \exp(\mathrm{i}u_0 d) \begin{bmatrix} \exp(\mathrm{i}\beta_L d_L) & 1 \\ \beta_L \exp(\mathrm{i}\beta_L d_L) & -\beta_L \end{bmatrix} \begin{bmatrix} A_L \\ B_L \end{bmatrix}. \quad (5.25)$$

By combining these equations one obtains a matrix equation

$$\exp(\mathrm{i}u_{0}d) \begin{bmatrix} A_{1} \\ B_{1} \end{bmatrix} = \begin{bmatrix} \exp(\mathrm{i}\beta_{1}d_{1}) & 1 \\ \beta_{1} \exp(\mathrm{i}\beta_{1}d_{1}) & -\beta_{1} \end{bmatrix}^{-1} \\ \times \prod_{l=2}^{L} \begin{bmatrix} 1 & \exp(\mathrm{i}\beta_{l}d_{l}) \\ \beta_{l} & -\beta_{l} \exp(\mathrm{i}\beta_{l}d_{l}) \end{bmatrix} \begin{bmatrix} \exp(\mathrm{i}\beta_{l}d_{l}) & 1 \\ \beta_{l} \exp(\mathrm{i}\beta_{l}d_{l}) & -\beta_{l} \end{bmatrix}^{-1} \\ \times \begin{bmatrix} 1 & \exp(\mathrm{i}\beta_{1}d_{1}) \\ \beta_{1} & -\beta_{1} \exp(\mathrm{i}\beta_{1}d_{1}) \end{bmatrix} \begin{bmatrix} A_{1} \\ B_{1} \end{bmatrix} \\ \equiv \begin{bmatrix} A(\gamma) & B(\gamma) \\ C(\gamma) & D(\gamma) \end{bmatrix} \begin{bmatrix} A_{1} \\ B_{1} \end{bmatrix}.$$
 (5.26)

In order to have non-trivial solutions, it is required that

$$A(\gamma)D(\gamma) - B(\gamma)C(\gamma) - \exp(iu_0d)[A(\gamma) + D(\gamma)] + \exp(i2u_0d) = 0, \tag{5.27}$$

which is a transcendental equation for the allowed values of  $\gamma$ . This equation has an infinite but countable number of roots, which will be denoted  $\gamma_m$ . Once these eigenvalues have been found, one can solve the amplitudes  $A_l$  and  $B_l$  using Eqs. (5.24) and (5.25). However, one of these remains undetermined. It can be fixed by normalizing the modes.

#### 5.4.2 Legendre polynomial expansion method

The problem with the preceding exact eigenmode method is that one must find zeroes of the transcendental equation (5.27) in a complex plane, which may be difficult. In order to avoid transcendental equation (5.27) one can approximate the exact modes using different kinds of expansions. One example is introduced by Morf [108,109]. He expressed the modes in Legendre and Chebyshev polynomials bases. The idea is, that since such polynomials form a complete base in the interval [-1,1] (see, e.g., Ref. [110], p. 652), the modes can be represented in these bases. Here we will use Legendre polynomials as base functions. The case with Chebyshev polynomials can be analyzed with slight modifications.

Let us write the mode  $X_l(x)$  in lth block as

$$X_l(x) = \sum_{m=0}^{\infty} p_m^l P_m(\xi),$$
 (5.28)

where  $P_m(\xi)$  is the mth Legendre polynomial,  $p_m^l$  are the polynomial coefficients of the lth mode and

$$\xi = \frac{2x - x_l - x_{l+1}}{x_{l+1} - x_l} \tag{5.29}$$

is a mapping from  $[x_l, x_{l+1}]$  to the interval [-1, 1]. If one truncates the sum to contain M polynomials, then the second derivative of the mode in the lth block can be written as

$$\frac{\mathrm{d}^2}{\mathrm{d}x^2} X_l(x) = \sum_{m=0}^{M-2} b_m P_m(\xi), \tag{5.30}$$

where the coefficients  $b_m$  are connected to the coefficients  $a_m$  as

$$b_m = \left(m + \frac{1}{2}\right) \sum_{p=m+2,m+4,\dots}^{M} (p+m+1)(p-m)a_p.$$
 (5.31)

In TE polarization, both the field and its derivative must be continuous across the block boundaries. One therefore obtains

$$\sum_{m=0}^{M_l} p_m^l = \sum_{m=0}^{M_{l+1}} p_m^{l+1} (-1)^m$$
 (5.32)

and

$$\frac{1}{d_l} \sum_{m=0}^{M_l} p_m^l m(m+1) = \frac{1}{d_{l+1}} \sum_{m=0}^{M_{l+1}} p_m^{l+1} (-1)^{m+1} m(m+1), \tag{5.33}$$

where  $d_l = x_{l+1} - x_l$  is the width of lth block. Pseudoperiodicity requires that

$$\sum_{m=0}^{M_L} p_m^L = \sum_{m=0}^{M_1} p_m^1 (-1)^m \exp(iu_0 d)$$
 (5.34)

and

$$\frac{1}{d_L} \sum_{m=0}^{M_L} p_m^L m(m+1) = \frac{1}{d_1} \sum_{m=0}^{M_1} p_m^1 (-1)^{m+1} m(m+1) \exp(\mathrm{i} u_0 d). \tag{5.35}$$

Thus one has 2L equations to eliminate the coefficients  $p_{M_l}^l$  and  $p_{M_l-1}^l$ . On combining these results, one obtains a matrix equation for the eigenvalues  $\gamma_m$  and the corresponding eigenvectors, which contain the polynomial coefficients  $p_m^l$ ,  $m=0,\ldots,M_l-1$ . In TM polarization one replaces all  $1/d_l$  in derivative terms by  $1/(\hat{n}_l^2d_l)$ , because the continuous function across the boundaries is the derivative of the field divided by  $\hat{n}_l^2$ .

In numerical calculations it is necessary to truncate the sum of the polynomials, but the maximum number of polynomials can differ from block to block.

#### 5.4.3 Fourier-expansion method

Since we are dealing with periodic elements, it is possible to express the permittivity distribution in the x direction in the form of a Fourier series. This method was introduced by Burckhardt [111,112] and developed further by Kaspar [113], Knop [114], and Nyyssonen and Kirk [102]. Also Tamir et al. used essentially the same method in the analysis of a sinusoidally modulated half-space [115,116].

Let us first assume TE polarization and write the relative permittivity of the grating as a Fourier-series

$$\hat{\epsilon}_r(x) = \sum_{m=-\infty}^{\infty} \epsilon_m \exp(i2\pi mx/d), \qquad (5.36)$$

where

$$\varepsilon_m = \frac{1}{d} \int_0^d \hat{\epsilon}_r(x) \exp(-i2\pi mx/d). \tag{5.37}$$

We look for a pseudoperiodic mode solution

$$X(x) = \sum_{l=-\infty}^{\infty} P_l \exp(iu_l x), \qquad (5.38)$$

where the coefficients  $P_l$  are unknown. Inserting Eqs. (5.36) and (5.38) into the Eq. (5.18), and using the orthonormality of the functions  $\exp(iu_m x)$  in the interval [0, d], one obtains a matrix equation

 $\mathbf{M}P = \gamma^2 P,\tag{5.39}$ 

where the vector P contains the coefficients  $P_l$  and M is a matrix with elements

$$M_{lm} = k^2 \varepsilon_{l-m} - u_m^2 \delta_{lm}. \tag{5.40}$$

Thus the mode eigenvalues  $\gamma_m$  are the eigenvalues of the matrix **M** and the corresponding eigenvector  $P_m$  gives the polynomial coefficients  $P_{lm}$ .

In TM polarization several formulations of the eigenvalue problem can be obtained, which all are equivalent in principle, but differ greatly when one considers numerical convergence. The most stable form is

$$N^{-1}(k^2I - KE^{-1}K)P = \gamma^2P,$$
 (5.41)

where  $E_{lm} = \varepsilon_{l-m}$ ,  $K_{lm} = u_l \delta_{lm}$ ,  $I_{lm} = \delta_{lm}$ ,  $N_{lm} = \xi_{l-m}$ , and  $\xi_l$  are the Fourier components of the function  $1/\hat{\varepsilon}_r$  [117–120].

One must truncate the matrices in numerical calculations in such a way that all propagating modes and a sufficient number of evanescent modes are included. The number of eigenvalues needed depends on the period of the element, on the refractive indices, and also on the state polarization.

#### 5.4.4 Boundary conditions

After the solution of the modes  $X_m(x)$  inside the grating with one of the methods discussed above, one has to determine the amplitudes  $a_m$  and  $b_m$  in Eq. (5.21) using the boundary conditions at each the boundaries  $z = z_j$ . In TE polarization we require that both  $E_y(x, z)$  and its z-derivative are continuous across each boundary.

In regions 1 (z < 0) and 3 (z > h) the field is expressed in the form of Rayleigh-expansions (5.9) and (5.6), respectively. The incident field is supposed to consist of either a single plane wave or a combination of plane waves that propagate in directions exactly opposite to those of the backward-diffracted orders. Thus the field in region 1 is expressed in the form

$$E_y^1(x,z) = \sum_{m=-\infty}^{\infty} A_m \exp\left[i(u_m x + r_m z)\right] + \sum_{m=-\infty}^{\infty} R_m \exp\left[i(u_m x - r_m z)\right], \quad (5.42)$$

where the coefficients  $A_m$  are the (known) amplitudes of the incident plane waves. In region 3 we write

$$E_y^3(x,z) = \sum_{m=-\infty}^{\infty} T_m \exp\left\{i \left[u_m x + t_m (z-h)\right]\right\}.$$
 (5.43)

Inside the *i*th grating layer we have the mode expansion

$$E_y^j(x,z) = \sum_{m=1}^{\infty} \left\{ a_m^j \exp\left[i\gamma_m^j(z-z_j)\right] + b_m^j \exp\left[-i\gamma_m^j(z-z_{j+1})\right] \right\} X_m^j(x).$$
 (5.44)

If we demand the continuity of both the field and its derivative across the boundaries z = 0 and z = h, we arrive at matrix equations

$$\begin{bmatrix} \mathbf{I} & \mathbf{0} \\ \mathbf{t} & \mathbf{0} \end{bmatrix} \begin{bmatrix} \mathbf{T} \\ \mathbf{R} \end{bmatrix} = \begin{bmatrix} \mathbf{P}^J \mathbf{E}^J & \mathbf{P}^J \\ \mathbf{P}^J \mathbf{\Gamma}^J \mathbf{E}^J & -\mathbf{P}^J \mathbf{\Gamma}^J \end{bmatrix} \begin{bmatrix} \mathbf{a}^J \\ \mathbf{b}^J \end{bmatrix}$$
(5.45)

and

$$\begin{bmatrix} \mathbf{0} & \mathbf{I} \\ \mathbf{0} & -\mathbf{r} \end{bmatrix} \begin{bmatrix} \mathbf{T} \\ \mathbf{R} \end{bmatrix} + \begin{bmatrix} \mathbf{I} & \mathbf{0} \\ \mathbf{r} & \mathbf{0} \end{bmatrix} \begin{bmatrix} \mathbf{A} \\ \mathbf{0} \end{bmatrix} = \begin{bmatrix} \mathbf{P}^{1} & \mathbf{P}^{1}\mathbf{E}^{1} \\ \mathbf{P}^{1}\mathbf{\Gamma}^{1} & -\mathbf{P}^{1}\mathbf{\Gamma}^{1}\mathbf{E}^{1} \end{bmatrix} \begin{bmatrix} \mathbf{a}^{1} \\ \mathbf{b}^{1} \end{bmatrix}. \tag{5.46}$$

Here  $I_{mn} = \delta_{mn}$ ,  $t_{mn} = t_m \delta_{mn}$ ,  $r_{mn} = r_m \delta_{mn}$ ,  $E^j_{mn} = \exp(i\gamma^j_m h_j)\delta_{mn}$ ,  $h_j = z_{j+1} - z_j$ ,  $\Gamma_{mn} = \gamma^j_m \delta_{mn}$ , the elements of vectors  $\boldsymbol{a}^j$ ,  $\boldsymbol{b}^j$ ,  $\boldsymbol{T}$ ,  $\boldsymbol{R}$ , and  $\boldsymbol{A}$  are the amplitudes  $a^j_m$ ,  $b^j_m$ ,  $T_m$ ,  $R_m$ , and  $A_m$ , respectively, and

$$P_{mn}^{j} = \langle \exp(iu_{m}x)|X_{n}^{j}(x)\rangle = \frac{1}{d} \int_{0}^{d} X_{n}^{j}(x) \exp(-iu_{m}x) dx$$
 (5.47)

are the projections of the modes into the base formed by the diffracted orders. These projections can be solved analytically in each modal method presented above.

Application of the boundary conditions at the surface between layers j and j+1 leads to the matrix equation

$$\begin{bmatrix} \mathbf{P}^{j}\mathbf{E}^{j} & \mathbf{P}^{j} \\ \mathbf{P}^{j}\Gamma^{j}\mathbf{E}^{j} & -\mathbf{P}^{j}\Gamma^{j} \end{bmatrix} \begin{bmatrix} \mathbf{a}^{j} \\ \mathbf{b}^{j} \end{bmatrix} = \begin{bmatrix} \mathbf{P}^{j+1} & \mathbf{P}^{j+1}\mathbf{E}^{j+1} \\ \mathbf{P}^{j+1}\Gamma^{j+1} & -\mathbf{P}^{j+1}\Gamma^{j+1}\mathbf{E}^{j+1} \end{bmatrix} \begin{bmatrix} \mathbf{a}^{j+1} \\ \mathbf{b}^{j+1} \end{bmatrix}.$$
(5.48)

Thus the vectors T and R can be obtained from the following set of linear equations:

$$\prod_{j=1}^{J} \begin{bmatrix} \mathbf{P}^{j} & \mathbf{P}^{j} \mathbf{E}^{j} \\ \mathbf{P}^{j} \mathbf{\Gamma}^{j} & -\mathbf{P}^{j} \mathbf{\Gamma}^{j} \mathbf{E}^{j} \end{bmatrix} \begin{bmatrix} \mathbf{P}^{j} \mathbf{E}^{j} & \mathbf{P}^{j} \\ \mathbf{P}^{j} \mathbf{\Gamma}^{j} \mathbf{E}^{j} & -\mathbf{P}^{j} \mathbf{\Gamma}^{j} \end{bmatrix}^{-1} \begin{bmatrix} \mathbf{I} & \mathbf{0} \\ \mathbf{t} & \mathbf{0} \end{bmatrix} \begin{bmatrix} \mathbf{T} \\ \mathbf{R} \end{bmatrix} \\
- \begin{bmatrix} \mathbf{0} & \mathbf{I} \\ \mathbf{0} & -\mathbf{r} \end{bmatrix} \begin{bmatrix} \mathbf{T} \\ \mathbf{R} \end{bmatrix} = \begin{bmatrix} \mathbf{I} & \mathbf{0} \\ \mathbf{r} & \mathbf{0} \end{bmatrix} \begin{bmatrix} \mathbf{A} \\ \mathbf{0} \end{bmatrix}.$$
(5.49)

If we choose a finite number of base functions  $\exp(iu_k x)$ , this set of equations truncates to a finite-size matrix equation. The main numerical problems in the solution of Eq. (5.49) are related to instabilities in the invertion of the matrix

$$\begin{bmatrix} \mathbf{P}^{j}\mathbf{E}^{j} & \mathbf{P}^{j} \\ \mathbf{P}^{j}\mathbf{\Gamma}^{j}\mathbf{E}^{j} & -\mathbf{P}^{j}\mathbf{\Gamma}^{j} \end{bmatrix}, \tag{5.50}$$

which can be avoided by recently introduced procedures [121].

In TM polarization one requires the continuity of the field and its normal derivative, divided by permittivity, at each layer boundary. This only results in minor modifications of the formalism presented above.

### 5.4.5 Comparison of modal methods

Having introduced three different modal methods, we feel the need to address their usefulness in different geometries, knowing that this can be a matter of opinion to some extent. The exact-eigenmode and Legendre-polynomial-expansion methods are most suitable for highly conducting lamellar gratings. Because of the assumption that the refractive index is constant in each block, they are not directly applicable to the analysis of continuous index-modulated gratings, even though one can approximate such structures by dividing the grating period into thin blocks with constant permittivity.

The problem with the exact mode representation occurs when the mode decays exponentially. Then the numerical rounding errors may grow exponentially and thus make solutions of modes badly inaccurate. This happens especially when the width of a single block is much larger than the wavelength. However, this can be at least partially avoided by dividing the blocks into smaller parts. Moreover, it is a rather demanding task to find the zeroes of Eq. (5.27), at least if some of the blocks have complex refractive indices  $\hat{n}_l$  (in that case one has to locate zeroes in the complex plane). Nevertheless, there exist methods to find the roots, see e.g., Refs. [107, 122]. For the computations, one can include only a finite number of modes. Then one must find those eigenvalues that have a modulus less than some constant  $\gamma_{\max}$ , which must be chosen in such a way that it is greater than  $k \max(|\hat{n}_l|)$ . Essentially, then one must find all eigenvalues inside a circle of this radius in the complex plane. One might first look for an approximative solution using either the Legendre polynomial expansion or the Fourier expansion method. Once such approximations have been found, one can use some optimization method to find the exact values.

With the Legendre polynomial method, the eigenvalues corresponding to the lowest-order modes converge rapidly, but the highest-order eigenvalues remain rather inaccurate: the number of sufficiently precise eigenvalues is typically only about one third of the total number of modes evaluated numerically. Therefore one must somehow choose the correct eigenvalues and neglect those that are inaccurate. Another problem is that the projections into the base  $\exp(iu_m x)$  contain Bessel functions, which usually cannot be evaluated as rapidly as the sinusoidal and cosinusoidal functions used in the exact mode methods.

The Fourier expansion method works best in the analysis of continuously index-modulated structures. With lamellar gratings, the permittivity distribution contains discontinuities, which makes the Fourier-series representation of the refractive-index distribution converge relatively slowly. Consequently the convergence of the lowest-order-eigenvalues is not as rapid as it is in the Legendre-polynomial expansion method. However, the eigenvalues associated with the highest modes are more accurate; all calculated eigenvalues and eigenvectors can be included in further computations. In spite of these considerations, the Fourier expansion method should be highly appreciated as it appears to be by far the easiest rigorous analysis method to implement numerically.

# 5.5 Rigorous coupled-wave analysis

Probably the most popular method to solve grating diffraction problems is the Rigorous Coupled-Wave Analysis (RCWA). The approach is slightly different from the modal

methods represented above, but it leads to the same numerical implementation as the Fourier-expansion method. The RCWA method was originally developed by Moharam and Gaylord [123] for planar volume gratings. One can find a good review of RCWA in Ref. [84]. The method has been generalized to surface relief gratings [124], 3D geometries [79,81], anisotropic gratings [125], etc.

First, let us assume TE polarization. The field outside the grating is given by Eqs. (5.9) and (5.6). Inside the modulated region, we start from the Helmholtz equation (2.20). Inside jth layer, located between  $z_j < z < z_{j+1}$ , the relative permittivity  $\hat{\epsilon}_r^j(x)$  is assumed z-invariant and pseudoperiodic. Instead of the separation of variables, we apply the ansatz [77]

$$E_y^j(x,z) = \sum_{l=-\infty}^{\infty} S_l^j(z) \exp(-iu_l x), \qquad (5.51)$$

where  $S_l^j(z)$  is the normalized amplitude of the lth space-harmonic field,  $u_l = u_0 + 2\pi m/d$ , and  $u_0 = k n_1 \sin \theta$  as before. The permittivity  $\hat{\epsilon}_r(x)$  is represented as a Fourier series

$$\hat{\epsilon}_r^j(x) = \sum_{p=-\infty}^{\infty} \epsilon_p^j \exp(i2\pi px/d). \tag{5.52}$$

Substitution Eqs. (5.51) and (5.52) into Eq. (2.20) yields the equation

$$\frac{\mathrm{d}^2 S^j(z)}{\mathrm{d}z^2} = \mathbf{A}^j S^j(z),\tag{5.53}$$

where the matrix  $A^{j}$  has the elements

$$A_{mp}^{j} = \alpha_m \delta_{mp} - k^2 \varepsilon_{m-p}^{j} \tag{5.54}$$

and the vector  $S^{j}(z)$  contains the amplitudes  $S_{m}^{j}(z)$ . The solution of Eq. (5.53) is

$$S_l^j(z) = \sum_{m=1}^{\infty} P_{lm}^j \left\{ a_m^j \exp\left[ -\gamma_m^j (z - z_j) \right] + b_m^j \exp\left[ \gamma_m^j (z - z_{j+1}) \right] \right\}, \tag{5.55}$$

where  $\gamma_m^j$  are the positive square-roots of the eigenvalues of the matrix  $\mathbf{A}^j$ , and  $P_{lm}^j$  are the elements of the corresponding eigenvectors. The coefficients  $a_m^j$  and  $b_m^j$  are solved using the boundary conditions. Thus the field inside the grating is similar to the field representation in the Fourier-expansion eigenmode method. The solution of the boundary conditions is equivalent to that already presented in Section 5.4.4.

In TM polarization, a similar procedure leads to the solution

$$H_y^j(x,z) = \sum_{l=-\infty}^{\infty} U_l^j(z) \exp(iu_l x), \qquad (5.56)$$

where

$$U_l^j(z) = \sum_{m=1}^{\infty} P_{lm}^j \left\{ a_m^j \exp\left[-\gamma_m(z - z_j)\right] + b_m^j \exp\left[\gamma_m(z - z_{j+1})\right] \right\}, \tag{5.57}$$

 $P_{lm}^{j}$  and  $\gamma_{m}^{j}$  are now the eigenvectors and the eigenvalues of the matrix

$$\mathbf{B}^{j} = (\mathbf{C}^{j})^{-1} \left[ \mathbf{K} (\mathbf{E}^{j})^{-1} \mathbf{K} - \mathbf{I} \right], \tag{5.58}$$

 $E^j_{mp}=\varepsilon_{m-p},~C^j_{mp}=\xi^j_{m-p}$  and  $\xi^j_m$  are the Fourier-coefficient of the function  $1/\hat{\epsilon}^j_r(x),$   $K_{mp}=u_m\delta_{mp},$  and I is the identity matrix [119,120].

Although RCWA is completely analogous to the Fourier-expansion modal method, one may find the former somewhat more intuitive, in particular when deriving various approximative methods for volume gratings [84]. In coupled-wave theory, the coupling between the diffraction orders appears to be due to the space-harmonics of the permittivity profile while in the modal method this coupling seems occur between the modes. However, this difference only takes place because of the way of choosing the ansatz.

### 5.6 Space-domain methods

The space-domain methods can be divided into two different categories: differential and integral methods [2]. In differential methods, the diffracted fields are obtained by integrating numerically the field equations over the grating volume. An example of differential methods [78] is the finite element method (FEM) [126,127]. The main problem with FEM is that one is typically lead to handle very large matrices. This is because the distance between neighboring grid points must be of the order of  $\lambda/10$  or less.

In integral methods [101,128], the field is represented as an integral of some unknown function over a surface that separates two homogeneous materials. The diffracted field is then obtained by solving an integral equation formed by using the Helmholtz equation and boundary conditions. Numerical implementation of integral methods can be rather difficult, but when properly implemented these methods can be very stable. The weakness of integral methods is that they can not be applied to index-modulated gratings.

It is also possible to use a volume integration method [129,130], in which the field is integrated over the grating volume. Using the Helmholtz equation and the appropriate boundary conditions one obtains an integral equation for the diffracted fields which is solved numerically in a suitable grid that divides the volume into cells with an approximately constant field.

# Chapter 6

# Diffraction analysis: continuous signals

#### 6.1 Introduction

In Chapter 5 we assumed that the diffractive element and the incident electromagnetic field are both pseudoperiodic, i.e., infinite. As a consequence, the outgoing fields are discrete superpositions of plane waves that propagate in different directions. Thus the far-field pattern is a set of discrete points with some relative intensities, given by the diffraction efficiencies of the diffraction orders. However, this situation is rather unphysical, since it implies, e.g., that the energy of the incident field is infinite.

If continuous far-field signals are required, one is forced to use either non-periodic diffractive elements or a finite illumination wave. In this Chapter we will consider three different kinds of systems. Firstly, we discuss finite diffractive elements with perfectly conducting aperture boundaries; the incident field may be either finite or infinite. The reason for the introduction of perfectly conducting boundaries is that then the spectrum of the mode eigenvalues necessarily becomes discrete. Secondly, we illuminate an infinite grating with a finite field, e.g., a Gaussian beam with its tails cut off. Since the illumination wave is finite, we can use methods developed for infinite periodic elements in the calculations. Finally, It is also possible to analyze diffraction of spatially partially coherent incident waves using the coherent-mode decomposition of the incident field (Section 4.5).

Here the analysis is performed by modal methods. It is also possible to use different space-domain methods in the analysis of non-periodic systems, including FEM [126] and the volume integral method [129].

# 6.2 Eigenmode method for modulated apertures

We will examine diffraction from an aperture, in which the refractive index distribution is piecewise constant (see Fig. 6.1). This is an extension of the analysis of unmodulated apertures [131] and grooves in a perfectly conducting surface [132]. The field inside the element can be solved using the exact eigenmode method introduced Section 5.4.1. We assume a single-layer lamellar structure inside the aperture, but the method can be generalized to multilevel profiles.

#### 6.2.1 Exact eigenmodes

We suppose that the (possible complex-valued) refractive-index distribution is of the form

$$\hat{n}(x) = \hat{n}_l \text{ when } x_l < x < x_{l+1},$$
(6.1)

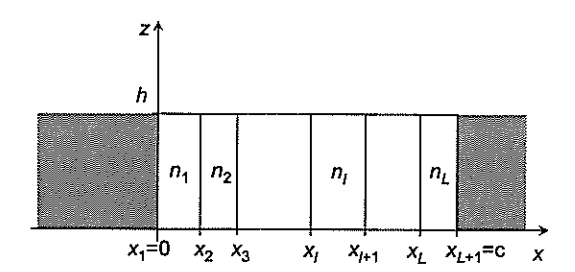


Fig. 6.1: Geometry of an index-modulated aperture in a perfectly conducting screen.

where  $x_1 = 0$  and  $x_{L+1} = c$ . As in Section 5.4.1 one can express the field in *l*th block,  $x_l < x < x_{l+1}$ , as [133]

$$U_y^l(x,z) = X_l(x) \left\{ a \exp(i\gamma z) + b \exp\left[-i\gamma(z-h)\right] \right\}, \tag{6.2}$$

where

$$X_l(x) = A_l \exp\left[i\beta_l(x - x_l)\right] + B_l \exp\left[-i\beta_l(x - x_l)\right]$$
(6.3)

and  $\beta_l$  is given by Eq. (5.23).

At each intermediate boundary  $x_2, \ldots, x_L$ , the field and either its derivative (in TE polarization) or the derivative divided by  $\hat{n}_l^2$  (in TM polarization) must be continuous. Outside the aperture, and therefore also at the aperture boundaries x=0 and x=c, either the field (in TE polarization) or its derivative (in TM polarization) must vanish. Let us consider only TM-polarization and introduce a new function

$$\bar{X}_l(x) = \frac{1}{\hat{n}_l} \frac{\mathrm{d}}{\mathrm{d}x} X_l(x). \tag{6.4}$$

In region  $x_l < x < x_{l+1}$ , one can solve the amplitudes  $A_l$  and  $B_l$  in terms of  $X_l(x_l)$  and  $\bar{X}_l(x_l)$ . Thus one obtains

$$\begin{bmatrix} X_l(x_{l+1}) \\ \bar{X}_l(x_{l+1}) \end{bmatrix} = \mathbf{M}_l(\gamma) \begin{bmatrix} X_l(x_l) \\ \bar{X}_l(x_l) \end{bmatrix}, \tag{6.5}$$

where

$$\mathbf{M}_{l}(\gamma) = \begin{bmatrix} \cos \left[\beta_{l}(x_{l+1} - x_{l})\right] & (\hat{n}_{l}^{2}/\beta_{l}) \sin \left[\beta_{l}(x_{l+1} - x_{l})\right] \\ -(\beta_{l}/\hat{n}_{l}^{2}) \sin \left[\beta_{l}(x_{l+1} - x_{l})\right] & \cos \left[\beta_{l}(x_{l+1} - x_{l})\right] \end{bmatrix}.$$
(6.6)

One can now recursively connect the values of X(x) and  $\bar{X}(x)$  at x=0 to those at x=c using the fact that these quantities are both continuous across the boundaries  $x=x_l$ . We obtain

$$\begin{bmatrix} X_L(c) \\ \bar{X}_L(c) \end{bmatrix} = \mathbf{M}(\gamma) \begin{bmatrix} X_1(0) \\ \bar{X}_1(0) \end{bmatrix}, \tag{6.7}$$

where

$$\mathbf{M}(\gamma) = \prod_{l=1}^{L} M_{L-l+1}(\gamma) = \begin{bmatrix} A(\gamma) & B(\gamma) \\ C(\gamma) & D(\gamma) \end{bmatrix}.$$
 (6.8)

Since  $E_z(x,z)$  must vanish at the perfectly conducting aperture boundaries,  $\bar{X}_1(0) = \bar{X}_L(c) = 0$ , and thus

$$C(\gamma) = 0. ag{6.9}$$

This equation is transcendental and the solutions may be hard to find. Once the eigenvalues  $\gamma_m$  of the modes have been found, one can recursively solve the values  $X_l(x_l)$  and  $\bar{X}_l(x_l)$  and then the modal function  $X_m(x)$ .

In TE polarization, all explicit  $\hat{n}_l$ :s must be removed from the matrices  $M_l(\gamma)$ , and the field  $E_y$  must vanish at the boundaries, which leads to an eigenvalue equation  $B(\gamma) = 0$ .

### 6.2.2 Polynomial expansion of the modes

In the numerical solution of Eq. (6.9) one may miss some of the eigenvalues  $\gamma_m$  unless the search is performed carefully. However, it is possible to use the Legendre polynomial expansion of the modes as in Section 5.4.2. With this method, all the lowest-order eigenvalues will always be found. Since the eigenvalues found by the polynomial expansion method are not exact, one can refine them with the aid of Eq. (6.9).

The Legendre polynomial expansion of the modes in the lth block is expressed in Eq. (5.28). Similarly to Section 5.4.2, one can now eliminate coefficients  $p_{M_l}^l$  and  $p_{M_l-1}^l$ . But instead of the pseudoperiodicity, we require that either (in TE polarization)

$$\sum_{m=0}^{M_1} p_m^1 (-1)^m = \sum_{m=0}^{M_L} p_m^L = 0$$
 (6.10)

or (in TM polarization)

$$\frac{1}{\hat{n}_1 d_1} \sum_{m=0}^{M_1} p_m^1 (-1)^{m+1} m(m+1) = \frac{1}{\hat{n}_L d_L} \sum_{m=0}^{M_L} p_m^L m(m+1) = 0.$$
 (6.11)

With these modifications, one can form a matrix equation almost similar to that in Section 5.4.2, which can be solved for the eigenvalues  $\gamma_m$  and corresponding polynomial coefficients  $p_m^l$ . Once the eigenvalues and the polynomial coefficients are found, one is able to construct the modes.

### 6.2.3 Boundary conditions

Having solved the eigenmodes of the modulated aperture, we use the boundary conditions at z = 0 and z = h to determine the reflected and the transmitted field. Let us consider TE polarization. One writes the incident, the reflected and the transmitted fields using their angular spectrum representations, i.e.,

$$E_y^{\text{in}}(x,z) = \int_{-n_1/\lambda}^{n_1/\lambda} A(\alpha) \exp\left\{i2\pi \left[\alpha x + r(\alpha)z\right]\right\} d\alpha, \tag{6.12}$$

$$E_y^r(x,z) = \int_{-\infty}^{\infty} R(\alpha) \exp\left\{i2\pi \left[\alpha x - r(\alpha)z\right]\right\} d\alpha, \tag{6.13}$$

$$E_y^{t}(x,z) = \int_{-\infty}^{\infty} T(\alpha) \exp\left\{i2\pi \left[\alpha x + t(\alpha)(z-h)\right]\right\} d\alpha, \tag{6.14}$$

where

$$r(\alpha) = \begin{cases} \sqrt{(n_1/\lambda)^2 - \alpha^2} & \text{if } |\alpha| \le n_1/\lambda \\ i\sqrt{\alpha^2 - (n_1/\lambda)^2} & \text{otherwise} \end{cases}$$
 (6.15)

and

$$t(\alpha) = \begin{cases} \sqrt{(n_3/\lambda)^2 - \alpha^2} & \text{if } |\alpha| \le n_3/\lambda \\ i\sqrt{\alpha^2 - (n_3/\lambda)^2} & \text{otherwise.} \end{cases}$$
 (6.16)

We also assumed that the incident field arrives from (minus) infinity, and therefore possesses no evanescent components. The integration limits  $-n_1/\lambda$  and  $n_1/\lambda$  in Eq. (6.12) can be replaced by  $-\infty$  and  $\infty$  by defining the angular spectrum of the incident field  $A(\alpha)$  to be zero outside the interval  $[-n_1/\lambda, n_1/\lambda]$ . The angular spectra  $R(\alpha)$  and  $T(\alpha)$  are the two unknown functions to be solved.

Inside the aperture, the field is represented by Eq. (6.2). The boundary conditions require that both  $E_y$  and  $\partial E_y/\partial z$  are continuous inside the aperture and that  $E_y$  vanishes outside the aperture. Thus we obtain a set equations [133]

$$\int_{-\infty}^{\infty} [A(\alpha) + R(\alpha)] \exp(i2\pi\alpha x) d\alpha = \sum_{m=1}^{\infty} X_m(x) \left[ a_m + b_m \exp(i\gamma_m h) \right], \quad (6.17)$$

$$2\pi \int_{-\infty}^{\infty} r(\alpha) \left[ A(\alpha) - R(\alpha) \right] \exp(i2\pi\alpha x) d\alpha = \sum_{m=1}^{\infty} X_m(x) \gamma_m \left[ a_m - b_m \exp(i\gamma_m h) \right], \quad (6.18)$$

$$\int_{-\infty}^{\infty} T(\alpha) \exp(i2\pi\alpha x) d\alpha = \sum_{m=1}^{\infty} X_m(x) \left[ a_m \exp(i\gamma_m h) + b_m \right], \quad (6.19)$$

$$2\pi \int_{-\infty}^{\infty} t(\alpha) T(\alpha) \exp(i2\pi\alpha x) d\alpha = \sum_{m=1}^{\infty} X_m(x) \gamma_m \left[ a_m \exp(i\gamma_m h) - b_m \right], \quad (6.20)$$

which can be solved in at least two different ways. Firstly, one can discretize the angular spectra, i.e., let  $A(\alpha) \to A_l = A(\alpha_l)$  and so on. If the difference between the points  $\alpha_l$  and  $\alpha_{l+1}$  is constant, the element acts like a periodic array of index-modulated apertures separated by perfectly conducting screen sections. The period increases when the sampling distance is reduced. The solution of this system is thus reduced to the analysis of grating diffraction. If the separation between the points is not constant, the physical interpretation is less clear.

The second method to solve Eqs. (6.17)-(6.20) proceeds as follows. We multiply Eqs. (6.17) and (6.19) by  $\exp(-i2\pi\alpha x)$ , and then integrate x from  $-\infty$  to  $\infty$  to obtain

$$A(\alpha) + R(\alpha) = \sum_{m=1}^{\infty} I_m(\alpha) \left[ a_m + b_m \exp(i\beta_m h) \right], \qquad (6.21)$$

$$T(\alpha) = \sum_{m=1}^{\infty} I_m(\alpha) \left[ a_m \exp(i\beta_m h) + b_m \right], \qquad (6.22)$$

where (note that the mode vanishes outside the aperture)

$$I_m(\alpha) = \int_{-\infty}^{\infty} X_m(x) \exp(-i2\pi\alpha x) dx.$$
 (6.23)

One can now substitute the functions  $R(\alpha)$  and  $T(\alpha)$  into Eqs (6.18) and (6.20), multiply them by  $X_p^*(x)$  and integrate x from 0 to c. This yields a doubly infinite system of linear equations:

$$\sum_{m=1}^{\infty} (K_{pm} + \gamma_m C_m \delta_{pm}) a_m + \sum_{m=1}^{\infty} (K_{pm} - \gamma_m C_m \delta_{pm}) \exp(i\gamma_m h) b_m = 4\pi \int_{-\infty}^{\infty} I_p^*(\alpha) A(\alpha) d\alpha,$$
(6.24)

$$\sum_{m=1}^{\infty} (L_{pm} - \gamma_m C_m \delta_{pm}) \exp(i\gamma_m h) a_m + \sum_{m=1}^{\infty} (L_{pm} + \gamma_m C_m \delta_{pm}) b_m = 0,$$
 (6.25)

where

$$K_{pm} = 2\pi \int_{-\infty}^{\infty} r(\alpha) I_p^*(\alpha) I_m(\alpha) d\alpha, \qquad (6.26)$$

$$L_{pm} = 2\pi \int_{-\infty}^{\infty} t(\alpha) I_p^*(\alpha) I_m(\alpha) d\alpha, \qquad (6.27)$$

and

$$C_m = \int_0^c |X_m(x)|^2 dx.$$
 (6.28)

Once the amplitudes  $a_m$  and  $b_m$  have been solved, one can calculate the angular spectra of the reflected and transmitted fields,  $R(\alpha)$  and  $T(\alpha)$ , from Eqs. (6.21) and (6.22). In TM polarization, one must slightly modify the preceding derivation.

The most serious numerical problem in this method is the calculation of the matrix elements  $K_{pm}$  and  $L_{pm}$ . In general, these integrals must be evaluated numerically, which is rather time consuming.

The most convenient quantity for the description of the energy of the transmitted and the refracted field is the radiant intensity. Since the field is assumed to be completely coherent, the radiant intensities of the diffracted fields are

$$J^{t}(\theta) = \left(\frac{n_3 \cos \theta}{\lambda}\right)^2 \left| T\left(\frac{n_3 \sin \theta}{\lambda}\right) \right|^2 \tag{6.29}$$

$$J^{r}(\theta) = \left(\frac{n_1 \cos \theta}{\lambda}\right)^2 \left| R\left(\frac{n_1 \sin \theta}{\lambda}\right) \right|^2, \tag{6.30}$$

where  $\theta$  is the angle between the z-axis and the direction of the observation point. For comparison, the radiant intensity of the incident field without the aperture is

$$J^{\text{in}}(\theta) = \left(\frac{n_1 \cos \theta}{\lambda}\right)^2 \left| A\left(\frac{n_1 \sin \theta}{\lambda}\right) \right|^2. \tag{6.31}$$

### 6.3 Periodic elements with finite incident beam

In Chapter 5 we solved the grating diffraction problem assuming that the incident beam is either a plane wave or a superposition of plane waves that propagate in the directions exactly opposite to reflected diffraction orders. Here we generalize the discussion to the case of an incident beam with a continuous angular spectrum.

We consider an arbitrary grating of period d and write the incident field as

$$E_y^{\text{in}}(x,z) = \int_0^{2\pi/\lambda} \sum_{m=-M}^M A_m(u_0) \exp\{i[u_m(u_0)x + r_m(u_0)z]\} du_0, \tag{6.32}$$

where  $A_m(u_0) = A(u_m/2\pi) = A(u_0/2\pi + m/d)$ ,  $u_0 = kn_1\sin\theta$ , and the summation contains only the homogeneous waves. In Eq. (6.32) we scan  $u_0$  over the angular range between two adjacent diffraction orders, solve the diffraction problem for each incident angle  $\theta$ , and superimpose the results coherently. The required density of sampling points depends on the complexity of  $A(\alpha)$ . In some cases, particularly when  $d \gg \lambda$ , as few as  $\sim 10$  sampling points may be adequate for accurate results. This means that one needs to solve the grating diffraction problem only for those  $\sim 10$  incident angles.

A non-periodic diffractive structure illuminated by a finite beam can be analyzed accurately with the aid of the above-described method. One replaces the element by a grating, which repeats itself only outside the region in which the incident field has a non-negligible amplitude. The choice of the grating period d depends on the diffractive structure and it must be tested by observing the convergence of the outgoing fields when d is increased. The advantage of the present approach over the exact treatment of non-periodic structures is computational efficiency. The numerical integrations required in the analysis of non-periodic elements are typically more time-consuming than the angular scan in grating theory.

### 6.4 Diffraction of spatially partially coherent fields

In both grating-diffraction analysis and the analysis of non-periodic elements we have assumed that the incident field is spatially completely coherent.

If the illumination is spatially partially coherent, the diffraction problem can be solved elegantly by application of the coherent mode decomposition of the incident field [134], introduced in Section 4.5. The angular correlation function of the incident field can then be written as

$$A^{\text{in}}(\alpha_1, \alpha_2) = \sum_{n=0}^{\infty} c_n A_n^*(\alpha_1) A_n(\alpha_2), \tag{6.33}$$

where the coherent modes  $A_n(\alpha)$  and the weights  $c_n$  can be found by solving Eq. (4.27). Since the functions  $A_n(\alpha)$  are spatially fully coherent, one can now solve the diffraction problem for each of them separately, with methods introduced above. The angular spectra of the forward- and backward-diffracted fields corresponding to the mode  $A_n(\alpha)$  are denoted by  $T_n(\alpha)$  and  $R_n(\alpha)$ , respectively. The angular correlation functions of the partially coherent forward- and backward-diffracted fields are now

$$A^{t}(\alpha_{1}, \alpha_{2}) = \sum_{n=0}^{\infty} c_{n} T_{n}^{*}(\alpha_{1}) T_{n}(\alpha_{2}),$$

$$A^{t}(\alpha_{1}, \alpha_{2}) = \sum_{n=0}^{\infty} c_{n} R_{n}^{*}(\alpha_{1}) R_{n}(\alpha_{2}).$$

$$(6.34)$$

The energy carried into the far-zone by the diffracted fields is described by the radiant intensity, given by Eq. (4.24).

# Chapter 7

# Approximate methods

The main problem with the rigorous methods presented in Chapters 5 and 6 is that they usually require heavy computations: if either the grating period or the aperture of a non-periodic element is much larger than the wavelength, one needs to solve large eigenvalue and boundary problems. Even more serious problems are encountered in three-dimensional geometries. Whenever possible, one therefore prefers approximate methods over rigorous ones. Here we consider two approximate methods: thin element approximation and first-order two-wave coupled-wave theory. Several other methods such as Raman-Nath theory [135–138] and effective medium theory [62,139,140], exist.

### 7.1 Thin element approximation

Let us suppose that the refractive index distribution of the element is

$$\hat{n}(x,y,z) = n(x,y,z) + i\kappa(x,y,z), \tag{7.1}$$

where n is the real refractive index and  $\kappa$  describes the absorption of the material. Then, calculating the optical path [3], one obtains a relationship between the incident field  $U^{\text{in}}(x,y,0)$  and the transmitted field  $U^{\text{t}}(x,y,h)$  in the form

$$U^{t}(x, y, h) = t(x, y)U^{in}(x, y, 0),$$
 (7.2)

where

$$t(x,y) = A(x,y) \exp\left[i\Phi(x,y)\right] \tag{7.3}$$

is known as the complex-amplitude transmission function. In Eq. (7.3)

$$A(x,y) = \exp\left[-k \int_0^h \kappa(x,y,z) dz\right]$$
 (7.4)

and

$$\Phi(x,y) = k \int_0^h n(x,y,z) dz$$
 (7.5)

are the amplitude and phase transmittance functions, respectively. If  $\kappa=0$ , the material is dielectric and the element modulates only the phase of the incident field. It is appropriate to note that although the thin-element approximation is rather good when the smallest feature size of the element is at least an order of a magnitude greater than the wavelength, it can fail dramatically when the feature size is reduced: see, e.g., Refs. [2,141–144].

Let us assume that the element is a grating with periods  $d_x$  and  $d_y$  in x and y directions, respectively, and that it is illuminated by a unit-amplitude plane wave  $U^{\text{in}}(x,y,z)=1$ . Then the amplitudes of the diffracted orders are

$$T_{mn} = \frac{1}{d_x d_y} \int_0^{d_x} \int_0^{d_y} t(x, y) \exp\left[-i2\pi (mx/d_x + ny/d_y)\right] dx dy.$$
 (7.6)

In the case of non-periodic elements, the angular spectrum is obtained by calculating the Fourier transform of the diffracted field at z = h:

$$T(\alpha, \beta) = \iint_{A} t(x, y) U^{\text{in}}(x, y, 0) \exp\left[-i2\pi(\alpha x + \beta y)\right] dxdy, \tag{7.7}$$

where A is the aperture of the element. Since the diffracted field is paraxial, its radiant intensity is proportional to  $|T(\alpha,\beta)|^2$ .

The complex-amplitude transmittance method can also be used when the incident field is spatially partially coherent, with cross-spectral density function  $W^{\text{in}}(x_1, y_1, z_1, x_2, y_2, z_2)$ , where we have omitted the frequency dependence. Then the cross-spectral density function of the transmitted field at the plane z = h is

$$W^{t}(x_1, y_1, h, x_2, y_2, h) = t^{*}(x_1, y_1)t(x_2, y_2)W^{in}(x_1, y_1, 0, x_2, y_2, 0).$$
(7.8)

#### 7.2First-order two-wave coupled-wave theory

Consider a cosinusoidal permittivity distribution

$$\hat{\epsilon}_r(x,z) = \epsilon_r + \Delta \epsilon_r \cos(2\pi x/d). \tag{7.9}$$

Neglecting the second derivatives in RCWA (Section 5.5) and assuming that only two propagating orders, m=0 and m=-1, exist, one can obtain analytic expressions for their space-harmonic amplitudes [84, 145]:

$$S_{-1}(z) = i \exp(-igz/2s) \frac{\sin\left[\sqrt{g^2 + 4f^2(z/2s)}\right]}{\sqrt{(1 + (g/2f)^2}}$$
(7.10)

and

$$S_0(z) = \exp(-igz/2s) \left\{ \cos\left[\sqrt{g^2 + 4f^2}(z/2s)\right] + \frac{i\sin\left[\sqrt{g^2 + 4f^2}(z/2s)\right]}{\sqrt{1 + (2f/g)^2}} \right\}.$$
 (7.11)

Here

$$g = (2\pi m/d)(u_0 + \pi m/d), \tag{7.12}$$

$$g = (2\pi m/d)(u_0 + \pi m/d), \qquad (7.12)$$
  

$$f = (\pi/\lambda)^2 \Delta \epsilon_r, \qquad (7.13)$$
  

$$s = k\sqrt{\epsilon_r} \cos \theta', \qquad (7.14)$$

$$s = k\sqrt{\epsilon_r}\cos\theta',\tag{7.14}$$

and  $\theta' = \arcsin \left[ (n_1/\sqrt{\epsilon_r}) \sin \theta \right]$  is the refraction angle of the incident wave inside the grating when  $\Delta \epsilon_r = 0$ .

If the incident beam arrives at the Bragg angle

$$\theta_B = \arcsin(\lambda/2n_1 d),\tag{7.15}$$

and if  $n_3 = n_1 = \sqrt{\epsilon_r}$ , one obtains

$$\eta_{-1} = |S_{-1}(h)|^2 = \sin^2\left(\frac{\pi\Delta\epsilon_r h}{2\sqrt{\epsilon_r \lambda}\cos\theta}\right).$$
(7.16)

Thus it is possible to archive 100% diffraction efficiency,  $\eta_{-1} = 100\%$ , if the grating parameters satisfies the condition

$$\frac{\pi \Delta \epsilon_r h}{2\sqrt{\epsilon_r} \lambda \cos \theta} = \frac{\pi}{2} + n\pi. \tag{7.17}$$

It is convenient to characterize the validity range of the first-order two-wave coupled-wave approximation using the Klein-Cook parameter [146]  $Q=4\pi^2h/kd^2$  and the Raman-Nath parameter [135]  $v=kh\Delta\epsilon_r$ . The two-wave approximation is rather accurate if  $Q\gg 1$  and  $Q/\nu\gg 1$  [84,99,100,147].

# Chapter 8

# Design of diffractive elements

### 8.1 Design freedoms

The basic design geometry in diffractive optics is shown in Fig. 8.1. An incident electromagnetic field  $\{E^{\rm in}(r,t),H^{\rm in}(r,t)\}$  arrives from  $z=-\infty$ . With the aid of an element at z=0, one wants to generate some signal function s[E(r,t),H(r,t)] inside the signal window  $\mathcal{W}$ . There may exist an entire family of fields  $\{E^{\rm s}(r,t),H^{\rm s}(r,t)\}$ , which all generate the required signal s. On the other hand, the design task may be impossible because the field must satisfy Maxwell's equations (2.3)–(2.6). Also fabrication constraints may limit the set of possible optical elements. Thus, instead of the exact signal field  $\{E^{\rm s}(r,t),H^{\rm s}(r,t)\}$ , one typically obtains a diffracted field  $\{E^{\rm d}(r,t),H^{\rm d}(r,t)\}$ , which is approximately equal to the signal in  $\mathcal{W}$ . Therefore one also has to investigate the signal error

$$s[\mathbf{E}^{e}(\mathbf{r},t),\mathbf{H}^{e}(\mathbf{r},t)] = s[\mathbf{E}^{s}(\mathbf{r},t),\mathbf{H}^{s}(\mathbf{r},t)] - s[\mathbf{E}^{d}(\mathbf{r},t),\mathbf{H}^{d}(\mathbf{r},t)]. \tag{8.1}$$

Fortunately, in most cases only some properties of the signal field need to be fixed. For example, one may define the signal as a distribution of the electric energy density, leaving other properties of the field in  $\mathcal W$  arbitrary. Finally, the entire field outside the signal window can be arbitrary (this is known as the amplitude freedom). In general, all unfixed properties of the field are called design freedoms [148]. These freedoms can be used, e.g., to maximize the diffraction efficiency of the element.

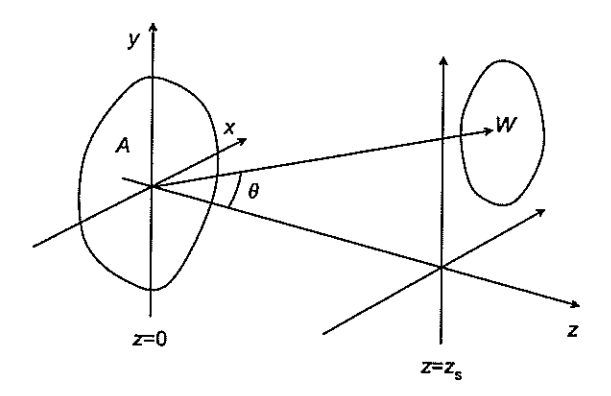


Fig. 8.1: Geometry of design problem.

### 8.2 Upper bound of the diffraction efficiency

Consider a thin element (Section 7.1) between the planes z=0 and z=h, illuminated by a scalar field  $U^{\rm in}(x,y,z)$ . The signal is the intensity distribution of the field inside  $\mathcal{W}$ , located at  $z=z_s$ , and the signal field is denoted by  $U^s(x,y,z)$ . We assume  $U^s(x,y,z_s)=0$  outside  $\mathcal{W}$  and  $U^s(x,y,z_s)=0$  outside  $\mathcal{A}$ . Then the efficiency of an element that modulates the complex amplitude of the incident field in exactly the required fashion, is

$$\eta = \frac{1}{\alpha^2} \frac{\iint_{\mathcal{A}} |U^{\text{s}}(x, y, h)|^2 \mathrm{d}x \mathrm{d}y}{\iint_{\mathcal{A}} |U^{\text{in}}(x, y, 0)|^2 \mathrm{d}x \mathrm{d}y},\tag{8.2}$$

where

$$\alpha = \max_{(x,y)\in\mathcal{A}} \frac{|U^{s}(x,y,h)|}{|U^{in}(x,y,0)|}.$$
(8.3)

This result is based on the complex-amplitude transmittance method.

Next we assume a phase-only Fourier-element with amplitude freedom. Then the upper bound of the efficiency is [149,150]

$$\eta = \frac{\left[\iint_{-\infty}^{\infty} |U^{\text{in}}(x, y, 0)| |U_0^s(x, y, h)| \cos \left[\Delta \phi(x, y)\right] dx dy\right]^2}{\iint_{-\infty}^{\infty} |U^{\text{in}}(x, y, 0)|^2 dx dy \iint_{-\infty}^{\infty} |U_0^s(x, y, h)|^2 dx dy},$$
(8.4)

where

$$\Delta \phi(x, y) = \arg \left[ U^{s}(x, y, h) \right] - \arg \left[ U_{0}^{s}(x, y, h) \right]. \tag{8.5}$$

is the phase difference between the signal field without noise,  $U_0^s(x, y, h)$ , and the signal field with noise allowed,  $U^s(x, y, h)$ .

Using Eqs. (8.2) and (8.4), one can optimize the phase of the signal field to obtain a maximum diffraction efficiency [151, 152]. Remarkably, it is not necessary to actually design any diffractive element for this purpose. Once the phase of the signal field has been determined, one can calculate the complex-amplitude transmittance function of the element using Eq. (7.2).

## 8.3 Design methods

In ray optics, one can design diffractive elements to deflect rays into desired directions with the aid of Eqs. (5.4) and (5.5), which determine the local period of the element [153]. Thus one can design, e.g., optical map transform elements [154-157].

In the paraxial domain, the incident field is described by a single scalar function and the thin element approximation is employed. Three different types of methods exist: direct, indirect and iterative. In direct design, one optimizes the structure of the element to generate a desired signal using, e.g., direct binary search [158] with simulated annealing [159]. It is also possible to optimize analytically the phase functions of certain diffractive elements using variational methods [160, 161].

In indirect design, one propagates the signal field to the element plane. Then the complex-amplitude transmittance function of the element is obtained using Eq. (7.2). If

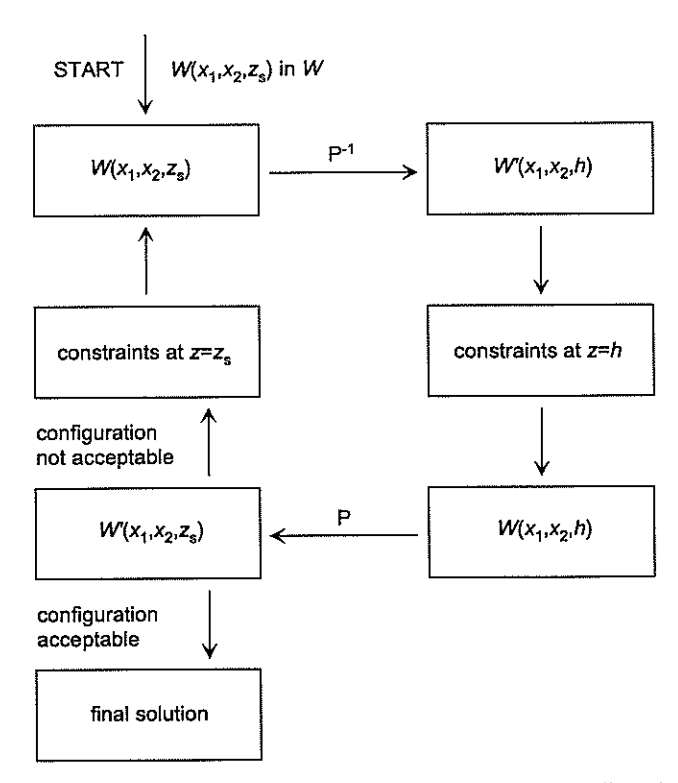


Fig. 8.2: Iterative Fourier-Transform algorithm for spatially partially coherent light.

the complex-amplitude transmittance function is unrealizable, one can use the design freedoms to optimize the signal field.

In iterative methods, the satisfaction of certain constraints is demanded both at the signal plane and at the element plane. Several iterative methods, such as Iterative Fourier transform algorithm (IFTA) [162–167], Yang-Gu algorithm [168, 169], and Fresnel pingpong algorithm [170], exist. If rigorous theory is used, only direct design methods are applicable because the inverse diffraction problem can not be solved [141, 171].

## 8.4 IFTA for spatially partially coherent light

We proceed to extend IFTA to spatially partially coherent scalar fields. The algorithm is introduced in Fig. 8.2. The propagation of the cross-spectral density function from the element plane z = h to the signal plane  $z = z_s$  is denoted by the operator  $\mathcal{P}$  and governed by Eq. (4.20).

At the first step, one constructs a cross-spectral density function that satisfies the signal constraints at  $z=z_s$ . This function is propagated to the plane z=h using the operator  $\mathcal{P}^{-1}$ . Then the element-plane constraints are applied. Using operator  $\mathcal{P}$ , the cross-spectral density function is propagated back to the signal plane  $z=z_s$ . If the

signal is obtained with acceptable accuracy, the algorithm is stopped. Otherwise, the cross-spectral density function is deformed as little as possible to fulfill the signal plane constraints. This procedure is continued until the required signal is obtained or until the iteration stagnates.

Since  $\mathcal{P}$  and  $\mathcal{P}^{-1}$  can be evaluated by applying the FFT algorithm (Section 3.1), this method is called the iterative Fourier transform algorithm. If a 3D geometry is concerned, 4D FFT is required in the partially coherent case. However, if the fields are assumed completely coherent, the algorithm separates into two identical completely coherent IFTA [165–167]. The quantization of the element can be carried out iteratively as in completely coherent IFTA [172].

Let us consider reshaping of a uniform-intensity Schell-model field

$$W^{\text{in}}(x_1, x_2, 0) = \exp\left[-(x_1 - x_2)^2 / 2\sigma_g^2\right]$$
 (8.6)

into a far-field flat-top distribution

$$A^{s}(\alpha, \alpha, h) = A_0 = 1/(\alpha_{\text{max}} - \alpha_{\text{min}}), \tag{8.7}$$

when  $\alpha_{\min} \leq \alpha \leq \alpha_{\max}$ . The following design freedoms are available:

- 1. The angular degree of coherence inside the signal window may be arbitrary (coherence freedom).
- 2. The entire angular correlation function outside the signal window may be arbitrary (amplitude freedom).
- 3. The angular self-correlation function  $A(\alpha, \alpha)$  needs to be only proportional to  $A_0$  (scale freedom).

The element is inside an opaque aperture of width a. The diffractive element is a phase-only element with a continuous phase profile.

We look for the cross-spectral density function  $W^s(x_1, x_2, h)$ . The iteration is started by taking a random initial distribution of the complex degree of coherence inside the signal window,  $\nu^s(\alpha_1, \alpha_2)$ , and forming the signal angular correlation function

$$A^{s}(\alpha_1, \alpha_2) = \sqrt{A^{s}(\alpha_1, \alpha_1)A^{s}(\alpha_2, \alpha_2)}\nu^{s}(\alpha_1, \alpha_2). \tag{8.8}$$

The complex-amplitude transmittance function of the element in each iteration  $k \leq K$ , where K is the total number of iterations, is chosen to be  $t_k(x) = \exp[i\phi_k(x)] = T_k(x,0)$ , where

$$T_k(x_1, x_2) = T'_k(x_1, x_2)/|T'_k(x_1, x_2)|,$$
 (8.9)

and

$$T'_k(x_1, x_2) = W^{s}(x_1, x_2, h) / W^{in}(x_1, x_2, 0).$$
(8.10)

The first  $K_1$  iteration are performed with only coherence freedom. This was found to improve the final efficiency. Next  $K_2$  iterations are done by allowing also the amplitude freedom. Finally,  $K_3$  iterations with all design freedoms are performed.

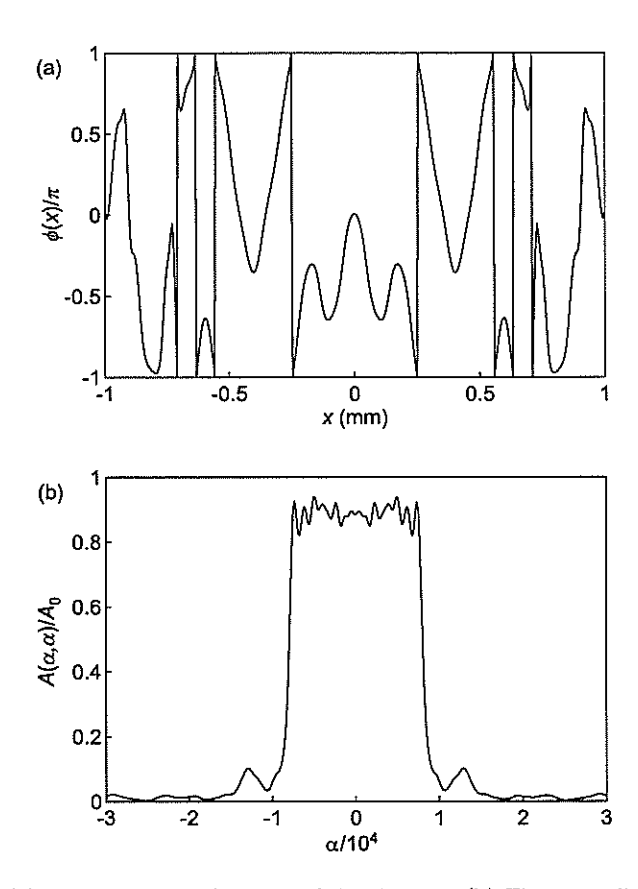


Fig. 8.3: (a) Required phase function of the element. (b) The normalized angular self-correlation function  $A(\alpha, \alpha)/A_0$ .

Figure 8.3a illustrates the phase function obtained when a=2 mm,  $\sigma_g=0.4$  mm,  $\alpha_{\rm max}=-\alpha_{\rm min}=7875,~\lambda=514$  nm,  $K_1=10,~K_2=10,~{\rm and}~K_3=5.$  Figure 8.3b shows the corresponding angular self-correlation function  $A(\alpha,\alpha)/A_0$  and Fig. 8.4 shows the modulus of the angular correlation function inside the signal window.

Although only 25 iterations are needed, the design process is rather slow compared to the design of a corresponding element for coherent light. This is because here one must Fourier transform 2D matrices instead of 1D arrays. The uniformity error of the preceding flat-top distribution is as large as ~ 10% even though a continuous phase-profile was allowed. It may be possible to obtain better results by choosing the initial angular correlation function properly, so that the signal wave would be bandlimitted within the aperture of the element [173].

However, this has not been attempted in the case of spatially partially coherent light.

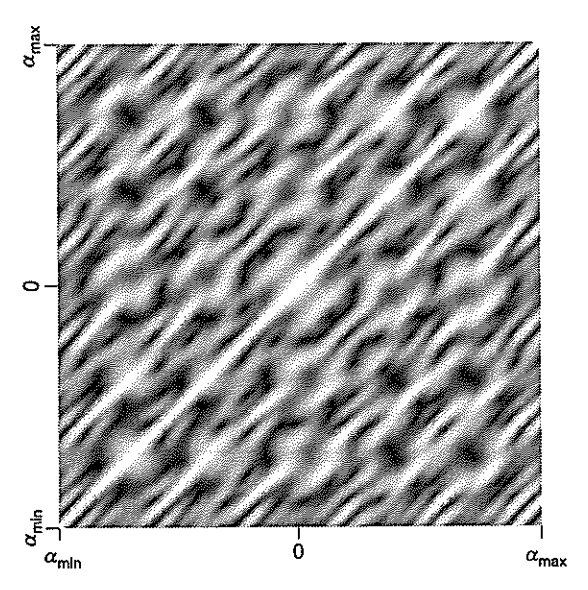


Fig. 8.4: Modulus of the angular correlation function  $\nu(\alpha_1,\alpha_2)$  inside the signal window.

#### Non-paraxial Gaussian to flat-top beam shaping 8.5

Elements, that reshape an incident Gaussian beam of width w into a field with a flattop radiant intensity distribution, as illustrated in Fig. 8.5a, are required frequently in a many technical applications [56]. If the flat-top opening angle  $\Omega$  is small, one can use paraxial design methods. However, with wide opening angles such paraxial designs fail and rigorous design methods are required.

Since both the incident field and the signal field are symmetric, the structure of the diffractive element is also chosen to be symmetric. The structure is described using the set of parameters  $\{x_l, h_l\}$  defined in Fig. 8.5b. In this example, the design is started from a  $1 \to 5$  array illuminator of period d, with  $|T_m|^2$  equal for  $|m| \le 5$ . The element is illuminated by a Gaussian beam of width  $w \sim \sqrt{2 \ln 2} d/\pi$ .

Using paraxial direct design, the set  $\{x_l, h_l\}$  is optimized to produce a uniform radiant intensity distribution  $|T(\alpha)|^2$  over the range  $|\alpha| \leq 5/d$ . The optimal parameters are found to be

$$\{x_1, \dots, x_4\} = \{0.173d, 0.289d, 0.366d, 0.446d\},$$

$$\{h_1, \dots, h_4\} = \{0.56\lambda, 0.66\lambda, 1.03\lambda, 1.77\lambda\},$$

$$(8.11)$$

$$\{h_1, \dots, h_d\} = \{0.56\lambda, 0.66\lambda, 1.03\lambda, 1.77\lambda\},$$
 (8.12)

and w = 0.38d. The element is then analyzed rigorously using the methods introduced in Chapter 6. The radiant intensities with opening angles  $\Omega=15.4^{\circ},~\Omega=23.0^{\circ},$  and  $\Omega = 47.2^{\circ}$ , corresponding the periods  $d = 15\lambda$ ,  $d = 10\lambda$  and  $d = 5\lambda$  are shown in Fig. 8.6, where we have normalized  $J^{in}(0) = 1$ .

The  $d = 5\lambda$  element is further optimized using rigorous direct optimization. The

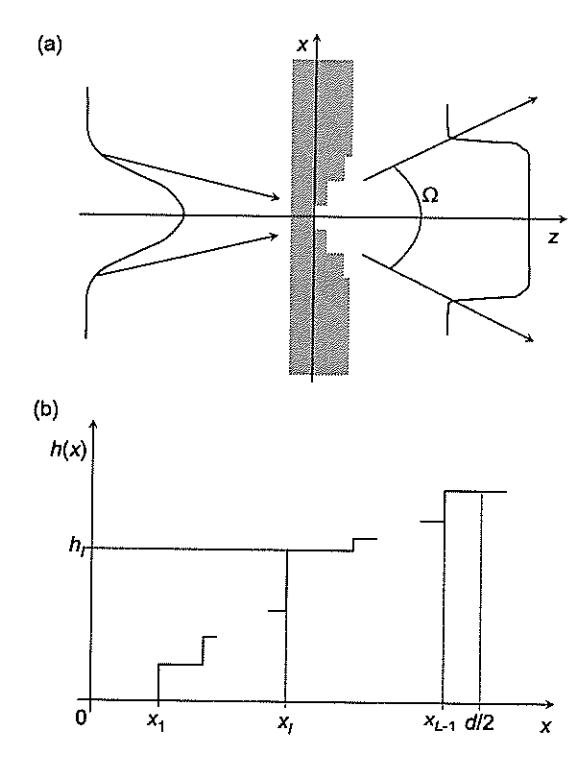


Fig. 8.5: Geometry of Gaussian to flattop-element.

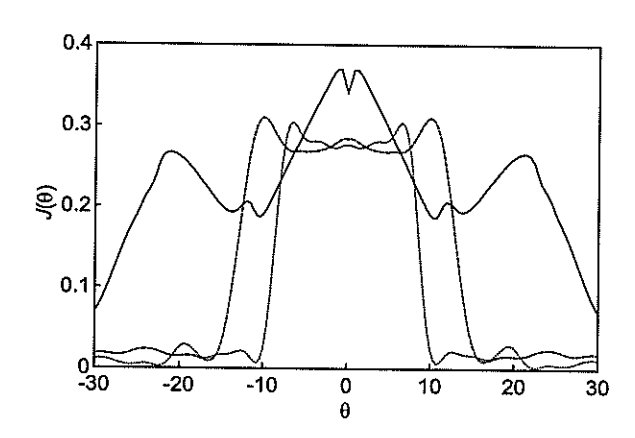


Fig. 8.6: Radiant intensity of the flattop element with different opening angle of signal  $\Omega$ . Solid line:  $\Omega=47.2^{\circ}$ . Dashed line:  $\Omega=23.0^{\circ}$ . Dotted line:  $\Omega=15.4^{\circ}$ .

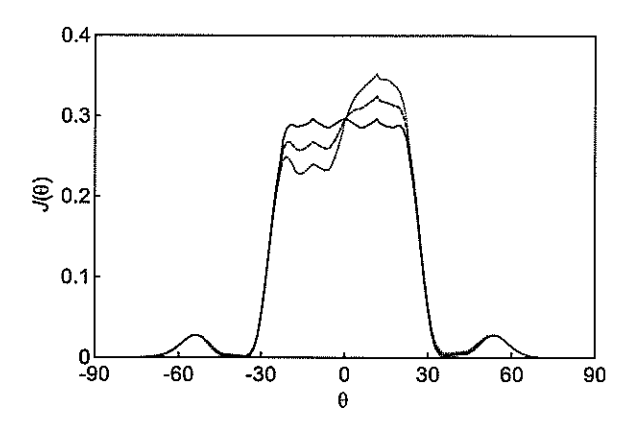


Fig. 8.7: Effect of the lateral positioning error in the signal fidelity of the Gaussian to flattop element. Solid line: no error. Dashed line: positioning error 0.02λ. Dotted line: positioning error  $0.04\lambda$ .

refined parameters are

$$\{x_1, \dots, x_3\} = \{0.173d, 0.366d, 0.446d\},$$
 (8.13)  
 $\{h_1, \dots, h_3\} = \{0.57\lambda, 0.87\lambda, 1.40\lambda\},$  (8.14)

$$\{h_1, \dots, h_3\} = \{0.57\lambda, 0.87\lambda, 1.40\lambda\},$$
 (8.14)

and w = 0.38d. The corresponding radiant intensity is shown in Fig. 8.7 (solid line). In Fig. 8.7, the effect of lateral position error of the element is illustrated, demonstrating high sensitivity. In Ref. [56], experimental demonstration of a rigorously designed Gaussian to flat-top element in the non-paraxial region is reported. Elements of this type would be extremely useful as line-focus generators, but the sensitivity to positioning errors limits their use.

# Chapter 9

# Coherence and diffraction

In this Chapter we investigate how diffraction changes the coherence properties of the electromagnetic field. The most familiar way to reduce coherence is the use of a rotating diffuser [174–176]. Alternatively one can employ an acousto-optic device, in which an acoustic pressure wave in a liquid or solid-state material forms a moving grating [177–182]. Here we introduce another method to realize a moving grating: the grating vibrator.

On the other hand, diffraction can improve the coherence properties of the field even in a homogeneous medium, as predicted by the Van Cittert-Zernike theorem [63]. Here we investigate how the spatial coherence properties of the field can be improved using the angular selectivity of a volume grating.

### 9.1 Grating vibrator

The geometry of a grating vibrator is illustrated in Fig. 9.1: the transducer P, which can be, e.g., a piezoelectric device, moves the grating periodically. We assume that the grating can be analyzed using the complex-amplitude transmittance method (Section 7.1). The complex-amplitude transmittance function is now time-dependent:

$$t(x,t) = \sum_{m=-\infty}^{\infty} T_m \exp\{i2\pi m[x + \Delta x(t)]/d\}, \qquad (9.1)$$

where

$$T_m = \frac{1}{d} \int_0^d t(x,0) \exp(-i2\pi mx/d) dx$$
 (9.2)

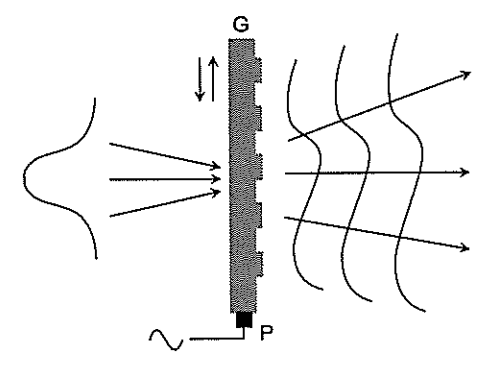


Fig. 9.1: Geometry of a grating vibrator.

and  $\Delta x(t)$  is the grating displacement, which is a periodic function of period T, i.e.,  $\Delta x(t+T) = \Delta x(t)$ . The incident spatially coherent field is assumed to be  $U(x,t) = U(x) \exp(-i\omega_0 t)$ . The cross-correlation function behind the grating is

$$\Gamma_{d}(x_{1}, x_{2}, \tau) = \langle U^{*}(x_{1}, t)t^{*}(x_{1}, t)U(x_{2}, t + \tau)t(x_{2}, t + \tau)\rangle$$

$$= U^{*}(x_{1})U(x_{2}) \sum_{m=-\infty}^{\infty} \sum_{n=-\infty}^{\infty} T_{m}^{*}T_{n} \exp\left[-i2\pi(mx_{1} - nx_{2})/d\right]$$

$$\times \exp\left(-i\omega_{0}\tau\right) \lim_{T \to \infty} \frac{1}{2T} \int_{-T}^{T} \exp\left\{i2\pi\left[m\Delta x(t) - n\Delta x(t + \tau)\right]/d\right\} dt.$$
(9.3)

In some important cases it is possible to evaluate the integral in Eq. (9.3) analytically. Let us assume that  $\Delta x(t) = a \sin(t/T)$  with a = constant. With the aid of the identity [110]

$$\exp(i\rho\sin\beta) = \sum_{p=-\infty}^{\infty} J_p(\rho) \exp(ip\beta), \tag{9.4}$$

where  $J_p$  is the Bessel function of the first kind, we obtain

$$\Gamma(x_1, x_2, \tau) = U^*(x_1)U(x_2) \sum_{m=-\infty}^{\infty} \sum_{n=-\infty}^{\infty} T_m^* T_n \exp\left[-i2\pi (mx_1 - nx_2)/d\right]$$

$$\times \exp(-i\omega_0 \tau) \sum_{n=-\infty}^{\infty} J_p(\rho_m) J_p(\rho_n) \exp(-ip\tau/T), \tag{9.5}$$

where  $\rho_m = 2\pi ma/d$ . The cross-spectral density function at the exit plane of the element is

$$W(x_{1}, x_{2}, \omega) = U^{*}(x_{1})U(x_{2}) \sum_{m=-\infty}^{\infty} \sum_{n=-\infty}^{\infty} T_{m}^{*}T_{n} \exp[-i2\pi(mx_{1} - nx_{2})/d]$$

$$\times \sum_{n=-\infty}^{\infty} J_{p}(\rho_{m})J_{p}(\rho_{n})\delta[\omega - (\omega_{0} + pf)], \qquad (9.6)$$

where  $\delta(x)$  is the Dirac delta function and f=1/T. This cross-spectral density function can be propagated to any observation plane using Eq. (4.20). The angular correlation function is

$$A(\alpha_1, \alpha_2, \omega) = \sum_{m=-\infty}^{\infty} \sum_{n=-\infty}^{\infty} T_m^* T_n A^*(\alpha_1 - m/d) A(\alpha_2 - n/d) \times \sum_{p=-\infty}^{\infty} J_p(\rho_m) J_p(\rho_n) \delta[\omega - (\omega_0 + pf)],$$

$$(9.7)$$

When the moving grating is realized using an acousto-optic device the beams corresponding to different diffraction orders are uncorrelated [177]. Equations (9.6) and (9.7) imply that in the case of vibrating grating the different diffraction orders are partially correlated.

### 9.2 Bragg selective gratings

As it was seen in Section 7.2, volume gratings can have a diffraction efficiency close to 100% when illuminated by a plane wave at the Bragg angle. However, the efficiency depends strongly on the angle of incidence and thus it is possible to improve the spatial coherence properties of an optical field using a volume grating as a filter [57, 183].

### 9.2.1 Coherence analysis

The grating, which is located between the planes z = 0 and z = h, is illuminated by a spatially partially coherent field with angular correlation function

$$A^{\text{in}}(\alpha_1, \alpha_2, z) = \sqrt{A^{\text{in}}(\alpha_1, \alpha_1, z)A^{\text{in}}(\alpha_2, \alpha_2, z)}\nu^{\text{in}}(\alpha_1, \alpha_2, z). \tag{9.8}$$

The cross-spectral density function behind the element is

$$W^{t}(x_{1}, x_{2}, h) = \sum_{m=-\infty}^{\infty} \sum_{n=-\infty}^{\infty} W_{mn}^{t}(x_{1}, x_{2}, h),$$
(9.9)

where

$$W_{mn}^{t}(x_{1}, x_{2}, h) = \exp\left[i2\pi(mx_{1} - nx_{2})/d\right] \times \int \int_{-\infty}^{\infty} A^{in}(\alpha_{1}, \alpha_{2}, 0)T_{m}^{*}(\alpha_{1})T_{n}(\alpha_{2}) \exp\left[-i2\pi(\alpha_{1}x_{1} - \alpha_{2}x_{2})\right] d\alpha_{1}d\alpha_{2}$$
(9.10)

and  $T_m(\alpha)$  is the amplitude of the *m*th diffracted order when the grating is illuminated by a plane wave with incident angle  $\theta$ , and  $\alpha = (n_1/\lambda) \sin \theta$ .

The angular correlation function at the plane z = h is

$$A^{t}(\alpha_1, \alpha_2, h) = \sum_{m=-\infty}^{\infty} \sum_{n=-\infty}^{\infty} A^{t}_{mn}(\alpha_1, \alpha_2, h), \tag{9.11}$$

where

$$A_{mn}^{t}(\alpha_{1}, \alpha_{2}, h) = A^{in}(\alpha_{1} - m/d, \alpha_{2} - n/d, 0)T_{m}^{*}(\alpha_{1} - m/d)T_{n}(\alpha_{2} - n/d).$$
 (9.12)

If the beams corresponding to different diffracted orders do not overlap in the far-zone, we need only to calculate the angular correlation function  $A^{\rm t}_{mm}(\alpha_1,\alpha_2,h)$  to determine the coherence properties of the *m*th-order diffracted beam. We obtain

$$A_{mm}^{t}(\alpha_1, \alpha_2, z) = \sqrt{A_{mm}^{t}(\alpha_1, \alpha_1, h)A_{mm}^{t}(\alpha_2, \alpha_2, h)}\nu_{mm}^{t}(\alpha_1, \alpha_2, h), \tag{9.13}$$

where

$$A_{mm}^{t}(\alpha,\alpha,h) = |T_{m}(\alpha - m/d)|^{2} A^{in}(\alpha - m/d,\alpha - m/d,0)$$

$$(9.14)$$

and

$$\nu_{mm}^{t}(\alpha_{1}, \alpha_{2}, h) = \frac{T_{m}^{*}(\alpha_{1} - m/d)}{|T_{m}(\alpha_{1} - m/d)|} \frac{T_{m}(\alpha_{2} - m/d)}{|T_{m}(\alpha_{2} - m/d)|} \nu^{in}(\alpha_{1} - m/d, \alpha_{2} - m/d, 0). \quad (9.15)$$

Thus the angular self-correlation function of the mth-order diffracted beam is determined by the angular correlation function of the incident beam and the amplitude  $T_m(\alpha)$ , while the absolute value of the complex degree of angular correlation is a shifted replica of the corresponding incident quantity.

#### 9.2.2 Examples

We consider three different gratings:

1. A binary surface-relief grating with permittivity distribution

$$\epsilon_r(x,z) = \begin{cases} n_1^2 & \text{when } 0 \le x \le d/2\\ n_3^2 & \text{when } d/2 \le x < d \end{cases}, \tag{9.16}$$

where  $d = \lambda$ ,  $h = 1.634\lambda$ ,  $n_1 = 1.5$ ,  $n_3 = 1.0$ .

2. A sinusoidal index-modulated grating with

$$\epsilon_r(x, z) = \epsilon_r + \Delta \epsilon_r \cos(2\pi x/d),$$
(9.17)

where  $\sqrt{\epsilon_r} = n_1 = n_3 = 1.5$ ,  $\Delta \epsilon_r = 0.04545$ ,  $d = 0.8\lambda$ , and  $h = 30\lambda$ .

3. A sinusoidal index-modulated grating with  $n_1 = n_3 = 1$ ,  $\sqrt{\epsilon_r} = 2.25$ , and  $h = 2000\lambda$  with either (a)  $\Delta \epsilon_r = 1.091 \times 10^{-3}$  and  $d = 1.10\lambda$  or (b)  $\Delta \epsilon_r = 1.057 \times 10^{-3}$  and  $d = 0.99\lambda$ .

Grating 1 has been optimized in Ref. [184] to have a maximum -1st order diffraction efficiency at Bragg incidence, while the permittivities of gratings 2, 3a, and 3b are optimized using Eq. (7.17). We assume that the incident field is a TE polarized Gaussian Schell-model beam arriving at the first Bragg angle of the grating:

$$W^{\text{in}}(x_1, x_2, 0) = \exp\left[-(x_1^2 + x_2^2)/w^2\right] \exp\left[-(x_1 - x_2)^2/2\sigma^2\right] \exp\left[-i\pi(x_1 - x_2)/d\right]. \tag{9.18}$$

Here w and  $\sigma$  are the  $e^{-2}$  half-width of the intensity distribution and the  $e^{-1/2}$  half-width of the complex degree of spatial coherence, respectively.

In Fig. 9.2 the diffraction efficiency of the zeroth and first diffraction orders of grating 1 with a plane wave illumination are shown. Although the element is a binary lamellar element, the maximum efficiency of the first order is over 95%. However, the angular selectivity is rather weak and it is not possible to have significant improvement of coherence.

In Fig. 9.3 the efficiencies of grating 2 with plane wave illumination are shown. The efficiencies are close to those predicted by Eqs. (7.10) and (7.11). Grating 2 is then illuminated by a Gaussian Schell-model beam (9.18) with  $w = \sigma = 10\lambda$ . The angular self-correlation functions of the incident field and the zeroth and first order diffracted beams are illustrated in Fig. 9.4. Since  $w = \sigma$ , the form of the degree of coherence  $\nu^{\rm in}(\alpha, \alpha_{\rm B})$  (here  $\alpha_{\rm B} = (n_1/\lambda) \sin \theta_{\rm B}$  and  $\theta_{\rm B}$  is the first Bragg angle of the grating) is the same as the angular self-correlation function of the incident beam. The angular self-correlation function of the first-order diffracted beam is narrower than that of the incident beam, while, as shown in Eq. (9.15), the modulus of the complex degree of angular coherence remains unchanged. Thus the width of the spatial coherence distribution compared to the width of the far-zone intensity distribution has been improved.

The diffraction efficiencies of gratings 3a and 3b with plane wave illumination are illustrated in Figs. 9.5a and 9.5b. Even though both elements have been optimized to

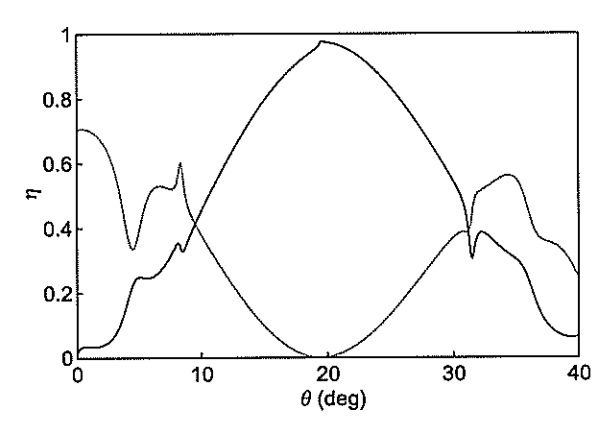


Fig. 9.2: Rigorously evaluated efficiencies  $\eta_{-1}$  (solid line) and  $\eta_0$  (dotted line) as functions of the angle of incidence  $\theta$ : fully coherent plane wave and grating 1.

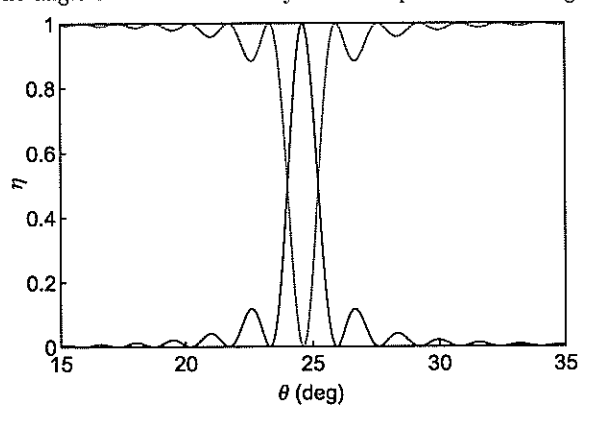


Fig. 9.3: Same as Fig. 9.2, but for grating 2.

produce 100% efficiencies according to Eq. (7.11), the rigorously calculated efficiency of the first order in the case of grating 3a is less than 50%, while grating 3b has an efficiency of  $\approx$  90% due to Fabry-Perot effects. If the elements are illuminated by a Gaussian-Schellmodel beam described by Eq. (9.18) with  $w = \sigma = 10\lambda$ , the first-order diffracted beams are almost completely spatially coherent. However, the efficiencies are low because of the strong angular selectivity: most of the transmitted energy propagates in the direction of the zeroth diffraction order.

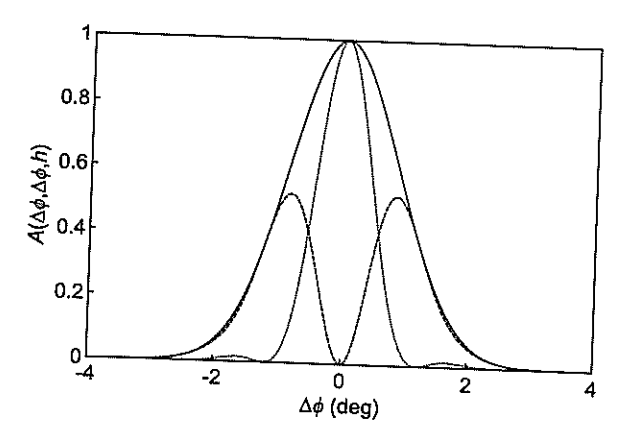


Fig. 9.4: Far-zone diffraction pattern of a Gaussian-Schell-model beam with  $w=\sigma=10\lambda$ , generated by grating 2. Solid line:  $A_{0,0}^t(\Delta\phi,\Delta\phi,h)$  when  $\Delta\epsilon_r=0$ . Dotted line:  $A_{0,-1}^t(\Delta\phi,\Delta\phi,h)$ . Dashed line:  $A_{0,0}^t(\Delta\phi,\Delta\phi,h)$ . Here  $\Delta\phi=\phi-\theta_{\rm B}$  if m=0 and  $\Delta\phi=\phi+\theta_{\rm B}$  if m=-1.

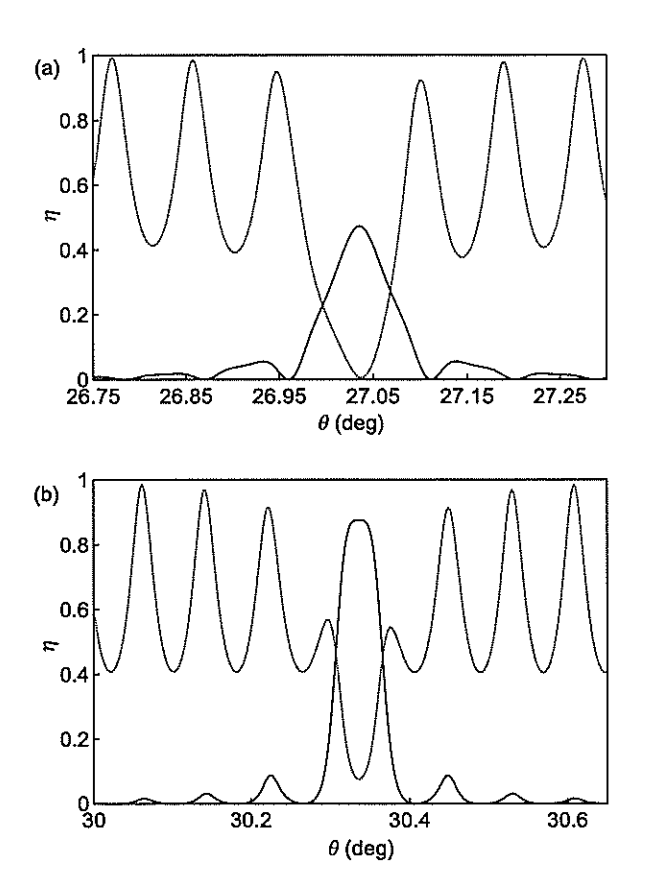


Fig. 9.5: Same as Fig. 9.2, but for (a) grating 3a and (b) for grating 3b.

# Chapter 10

# Propagation invariance and self-imaging

In this Chapter we investigate three topics. First, the Talbot effect [185] with spatially partially coherent illumination is analyzed. Then the validity of the paraxial approximation in the Lau effect [58] is evaluated. Finally, a novel quasi-rigorous analysis method of diffractive axicons is introduced for the analysis of approximate zeroth-order Bessel beams [186, 187] generated by diffractive axicons [188].

### 10.1 Talbot effect

The longitudinal periodicity of a laterally periodic completely spatially coherent field in the paraxial approximation is known as the Talbot effect [185,189]. Many applications, such as array illuminators [190–194] and interferometers [195] based on the Talbot effect have been suggested. Later it was found that in non-paraxial cases the Talbot patterns become strongly distorted [196, 197].

Consider the geometry in Fig. 10.1. A grating with complex-amplitude transmittance function

$$t(x;\omega) = \sum_{m=-\infty}^{\infty} T_m(\omega) \exp(i2\pi mx/d), \qquad (10.1)$$

where

$$T_m(\omega) = \frac{1}{d} \int_0^d t(x; \omega) \exp(-i2\pi mx/d) dx, \qquad (10.2)$$

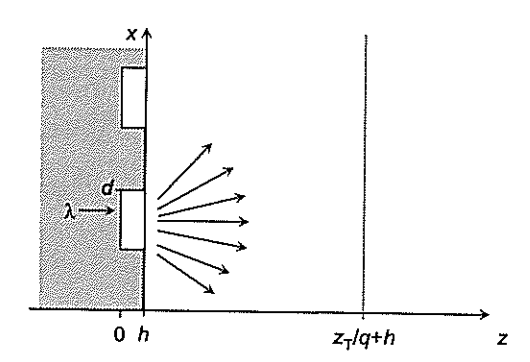


Fig. 10.1: Geometry of the Talbot effect.

is illuminated by a uniform-intensity Schell-model field with cross-spectral density function

$$W(x_1, x_2, 0; \omega) = S(\omega)\mu(x_1, x_2, 0; \omega), \tag{10.3}$$

where

$$S(\omega) = \frac{1}{\sqrt{\pi}\Gamma} \exp\left[-(\omega - \bar{\omega})^2/\Gamma^2\right]$$
 (10.4)

is the spectrum of the field (we assume a quasimonochromatic field, i.e.,  $\omega \gg \Gamma$ ), and

$$\mu(x_1, x_2, 0; \omega) = \exp\left[-(x_1 - x_2)^2 / 2\sigma^2(\omega)\right]$$
 (10.5)

is the complex degree of coherence. Then, using Eqs. (7.8) and (4.20), the spectral density at plane z = constant is found to be

$$S(x,z;\omega) = W(x,x,z;\omega)$$

$$= S(\omega) \sum_{m=-\infty}^{\infty} \sum_{n=-\infty}^{\infty} T_m^*(\omega) T_n(\omega) \exp\left[-i2\pi(m-n)x/d\right]$$

$$\times \int_{-\infty}^{\infty} \sqrt{2\pi}\sigma(\omega) \exp\left[-2\pi^2\sigma^2(\omega)(\alpha-m/d)^2\right]$$

$$\times \exp\left\{-i2\pi \left[w^*(\alpha;\omega) - w(\alpha-(m-n)/d;\omega)\right] \Delta z\right\} d\alpha, \quad (10.6)$$

where  $\Delta z = z - h$ , and  $w(\alpha; \omega)$  is given by Eq. (3.3). The intensity pattern observed at the plane z = constant is

$$I(x,z) = \int_0^\infty S(x,z;\omega) d\omega.$$
 (10.7)

In the coherent limit, i.e., when  $\sigma(\omega) \to \infty$ , one can use the expression

$$\delta(x) = \lim_{\alpha \to \infty} \left[ \alpha \exp(-\pi \alpha^2 x^2) \right]$$
 (10.8)

to obtain

$$S(x,z;\omega) = S(\omega) \left| \sum_{m=-\infty}^{\infty} T_m(\omega) \exp(i2\pi mx/d) \exp\left[i2\pi w(m/d;\omega)\Delta z\right] \right|^2.$$
 (10.9)

Using the paraxial approximation (3.6) in Eq. (10.6), we obtain

$$S(x,z;\omega) = S(\omega) \sum_{m=-\infty}^{\infty} \sum_{n=-\infty}^{\infty} T_m^*(\omega) T_n(\omega) \exp\left[-i2\pi(m-n)x/d\right]$$

$$\times \exp\left\{-\frac{1}{2}(m-n)^2 \left[\lambda \Delta z/\sigma(\omega)d\right]^2\right\} \exp\left[i\pi\lambda \left(m^2-n^2\right) \Delta z/d^2\right]$$
(10.10)

In the coherent limit, we find that  $S(x, h; \omega) = S(x, h + pz_T; \omega)$ , where

$$z_{\rm T} = 2d^2/\lambda \tag{10.11}$$

is called the Talbot distance and p is an integer. However, interesting intensity patterns can occur also at distances  $z = h + z_{\rm T}/q$ , where q is an integer [190,193].

### 10.1.1 Examples

Let us consider the diffraction pattern of a binary phase grating with  $d=50\lambda$ , fill factor c/d=1/2 and phase-delay  $\pi/2$  across the plane  $z=h+z_{\rm T}/4$  [190], and diffraction pattern of a 3-level grating

$$\phi(x) = \begin{cases} 3\pi/4, & 0 < x < d/4 \\ \pi, & d/4 < x < d/2 \\ 3\pi/4, & d/2 < x < 3d/4 \\ 0, & 3d/4 < x < d \end{cases}$$
(10.12)

with the same period at  $z = h = z_T/8$  [193]. According to the paraxial approximation they generate binary intensity patterns with fill factors 1/2 and 1/4, respectively.

In Fig. 10.2, the binary element with monochromatic illumination ( $\Gamma \to 0$ ) is analyzed. Strong intensity fluctuations are observed with spatially coherent illumination (Fig. 10.2a) [196,197]. However, when the spatial coherence is reduced, the fluctuations are smoothed out. At the same time the spot boundaries become more inclined. In Fig. 10.3, the same is illustrated for the three-level element. In both cases it is possible to find coherence conditions in which the spots are of high-quality flat-top form.

The effect of polychromatic, but spatially fully coherent illumination is illustrated in Figs. 10.4 and 10.5. The intensity fluctuations are smoothed out, but the resolution decreases faster than with spatially partially coherent monochromatic illumination. This is related to wavelength dependence of the Talbot distance  $z_{\rm T}$ .

### 10.2 Lau effect

If two gratings  $G_1$  and  $G_2$  are placed a distance  $\Delta z$  apart as in Fig. 10.6 and  $G_1$ , is illuminated by spatially incoherent quasimonochromatic light, high contrast fringes can be observed in the far-zone under some specific conditions. This effect, known as the Lau effect [58], has been analyzed using different paraxial approaches [189, 198–202] and different kinds of gratings [203–205]. Applications including interferometers [206–208] have been proposed. Similarities between the Talbot and Lau effects have been investigated in several papers [209–211, 189]. Recently, the validity of the paraxial approximation has been analyzed in Ref. [59].

We assume that both  $G_1$  and  $G_2$  can be treated as thin elements. The cross-spectral density function just behind the grating  $G_1$  can be written as

$$W(x_1, y_1, x_2, y_2, h_1) = I(x_1, y_1, h_1)\delta(x_1 - x_2, y_1 - y_2)/\delta(0, 0),$$
(10.13)

where the Dirac delta function is understood as a limit

$$\delta(x,y) = \lim_{\sigma \to 0} \left\{ \left( 2\pi\sigma^2 \right)^{-1} \exp\left[ -(x^2 + y^2)/2\sigma^2 \right] \right\}$$
 (10.14)

and  $I(x, y, h_1)$  is the intensity distribution after grating  $G_1$ , normalized as

$$\frac{1}{d} \int_0^d I(x_1, y_1, h_1) \mathrm{d}x_1 = 1. \tag{10.15}$$

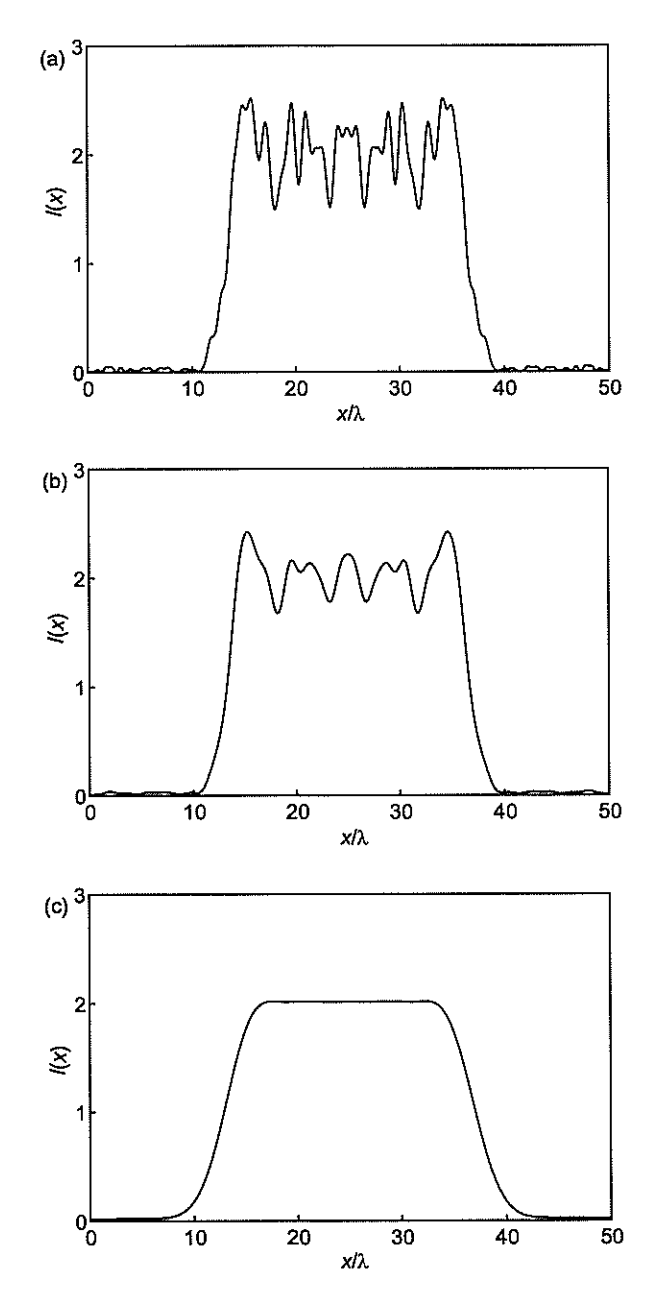


Fig. 10.2: Effect of spatial coherence in the spot array generated by a binary phase grating of period  $d=50\lambda$  at  $z=h+z_{\rm T}/4$ . (a) Full coherence  $\sigma(\bar{\omega})=\infty$ . (b)  $\sigma(\bar{\omega})=10d$ . (c)  $\sigma(\bar{\omega})=2d$ .

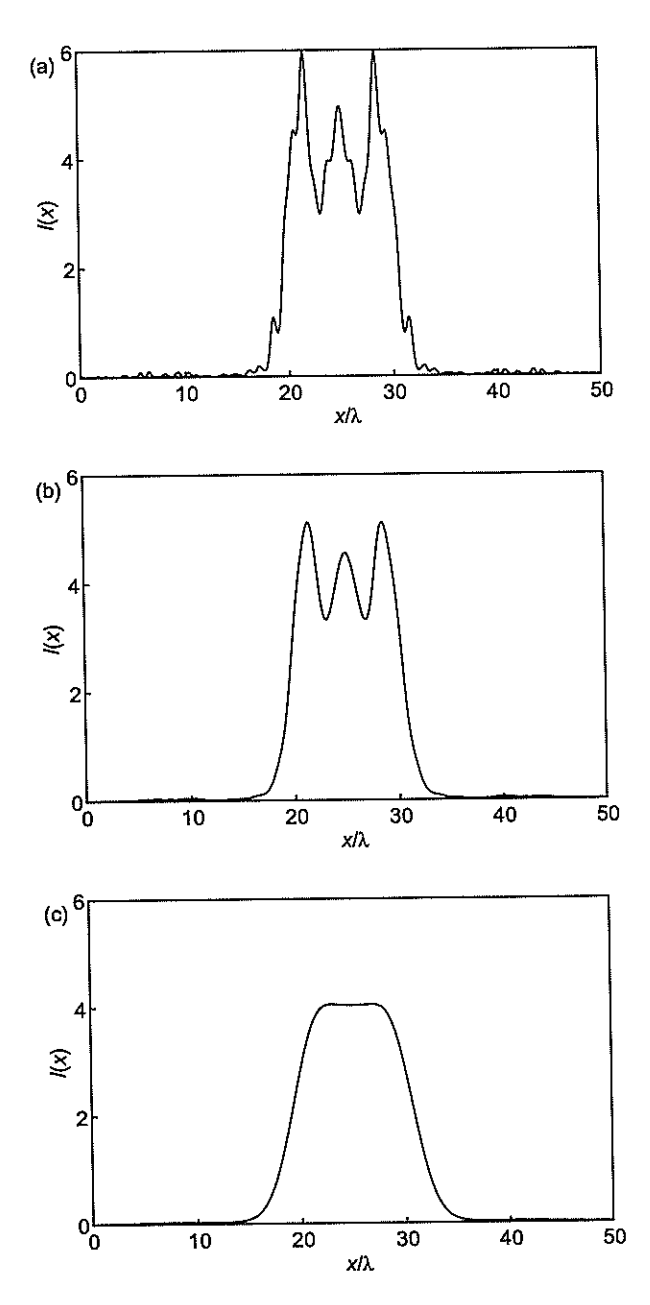
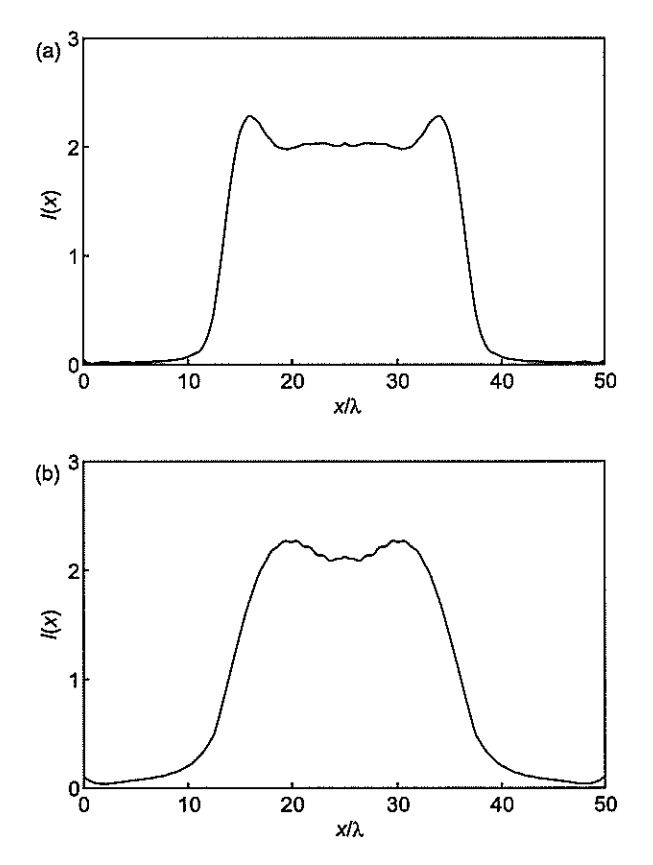


Fig. 10.3: Effect of spatial coherence in the spot array generated by a 3-level phase grating of period  $d=50\lambda$  at  $z=h+z_{\rm T}/8$ . (a) Full coherence  $\sigma(\bar{\omega})=\infty$ . (b)  $\sigma(\bar{\omega})=5d$ . (c)  $\sigma(\bar{\omega})=1.2d$ .



**Fig. 10.4:** Effect of polychromatic illumination in the spot array generated by a binary phase grating of period  $d=50\lambda$  at  $z=h+z_{\rm T}/4$ . (a)  $\bar{\omega}/\Gamma=50$ . (b)  $\bar{\omega}/\Gamma=10$ . The coherent case is shown in Fig. 10.2a.

Since  $I(x, y, h_1)$  is a periodic function, it can be expressed as a Fourier series

$$I(x_1, y_1, h_1) = \sum_{n = -\infty}^{\infty} C_n \exp(i2\pi nx/d),$$
 (10.16)

where the Fourier coefficients  $C_n$  are

$$C_n = \frac{1}{d} \int_0^d I(x_1, y_1, h_1) \exp(-i2\pi nx/d) dx.$$
 (10.17)

The complex-amplitude transmittance function of grating  $G_2$  is

$$t(x) = \sum_{p=-\infty}^{\infty} T_p \exp(i2\pi px/d), \qquad (10.18)$$

where

$$T_p = \frac{1}{d} \int_0^d t(x) \exp(-i2\pi px/d) dx.$$
 (10.19)

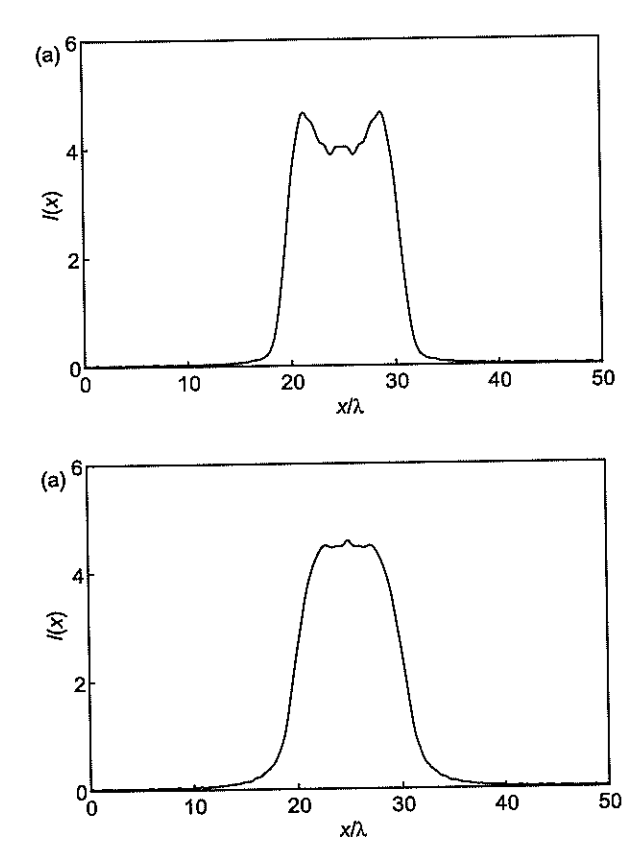


Fig. 10.5: Effect of polychromatic illumination in the spot array generated by a 3-level phase grating of period  $d=50\lambda$  at  $z=h+z_{\rm T}/8$ . (a)  $\bar{\omega}/\Gamma=50$ . (b)  $\bar{\omega}/\Gamma=15$ . The coherent case is shown in Fig. 10.3a.

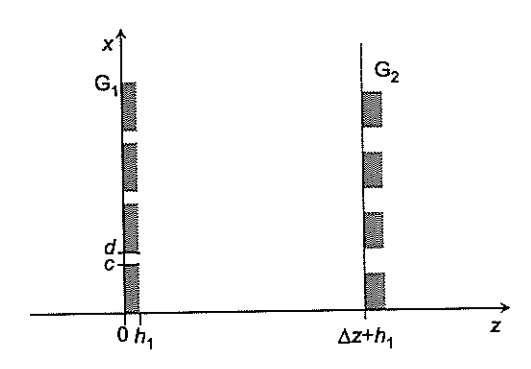


Fig. 10.6: The geometry of the Lau effect.

Using Eqs. (7.8) and (4.20), the angular self-correlation function (4.21) after  $G_2$  is found to be

$$A(\alpha,\beta) = \sum_{p=-\infty}^{\infty} \sum_{q=-\infty}^{\infty} C_{p-q} T_p^* T_q \exp\{-i2\pi [w^*(\alpha - p/d,\beta) - w(\alpha - q/d,\beta)]\Delta z\}, \quad (10.20)$$

where  $\omega(\alpha, \beta)$  is given by Eq. (3.3). Applying the paraxial approximation (3.6), Eq. (10.20) can be written as

$$A(\alpha,\beta) = \sum_{p=-\infty}^{\infty} \sum_{q=-\infty}^{\infty} C_{p-q} T_p^* T_q \exp[i\pi(p^2 - q^2)\lambda \Delta z/d^2] \exp[-i2\pi(p-q)\lambda \Delta z\alpha/d], (10.21)$$

which is a periodic function of period  $\Lambda = d/\lambda \Delta z$ . If grating  $G_1$  is a Ronchi ruling with infinitely narrow slits, i.e.,  $C_n = 1$  for all n, an analogy with the fully coherent Talbot effect can be observed [59,189].

#### 10.2.1 Examples

Let us assume that the first grating is a Ronchi ruling with infinity narrows slits. In Figs. 10.7, the angular self-correlation function is plotted, assuming that  $G_2$  is a binary amplitude grating with fill factor 1/2, and that the grating separation is  $\Delta z = z_{\rm T}$ , where  $z_{\rm T}$  is the Talbot distance. Strong fluctuations are observed even when the grating period is  $d=500\lambda$ , since the field after the incoherently illuminated grating  $G_1$  is inherently non-paraxial. In Fig. 10.8 the angular self-correlation function is shown, assuming a binary phase grating  $G_2$  with phase shift  $\phi=\pi/2$ , fill factor 1/2, and grating separation  $\Delta z=z_{\rm T}/4$ .

Let us assume that the slits of  $G_1$  have a finite width. In Fig. 10.9, the angular self-correlation function is illustrated with various widths of  $G_1$ , while  $G_2$  is the same as in Fig. 10.8a. The fluctuations are significantly reduced, but the edge resolution is simultaneously decreased.

## 10.3 Propagation-invariant fields

There exists a wide class of fields, which are beam-like (in a sense) and propagation invariant [186, 187, 212, 213], i.e., the transverse intensity profile is independent on the propagation distance. The simplest scalar example is the zeroth-order Bessel beam

$$U(x, y, z) = J_0(\alpha \rho) \exp(i\beta z), \qquad (10.22)$$

where  $\alpha^2 + \beta^2 = k^2$ ,  $\rho^2 = x^2 + y^2$  and  $J_0$  is the zeroth-order Bessel function. Since the Bessel function  $J_0(\rho)$  decays as  $1/\rho$  when  $\rho \to \infty$ , the energy of this field is infinite. Therefore the ideal Bessel beam is physically unrealizable.

There exist several ways to generate approximate zeroth-order Bessel beams, which are nearly propagation-invariant between some planes  $z=z_1$  and  $z=z_2$ . Since the zeroth-order Bessel beam is a conical wave, one can use an annular aperture to generate it [186, 214]. Alternatively, Fabry-Perot resonators [214] and refractive [215, 216] or diffractive axicons [188] may be used. Here we analyze an approximate Bessel beam generated by a diffractive axicon, i.e., a circular grating with constant local period, by using a novel quasi rigorous method.

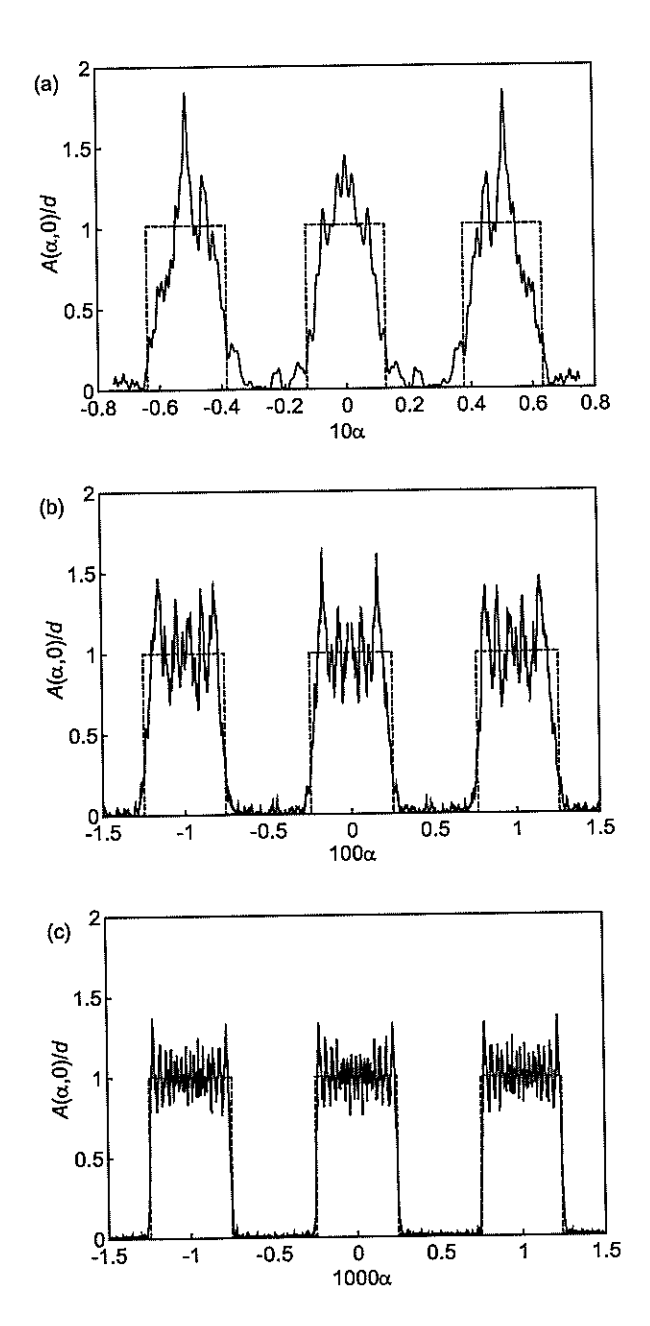


**Fig. 10.7:** Non-paraxial analysis of the far-zone diffraction pattern of a binary amplitude grating in the Lau set-up with grating separation  $\Delta z = z_T$ : (a)  $d/\lambda = 10$ ; (b)  $d/\lambda = 50$ ; (c)  $d/\lambda = 500$ . Solid line: non-paraxial analysis. Dashed line: paraxial analysis.

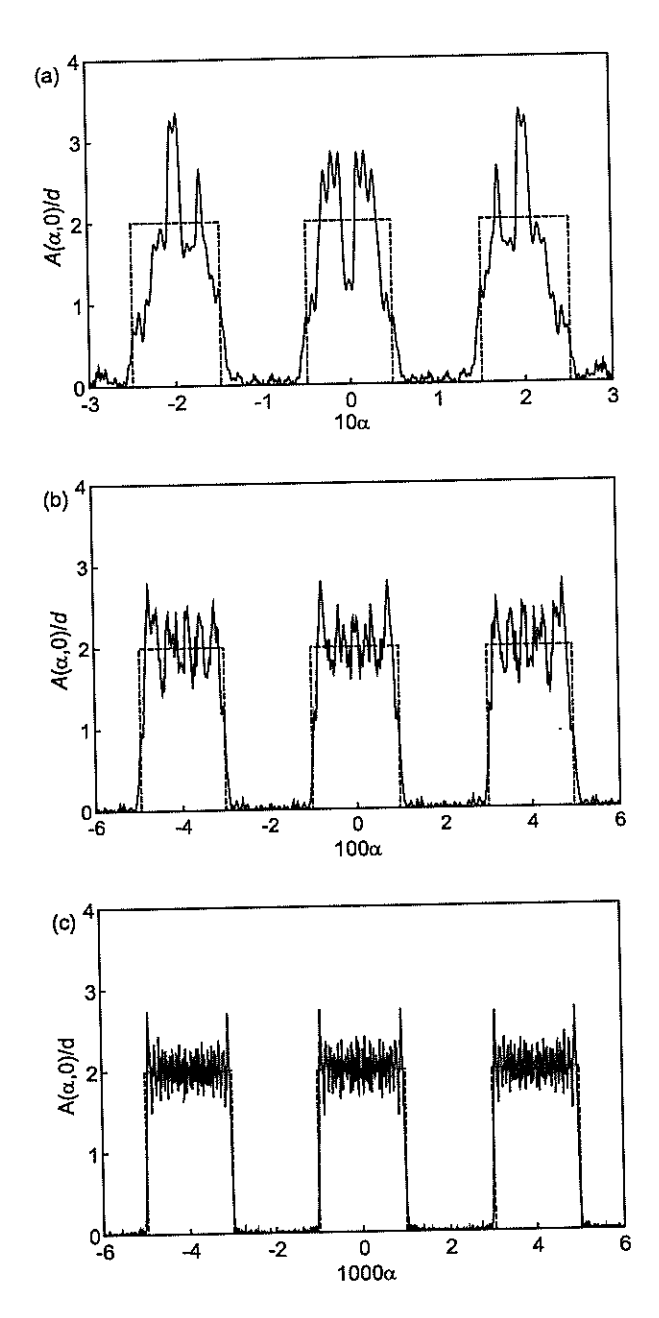


Fig. 10.8: Non-paraxial analysis of the far-zone diffraction pattern of a binary phase grating with phase delay  $\pi/2$  in the Lau set-up with grating separation  $\Delta z = z_{\rm T}$ : (a)  $d/\lambda = 10$ ; (b)  $d/\lambda = 50$ ; (c)  $d/\lambda = 500$ . Solid line: non-paraxial analysis. Dashed line: paraxial analysis.

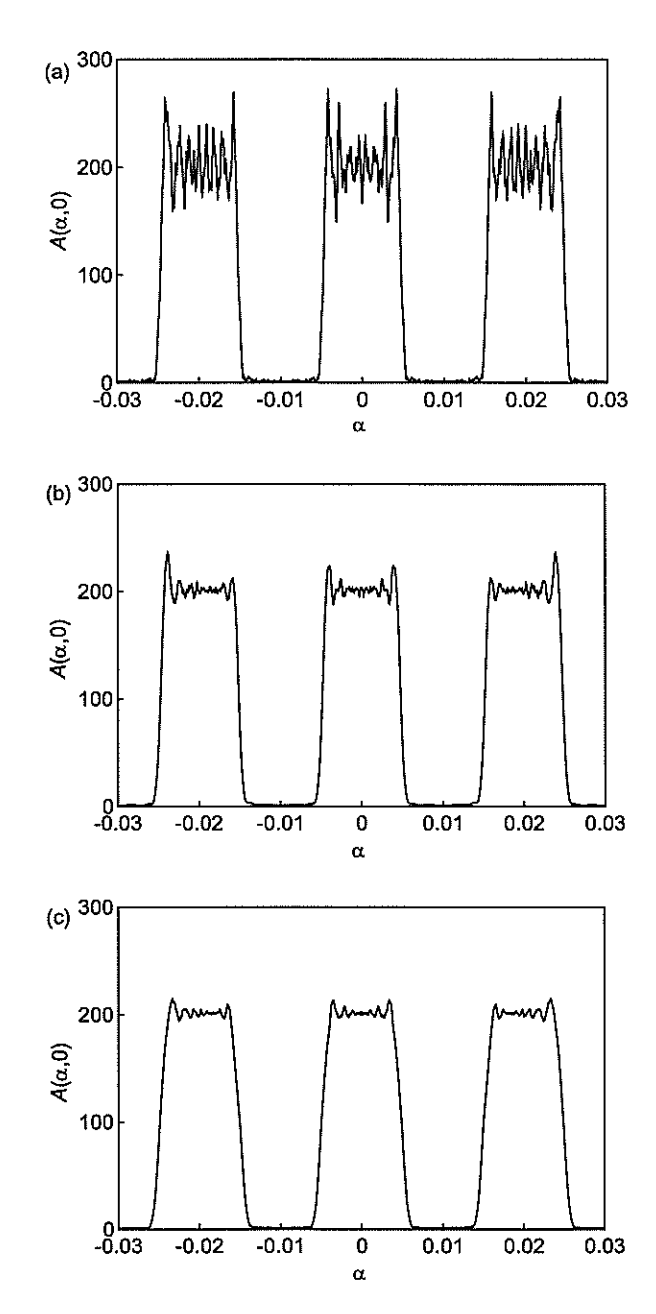


Fig. 10.9: Analysis of the effect of a finite slit width of the grating  $G_1$  in the far-zone diffraction pattern of a phase-only grating  $G_2$ . Here  $d/\lambda=100$  and the ratio c/d of the slit width and grating period is (a) c/d=0.01, (b) c/d=0.05, (c) c/d=0.1.

### Quasi-rigorous analysis of diffractive axicons

Let us assume that a diffractive axicon is located between the planes z = 0 and z = h, and illuminated by a completely coherent x-polarized field,

$$E^{\text{in}}(x, y, z) = \hat{x}E^{\text{in}}_{\tau}(x, y, z) = \hat{x}A_{x}(\rho)\exp(ikn_{1}z).$$
 (10.23)

Here  $\rho^2 = x^2 + y^2$ ,  $A_x(\rho)$  is the radially symmetric amplitude distribution, and  $n_1$  is the refractive index in the region  $z \leq 0$ . This is not necessarily an exact solution of Maxwell's equations, but if  $A_x(\rho)$  varies slowly compared to the wavelength, it is an excellent approximation.

Consider the coordinate system introduced in Fig. 10.10. At the point (x, y, x) we use local coordinates  $\hat{\rho}$  and  $\hat{\phi}$  and write the incident field as

$$\boldsymbol{E}_{x}^{\mathrm{in}}(\rho,\phi,z) = \hat{\rho} E_{\rho}^{\mathrm{in}}(\rho,\phi,z) + \hat{\phi} E_{\phi}^{\mathrm{in}}(\rho,\phi,z), \tag{10.24}$$

where

$$E_{\rho}^{\text{in}}(\rho,\phi,z) = A_x(\rho)\cos\phi\exp(\mathrm{i}kn_1z), \qquad (10.25)$$
  

$$E_{\phi}^{\text{in}}(\rho,\phi,z) = -A_x(\rho)\sin\phi\exp(\mathrm{i}kn_1z). \qquad (10.26)$$

$$E_{\phi}^{\text{in}}(\rho,\phi,z) = -A_x(\rho)\sin\phi\exp(\mathrm{i}kn_1z). \tag{10.26}$$

We assume that the grating diffraction problem can be treated locally, which permits a one-dimensional analysis. The field  $E_{\phi}$  after the element is

$$E_{\phi}^{t}(\rho,\phi,h) = E_{\phi}^{in}(\rho,\phi,0) \sum_{m=-\infty}^{\infty} T_{m} \exp(i2\pi m\rho/d) \exp\left[it_{m}(z-h)\right], \qquad (10.27)$$

where

$$t_m = \begin{cases} \sqrt{k^2 n_3^2 - (2\pi m/d)^2} & \text{when } |m| < dn_3/\lambda \\ i\sqrt{(2\pi m/d)^2 - k^2 n_3^2} & \text{otherwise.} \end{cases}$$
 (10.28)

and the Fourier amplitudes  $T_m$  of the transmitted field can be solved using the methods introduced in Chapter 5 in TE polarization.

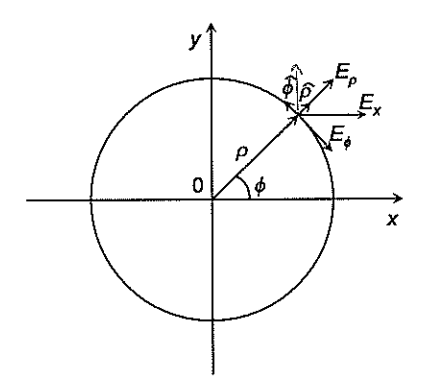


Fig. 10.10: Local coordinate system.

In TM polarization,  $H_{\phi}^{\text{in}}$  is obtained using Maxwell's equation (2.3). The field just behind the element assumes the form

$$H_{\phi}^{t}(\rho,\phi,h) = H_{\phi}^{in}(\rho,\phi,0) \sum_{m=-\infty}^{\infty} S_{m} \exp(i2\pi m/d) \exp\left[it_{m}(z-h)\right],$$
 (10.29)

where the coefficients  $S_m$  can also be solved using rigorous diffraction analysis.

Using Maxwell equation (2.4), the electric field components  $E_{\rho}^{t}$  and  $E_{z}^{t}$  can be easily solved. Switching back to the global coordinates, one obtains

$$E_x^{\rm t}(\rho,\phi,h) = A(\rho) \sum_{m=-\infty}^{\infty} \left[ (n_1 t_m/k) S_m \cos^2 \phi + T_m \sin^2 \phi \right] \exp(i2\pi m \rho/d), (10.30)$$

$$E_y^{t}(\rho, \phi, h) = A(\rho) \sin \phi \cos \phi \sum_{m=-\infty}^{\infty} [(n_1 t_m/k) S_m - T_m] \exp(i2\pi m \rho/d),$$
 (10.31)

$$E_z^{\rm t}(\rho,\phi,h) = -A(\rho)(n_1\lambda/d)\cos\phi \sum_{-\infty}^{\infty} mS_m \exp(\mathrm{i}2\pi m\rho/d). \tag{10.32}$$

The magnetic field components can be solved from Maxwell's equation (2.3) and the y-polarization can be treated analogously. Once the field components have been solved at z = 0, they can be propagated separately to the observation plane by means of Eq. (3.12).

Similarly one can analyze more complicated diffractive elements, which generate higherorder propagation-invariant fields. This method can also be extended to the analysis of diffractive lenses. The work in this direction is currently under way.

#### 10.3.2 Examples

Let us consider the following lamellar elements:

- 1. Binary element with  $h = \lambda$  and local period 1.5 $\lambda$ .
- 2. Four-level element with optimized [141] structure and local period  $1.5\lambda$ .
- 3. Binary element with  $h = \lambda$  and local period  $5\lambda$ .
- 4. Four-level element with optimized [141] structure and local period  $5\lambda$ .

We assume that the radius of the aperture of the element is  $40\lambda$  and that an opaque disk of radius  $5\lambda$  exists around the origin. The refractive indices are  $n_1 = 1.5$  and  $n_3 = 1$ . The 4-level structures have been optimized for maximum minus first order diffraction efficiency in both TE and TM polarization [141]. The binary elements have a fill factor of 1/2 and a profile height  $h = \lambda$ . The incident field is assumed to be a plane wave, i.e.,  $A(\rho) = 1$ .

Figure 10.11a illustrates axial intensities after gratings 1 and 2 under x-polarized illumination. Since only orders  $m=\pm 1$  and m=0 exist, the only effect introduced by the optimized element is an increased axial intensity. In Fig. 10.11b, the local period of the element is  $d=5\lambda$ . Strong interference between different diffraction orders takes place behind the binary element. In the case of 4-level element, this interference is reduced because the efficiencies of the diffraction orders other than m=-1 have decreased.

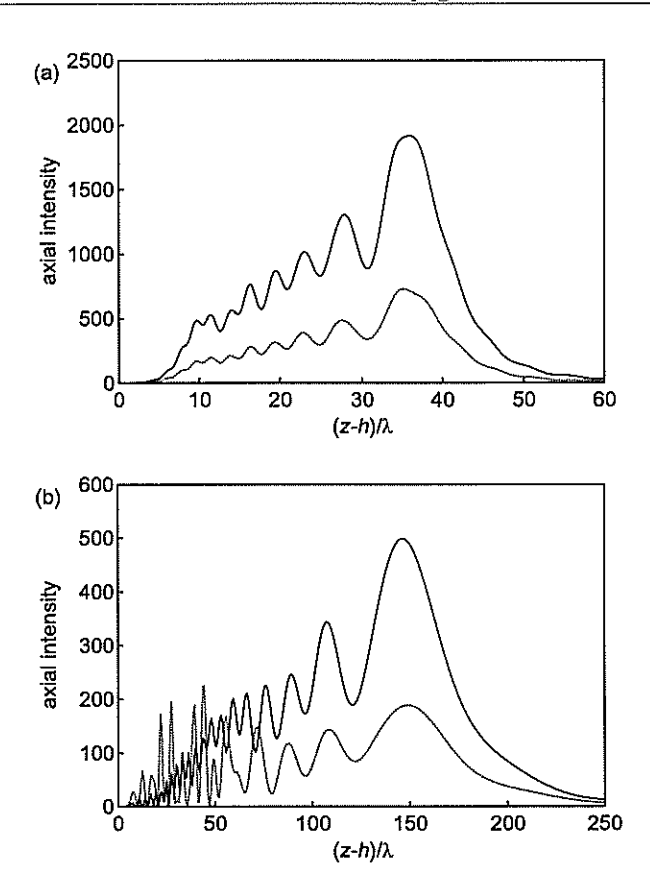


Fig. 10.11: Axial intensities: (a)  $d=1.5\lambda$ , (b)  $d=5.0\lambda$ . Dotted line: binary element. Solid line: optimized 4-level element.

Figures 10.12 and 10.13 illustrate the transverse intensity distributions at distances  $z=h+100\lambda$  and  $z=h+200\lambda$ , respectively, behind element 3, illuminated by an x-polarized plane wave. The radial intensity is an approximation of a Bessel function, and the width of the central peak remains approximately constant. Also the distribution is found to be almost radially symmetric, which was to be expected since the element operates close to the paraxial domain. Figure 10.14 illustrates the transverse intensity profile at the distance  $z=h+40\lambda$ . Due to the interference of several conical diffraction orders, the radial intensity is no longer a good approximation of the lowest-order Bessel function.

When the period d of the circular grating is reduced, the transverse intensity profile is no longer radially symmetric. Figure 10.15 shows the transverse intensity distribution at a distance  $z=h+40\lambda$ , behind grating 1 illuminated by an x-polarized plane wave. In Fig. 10.16, element 1 is illuminated by a circularly polarized field. The transverse intensity is now radially symmetric even though the local period is small. A symmetric intensity distribution is also obtained with unpolarized illumination.

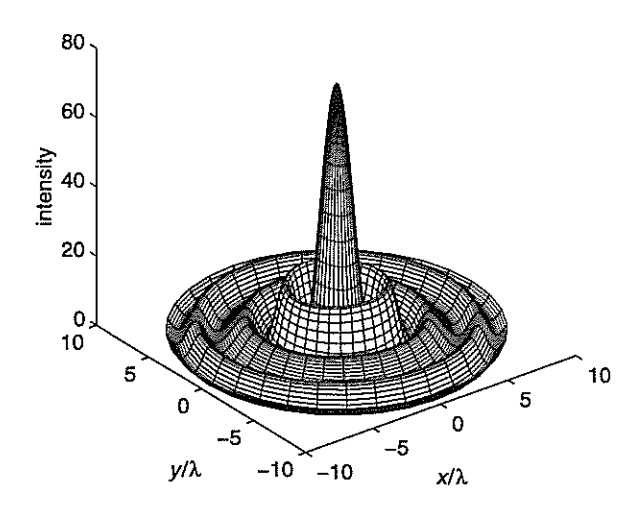
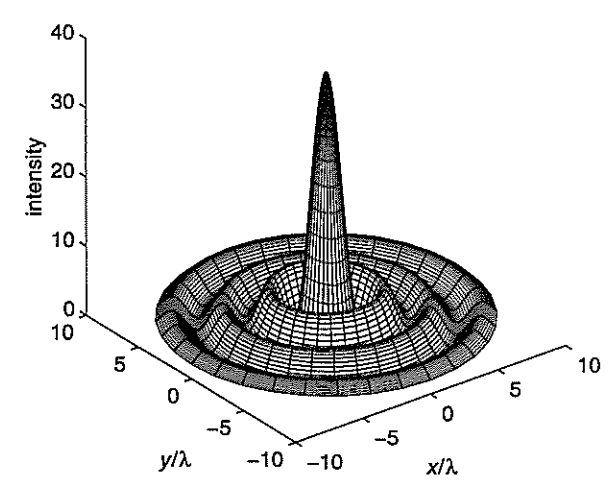
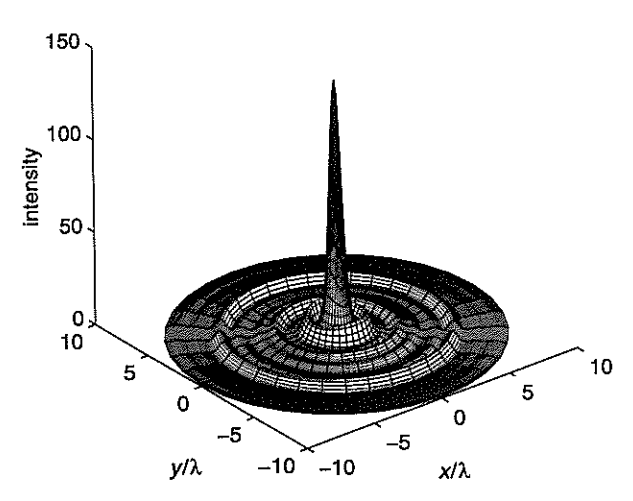


Fig. 10.12: Transverse intensity distribution at  $z=h+100\lambda$ . The period of the circular grating is  $d=5.0\lambda$ , and the element has a binary surface-relief profile. The incident field is linearly polarized.



**Fig. 10.13:** Same as Fig. 10.13, but at  $z = h + 200\lambda$ .



**Fig. 10.14:** Same as Fig. 10.12, but  $z = h + 40\lambda$ .

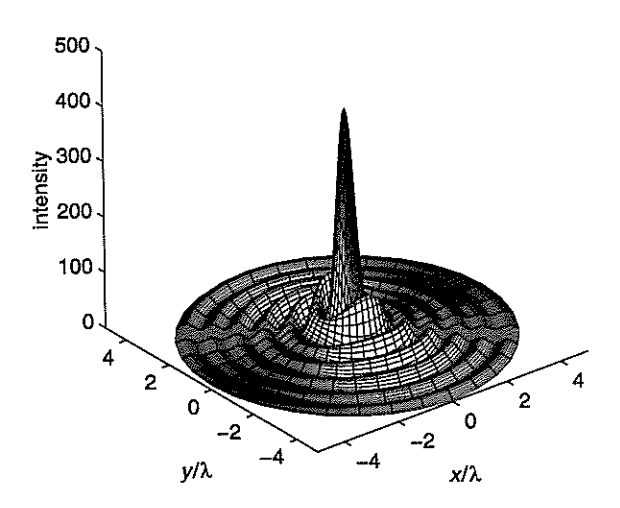


Fig. 10.15: Transverse intensity distribution at  $z=h+40\lambda$ . The period of the binary element is  $d=1.5\lambda$ . The incident field is a linearly x-polarized plane wave.

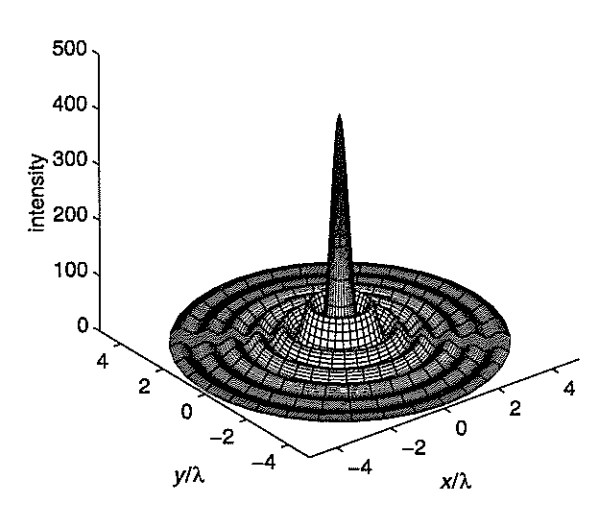


Fig. 10.16: Same as in Fig. 10.15, but the incident field is circularly polarized.

# Chapter 11

## Zeroth-order diffractive elements

### 11.1 Introduction

If the signal is encoded into the zeroth order of a diffractive element one speaks of a zeroth-order element. If the element is a grating with a period  $d < \lambda$ , only the zeroth transmitted and reflected diffraction orders can propagate and the element can be investigated using the effective medium theory [62,139,140]. These elements can be understood as artificial dielectric media [217–223] with effective refractive indices that depend strongly on the polarization state of the incident field. Therefore polarization dependent elements are possible [224–226]. Furthermore, applications such as grating antireflection surfaces [227] and guided-mode resonance filters [228–232] exist.

When a diffractive element is designed, one normally uses the amplitude freedom (Section 8.1) and thereby permits noise outside the signal window. Usually this noise concentrates in the immediate neighborhood of the signal window, where it may disturb the optical function of the element. One can eliminate this by enlarging the signal window (by including a zero-frame around the signal), which leads to more complicated elements and a considerable increase in the computational complexity. The other possibility is to use elements that control both the amplitude and the phase of the field. Such elements can be realized, e.g., by a double-layer technique [233], which however is difficult to calibrate. The alternative is the use of a carrier grating, which deflects the signal off-axis [24]. Here we consider complex-amplitude modulating elements, which deflect the noise off-axis and leave the signal on-axis [60,61].

## 11.2 Zeroth-order complex amplitude modulation

A lamellar grating with periods  $d_x$  and  $d_y$  in x and y directions, respectively, is divided into  $K \times L$  cells of equal size. With K cells in the 1D geometry, K diffraction orders separate the signal in the zeroth carrier-grating diffraction order and the noise that is deflected in higher carrier-grating orders. The depth and the fill factor associated with the cell (k,l) are denoted by  $h_{kl}$  and  $f_{kl}$ , respectively, and  $h=\lambda/(n-1)$ , where n is the refractive index of the element. We assume K=L and  $d_x=d_y=d=Kd_c$ , where  $d_c$  represents the carrier grating period. Figure 11.1 illustrates the geometry of a 1D grating with fill factor  $f_l=c_l/d_c$ .

If K = L = 1 ( $f_{11} = f$  and  $h_{11} = h$ ), the complex amplitude of the zeroth diffraction order is, according to the complex-amplitude transmittance theory,

$$T = 1 - f + f \exp\left[-ik(n-1)h\right]. \tag{11.1}$$

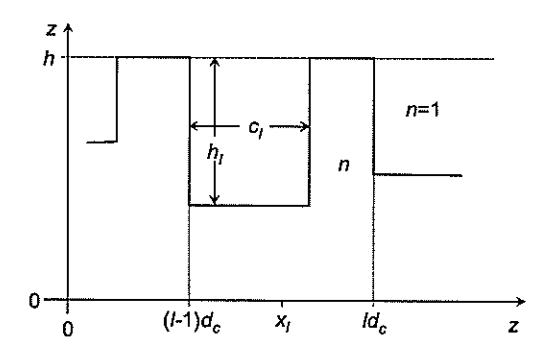


Fig. 11.1: Geometry of zeroth-order complex-amplitude encoding in one dimension.

This result is independent on the shape of the lamellar valley and it is valid also in 1D geometry. If we write  $T = A \exp(i\Phi)$ , where A is the amplitude and  $\Phi$  is the phase of the zeroth order, we obtain

$$f = 1 - \frac{1 - A^2}{2(1 - A\cos\Phi)} \tag{11.2}$$

and

$$\exp[ik(n-1)h] = \frac{A}{f}\exp(i\Phi) + 1 - \frac{1}{f}.$$
(11.3)

We sample the complex-amplitude distribution in cells (k, l) according to  $T_{kl} = T(x_k, y_l) = A_{kl} \exp(i\Phi_{kl})$ , where k = 1, ..., K and l = 1, ..., L. These amplitudes can be encoded into the zeroth diffraction order according to Eqs. (11.2) and (11.3). The shape and location of the valley can vary from cell to cell, since a lateral shift of the grating has no effect in the complex amplitude of the zeroth order (see Section 5.2.1).

#### 11.2.1 Examples

For fabrication reasons, only  $Q_f$  fill-factor values and  $Q_z$  depth values can often be realized. Choosing  $Q_f = Q_z = Q$  we consider Q = 8 in the 1D geometry of Fig. 11.1. In Fig. 11.2 the available phase and amplitude combinations are calculated using the complex-amplitude transmittance method and rigorous diffraction theory. The size of the cell in the rigorous calculations is  $d_c = 4\lambda$ , the refractive index is n = 1.5, and the effects of boundary reflections are ignored. In two-dimensional encoding, the minimum feature size required for a given carrier period is larger, and the allowed amplitude-phase combinations are more equally distributed in the amplitude/phase space [61].

Let us consider elements with two-point and three-point signals. Using Eq. (8.2), the required complex-amplitude transmittances are found to be

$$t(x) = \cos(2\pi x/d) \exp(i\psi_1) \tag{11.4}$$

and

$$t(x) \approx 0.809 \left[\cos(2\pi x/d) + \cos(6\pi x/d) \exp(i1.8089)\right] \exp(i\psi_2),$$
 (11.5)

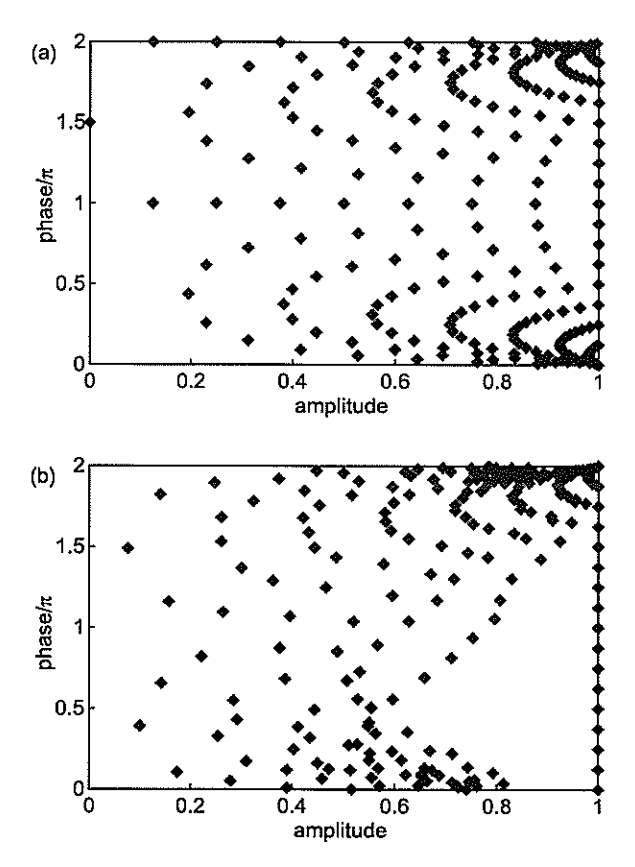


Fig. 11.2: Allowed phase-amplitude combinations, 8 quantization levels in both lateral and depth directions; (a) using scalar diffraction theory, (b) using rigorous diffraction theory with  $d_c=4\lambda$ .

where  $\psi_1$  and  $\psi_2$  are arbitrary phase factors). The efficiencies are 50% and 60%, respectively [60]. Using Eqs. (11.2) and (11.3), the required fill factors and depths can be calculated. Figures 11.3a and 11.3b show the profiles of these elements with L=25 and Q=16.

Figure 11.4 illustrates the uniformity and the noise of the encoded three-point element using complex-amplitude transmittance theory. The signal uniformity is defined as  $U = (\eta_{\text{max}} - \eta_{\text{min}})/(\eta_{\text{max}} + \eta_{\text{min}})$ , where  $\eta_{\text{max}}$  and  $\eta_{\text{min}}$  are the maximum and minimum efficiencies of the signal diffraction orders. The noise is defined to contain the energy in non-signal diffraction orders  $m = -10, \ldots, 10$ . The rigorous electromagnetic analysis of both elements can be found in Ref. [60].

The second example is a two-dimensional  $3 \times 3$  array. The optimal complex-amplitude transmission function is obtained using an iterative Fourier-transform algorithm with gradual clipping at the plane of the element, as introduced in Ref. [61]. The encoded structure of the element with K=L=64 and Q=16 is illustrated in Figure 11.5. In

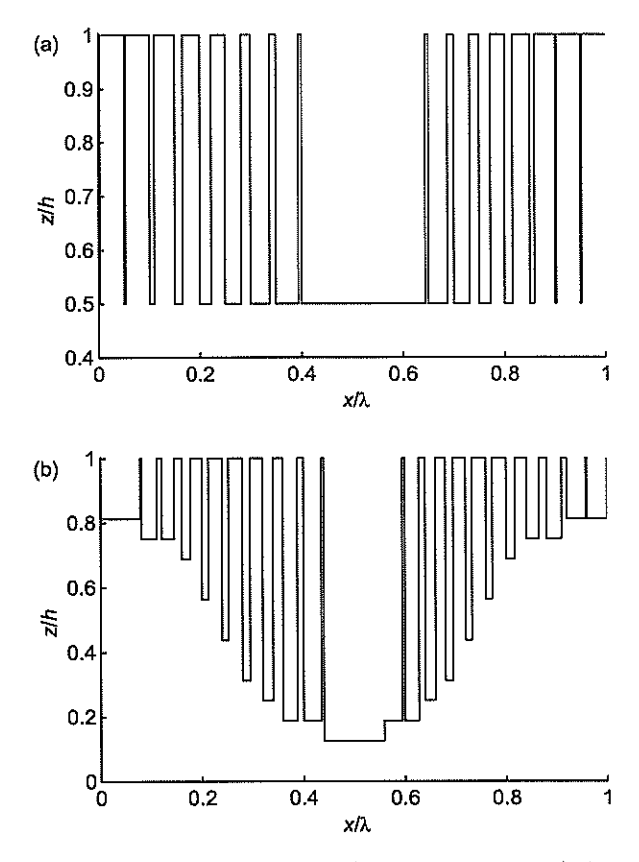
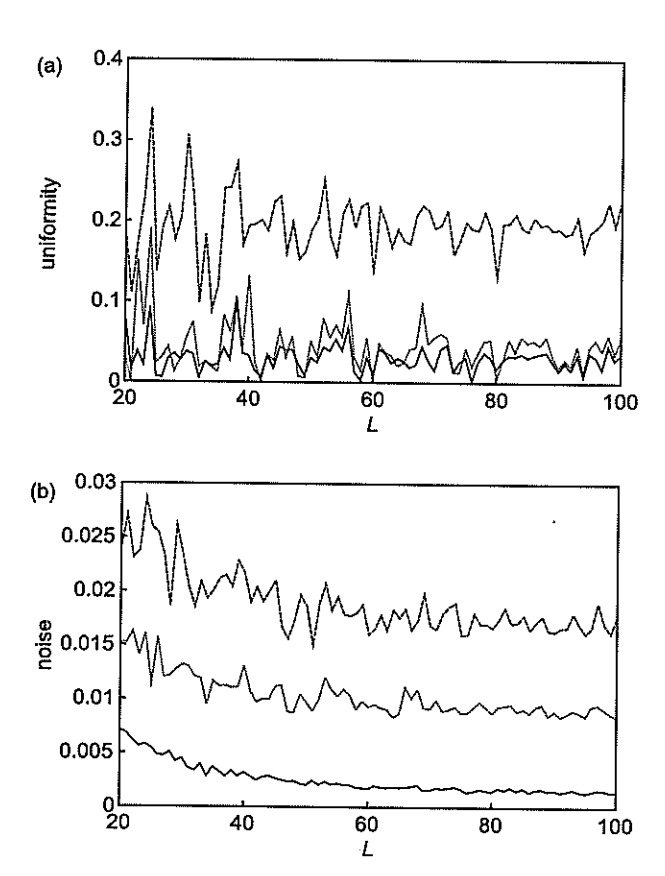


Fig. 11.3: Structures of encoded elements: a) two-point signal, b) three-point signal.

Fig. 11.6 the results of the complex-amplitude transmittance analysis of this element is shown. The noise is defined to contain non-signal orders in the range  $m=-10,\ldots,10$  and  $n=-10,\ldots,10$ . The noise and uniformity are plotted as a function of the number of cells L with different quantizations.

One can easily design diffractive elements which have the same signals as in our previous examples, but higher efficiencies. However, with our encoding method, the noise can be zero in quite a large neighborhood of the signal. The main negative feature in our encoding method is that elements with relatively simple signals, as in our examples (Figs. 11.3 and 11.5), have usually rather complicated structures.



**Fig. 11.4:** (a) Uniformity in  $\mathcal W$  and (b) the combined noise in the 21 central diffraction orders as a function of the number of sampling cells L for the three-beam element with Q=8 (dashed line), Q=16 (dotted line) and Q=32 (solid line).

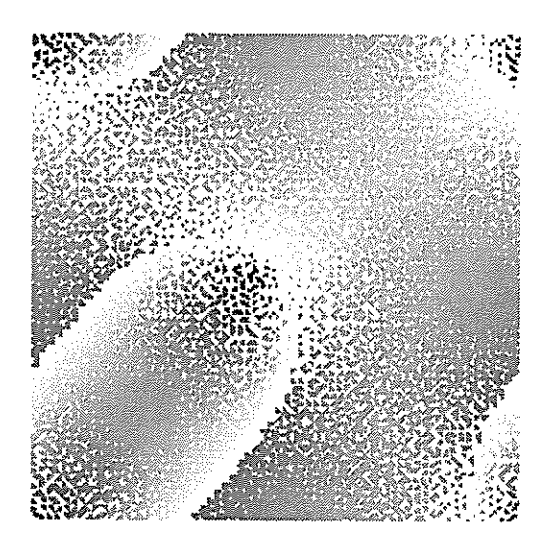


Fig. 11.5: Structure of one period of a  $3 \times 3$ -element: different gray levels indicate profile depth: in the white areas  $h_l = 0$ , and in the black areas  $h_l = h$ .

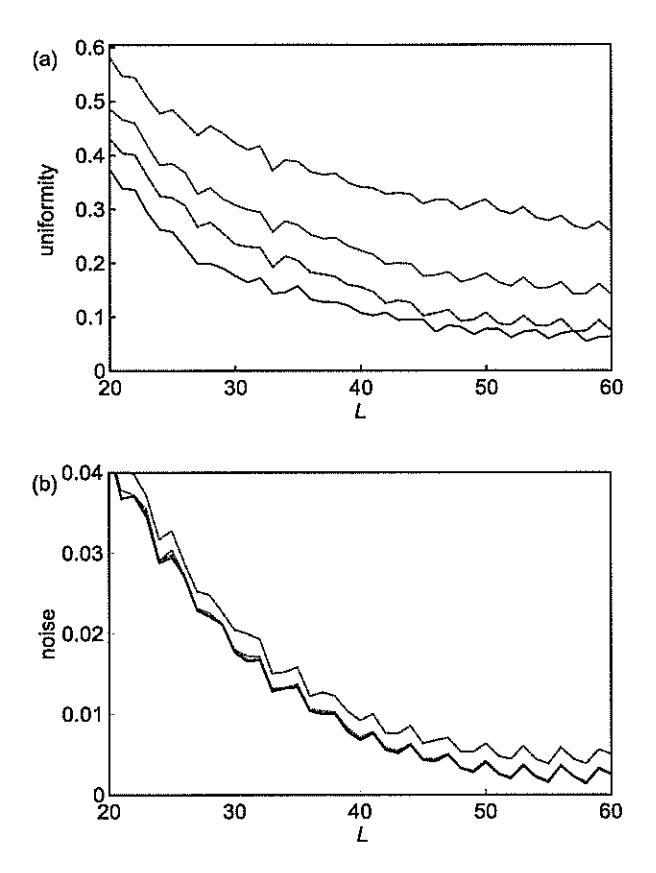


Fig. 11.6: Scalar analysis of (a) uniformity and (b) noise for a  $3\times 3$ -beam-splitter with  $Q=\infty$  (solid line), Q=64 (dashed line), Q=32 (dotted line) and Q=16 (dash-dotted line).

# Chapter 12

# Waveguide analysis with diffractive optics

In this Chapter we apply the rigorous diffraction analysis methods introduced in Chapter 5 to the analysis of modulated dielectric waveguides, which forms the basis of integrated optics [234]. This is achieved by replacing the original waveguide structure with a corresponding periodic element and choosing the period so large that the effect of periodicity becomes insignificant [235]. The advantage is that the spectrum of eigenvalues becomes discrete, which greatly simplifies the analysis. This goal can also be achieved by applying perfectly conducting boundary condition as in Section 6.2 [133]. However, the latter approach leads to somewhat more complicated calculations. Here we analyze the convergence of the mode eigenvalues, the problem of beam focusing into a planar waveguide, and scattering by waveguide discontinuities. Similarly one can investigate, e.g., output coupling [236, 237] directional couplers [238–242] and distributed Bragg reflectors [243, 244].

### 12.1 Waveguide modes

There exist different methods to solve the modes of a waveguide: see, e.g., Refs. [245–250]. Here we solve the modes using the eigenmode method presented in Chapters 5 and 6. We consider a planar waveguide located between a homogeneous substrate (x < 0) and a cover layer  $(x > d_g)$  with refractive indices  $n_s$  and  $n_c$ , respectively (Fig. 12.1), and TE polarization. The refractive index of the waveguide region  $(0 < x < d_g)$  is assumed to be piecewise constant:  $n(x) = n_l$  whenever  $x_l < x < x_{l+1}$ , with  $x_1 = 0$  and  $x_{L+1} = d_g$ .

The field must obey the Helmholtz equation in each homogeneous region and the

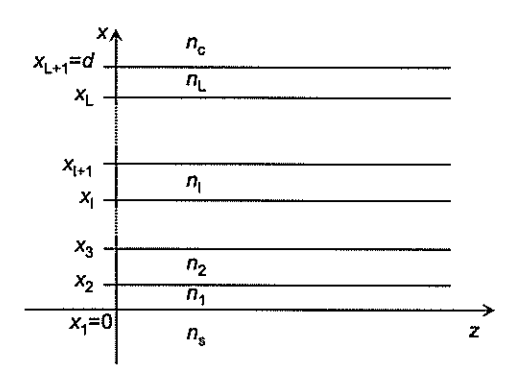


Fig. 12.1: Geometry of a planar waveguide.

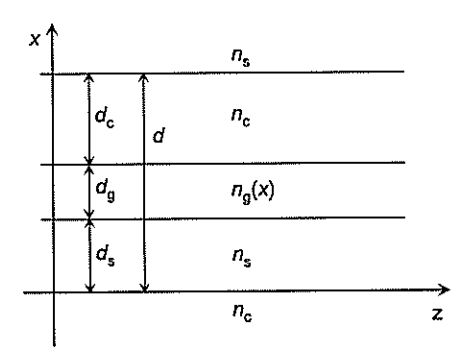


Fig. 12.2: Geometry of a waveguide with periodic boundary conditions

appropriate electromagnetic boundary conditions must be satisfied at each interface. The solution for the guided modes is

$$E_y(x,z) = X(x)Z(z), \tag{12.1}$$

where the function X(x) is

$$X(x) = \begin{cases} a_c \exp\left[-\beta_c(x - d_g)\right] & x > d_g \\ a_l \sin(\beta_l x) + b_l \cos(\beta_l x) & x_l < x < x_{l+1} \\ a_s \exp(\beta_s x) & x < 0, \end{cases}$$
(12.2)

we have defined

$$\beta_c = \sqrt{\gamma^2 - (kn_c)^2},$$
(12.3)
$$\beta_l = \sqrt{(kn_l)^2 - \gamma^2},$$
(12.4)

$$\beta_l = \sqrt{(kn_l)^2 - \gamma^2},\tag{12.4}$$

$$\beta_s = \sqrt{\gamma^2 - (kn_s)^2},\tag{12.5}$$

and the function Z(z) is given by Eq. (5.21). By applying the boundary conditions, one obtains a transcendental equation, which has zeros at  $\gamma = \gamma_m$ . Once the eigenvalues  $\gamma_m$ have been determined, all but one of the amplitudes  $a_s$ ,  $a_l$ ,  $b_l$  and  $a_c$  can be determined from the boundary conditions at  $x = x_l$ . The remaining amplitude is fixed by normalization of the modes  $X_m(x)$ . Similarly, radiating and evanescent modes can be solved. The spectrum of the guided modes is discrete, but the radiating and evanescent modes have continuous spectra.

The idea of replacing the waveguide by a corresponding periodic structure was introduced in Ref. [235]. Let us suppose that the waveguide shown in Fig. 12.1 is replaced by an infinite array of elements as illustrated in Fig. 12.2. The waveguide regions in each period are supposed to be identical with the original waveguide. The thickness of the substrate and cover layers in each period are supposed to be  $d_s$  and  $d_c$ , respectively. Thus the period of the resulting grating is  $d = d_s + d_q + d_c$ . Now the modes can be solved using modal methods introduced in Section 5.4.

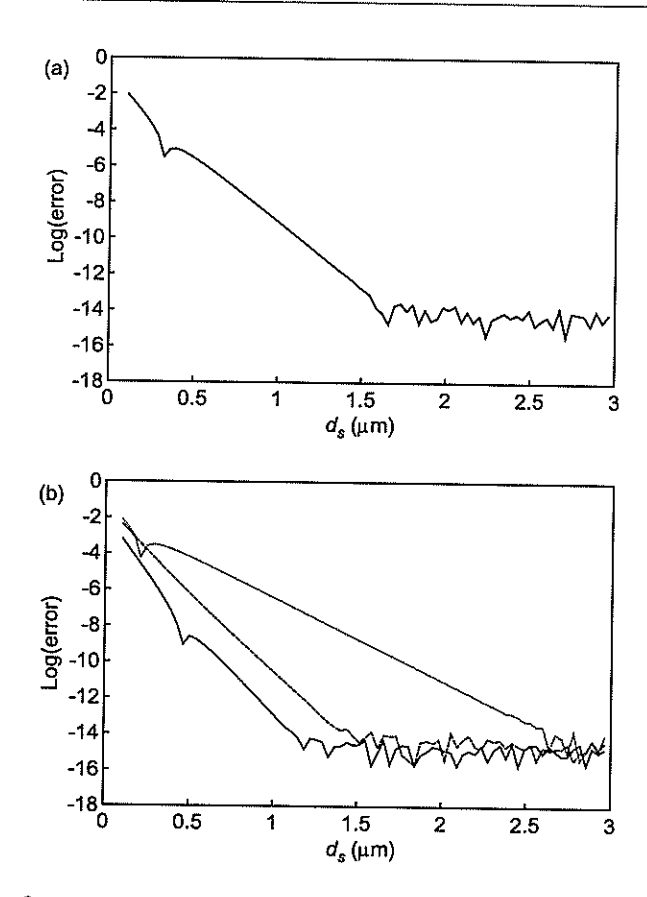


Fig. 12.3: Convergence of the eigenvalues using periodic boundary conditions: The logarithmic error of the eigenvalues when (a)  $d_g=0.21\,\mu\mathrm{m}$ , (b)  $d_g=0.70\,\mu\mathrm{m}$ . Solid lines: m=0. Dashed lines m=1. Dotted lines: m=2.

In Fig. 12.3 the convergence of the eigenvalues  $\gamma_m$  is shown as a function of  $d_s = d_c$ . The quantity log(error) is defined as  $\log |(\gamma_m - \gamma_m^e)/\gamma_m^e|$ , where  $\gamma_m^e$  and  $\gamma_m$  are the exact waveguide eigenvalue and the eigenvalue calculated with periodic boundary conditions, respectively. We have assumed a single-layer waveguide, refractive indices  $n_s = 1.55$ ,  $n_1 = 1.97$ ,  $n_c = 1$ , and  $\lambda = 0.6328~\mu\text{m}$ . The thickness of the waveguide layer is either  $d_g = 0.21~\mu\text{m}$  (single-mode waveguide, Fig. 12.3a) or  $d_g = 0.70~\mu\text{m}$  (three-mode waveguide, Figs. 12.3b). The grating eigenvalues are calculated using the Legendre-polynomial expansion method of the exact eigenmodes, introduced in Section 5.4.2.

## 12.2 Beam coupling into a planar waveguide

Let us consider the coupling of a Gaussian beam into a planar waveguide as illustrated in Fig. 12.2.

For comparison with the quasi-rigorous approach with periodic boundary conditions

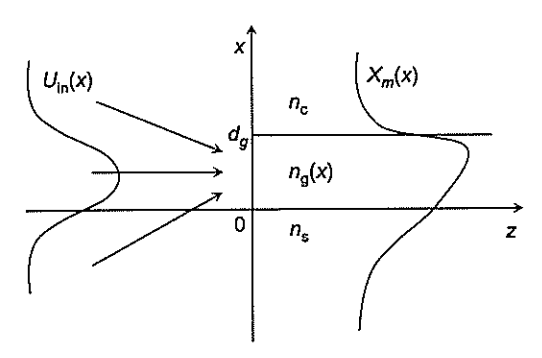


Fig. 12.4: The geometry of waveguide incoupling.

we apply a well-known overlap integral method [243,251]. Since the modes are orthonormal one can represent the incident beam in the base of the modes (provided that the base is complete). Then the coupling efficiency of an incident beam  $U^{\rm in}$  to the mth mode  $X_m(x)$  is

$$\eta = \left| \frac{\int_{-\infty}^{\infty} X_m^*(x) U_{\rm in}(x) dx}{\sqrt{\int_{-\infty}^{\infty} |X_m|^2 dx} \int_{-\infty}^{\infty} |U_{\rm in}(x)|^2 dx} \right|^2. \tag{12.6}$$

With periodic boundary conditions, the efficiency of input coupling can be directly calculated by applying the methods presented in Sections 5.4.4 and 6.3. Rather than having several sampling points in Eq. (6.32), one sampling point is used and the period of the element is increased to guarantee convergence. Thus one can directly apply Eq. (5.46).

In order to calculate the coupling efficiency, we define the energy flow P as

$$P = \int_{-d_*}^{d_g + d_c} \langle S_z(x, z) \rangle \mathrm{d}x, \tag{12.7}$$

where  $S_z(x, z)$  is the z-component of the Poynting vector of either the incident, the reflected or the transmitted field. The coupling efficiency into the mth mode is then

$$\eta_m = P_m / P^{\text{in}} = \frac{\gamma_n |a_n|^2 \sum_{l=-\infty}^{\infty} |P_{ln}|^2}{\sum_{l=-\infty}^{\infty} \Re(r_l) |A_l|^2},$$
(12.8)

where  $P_{ln}$  are the projections defined in Eq. (5.47) and  $A_l$  represent the sampled values of the incident angular spectrum.

We consider the coupling of an incident Gaussian beam into a planar waveguide. The Gaussian beam is written as

$$E_n^{\text{in}}(x,0) = E_0 \exp[-(x-x_0)^2/w^2], \tag{12.9}$$

where  $x_0$  and w define the beam position and width, respectively. In Figs. 12.5 and 12.6 the coupling efficiencies are shown as functions of w and  $x_0$ , using rigorous periodic boundary conditions and the overlap integral method, respectively.

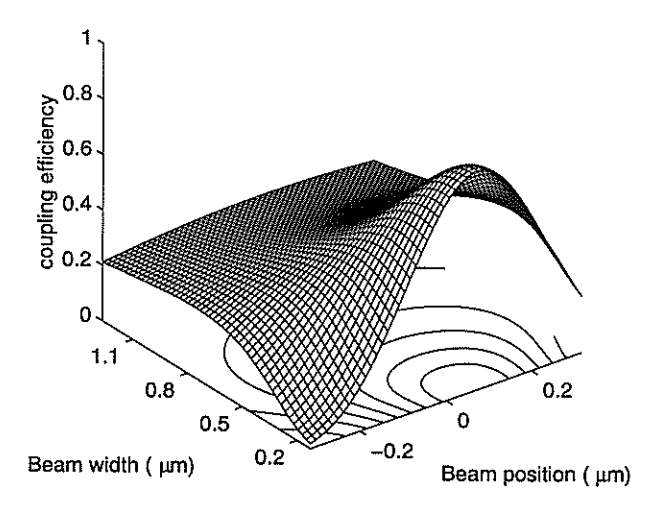


Fig. 12.5: Coupling efficiency as a function of beam width and incident beam position: rigorous grating theory.

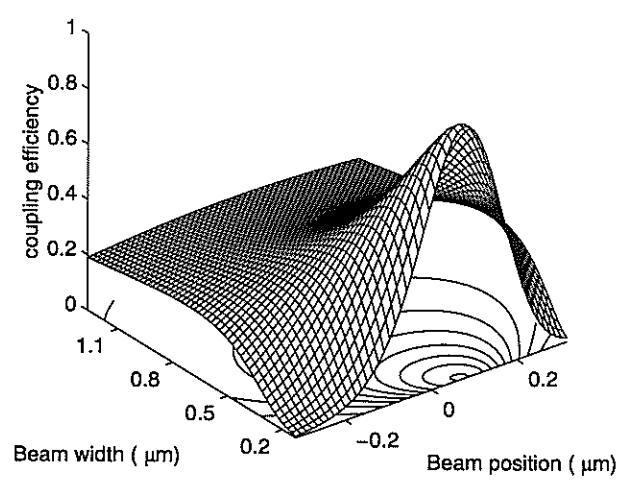


Fig. 12.6: Coupling efficiency as a function of beam width and incident beam position: overlap integral method.

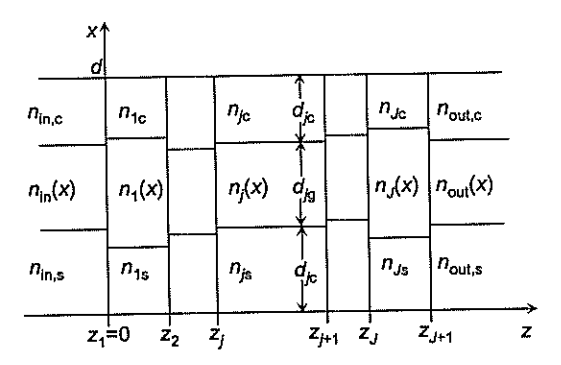


Fig. 12.7: Periodic waveguide with discontinuities.

Figures 12.5 and 12.6 show that the overlap integral method is rather accurate. However, when the width of the beam is narrow its predictions differ significantly from the rigorous results.

## 12.3 Waveguide discontinuities

Several different analysis methods of waveguide discontinuities, such as finite-element and boundary-element methods [252–255], integral methods [256,257], and the method of lines [258], exist. Here we treat similar problems using periodic boundary conditions.

Let us suppose a waveguide with discontinuities at the planes  $z = z_j$ , as in Fig. 12.7. Using the periodic boundary conditions, the modes in each slab  $z_j$  can be solved as shown in Section 5.4, while at each boundary one can apply the continuity expressed in Eq. (5.48). Thus the propagation of the modes is completely described by grating diffraction theory. The energy of each mode in region  $z_j < z < z_{j+1}$  is given by Eq. (12.7).

Let us consider the geometry of Fig. 12.8a. The wavelength is  $\lambda=1.2~\mu\mathrm{m}$  and the incident field contains only the zeroth-order mode. Figures 12.8b and 12.8c illustrate the output phase shift and efficiency. The phase shift is defined as the difference between the phases of the mode at z=h with and without modulation between the planes z=0 and z=h. The approximate value of the phase shift is obtained using the effective index of the mode as

$$\phi = \int_0^h \left[ \gamma_0(z) - \gamma_0^{\text{in}} \right] dz, \tag{12.10}$$

where  $\gamma_m^{\rm in}$  is the mode eigenvalue in the homogeneous regions z < 0 and z > h. Values of  $d_s$  and  $d_c$  are chosen to be sufficiently large to guarantee convergence.

This method also facilitates the analysis of smoothly modulated waveguides. One can then approximate the continuous refractive index distribution by a stack of multi-layer waveguides. In Fig. 12.9 a typical index-modulated waveguide structure is illustrated, which can be fabricated using two consecutive ion-exchange processes [259–261]. In the first step, a slit of width  $h=10~\mu{\rm m}$  is employed to generate the modulated area, and in the second step the basic waveguide refractive index distribution is generated [259, 262, 263]. Here  $n_s=1.523,\,n_c=1,$  and  $d_g=5~\mu{\rm m}.$ 

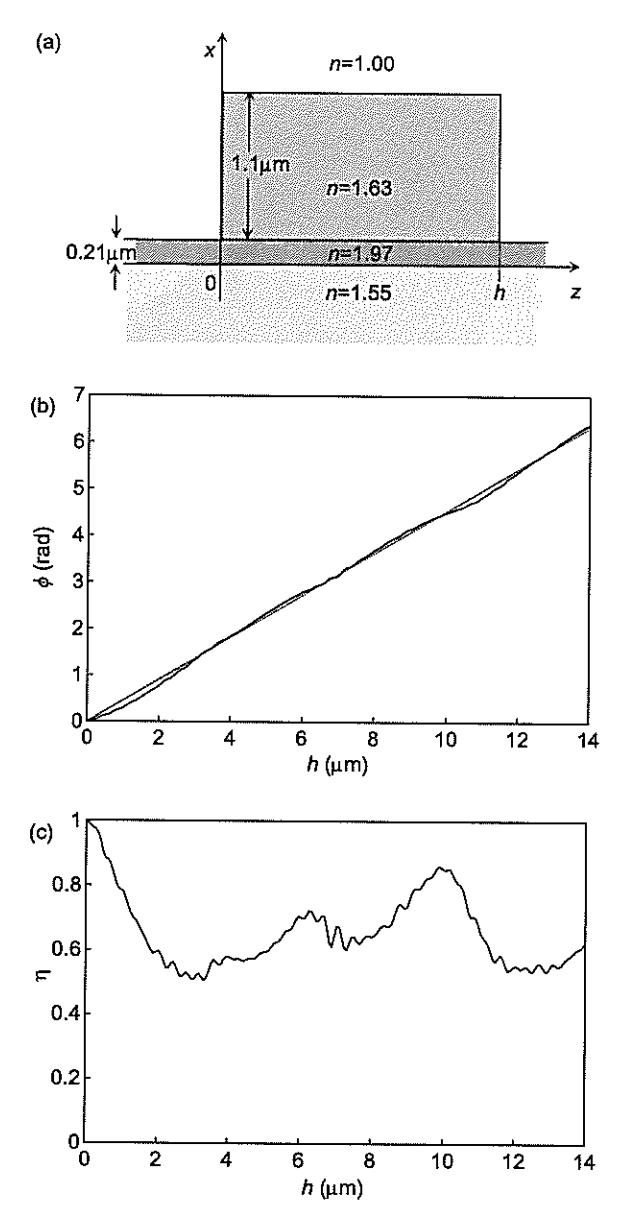


Fig. 12.8: The output of a cover-layer modulated waveguide. (a) The structure of the element and (b) the phase difference. Solid line: rigorous calculation. Dashed line: effective index approximation. (c) Output efficiency.

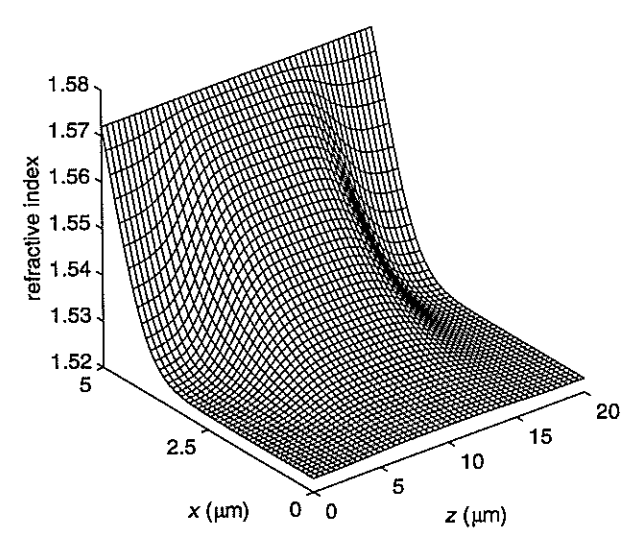
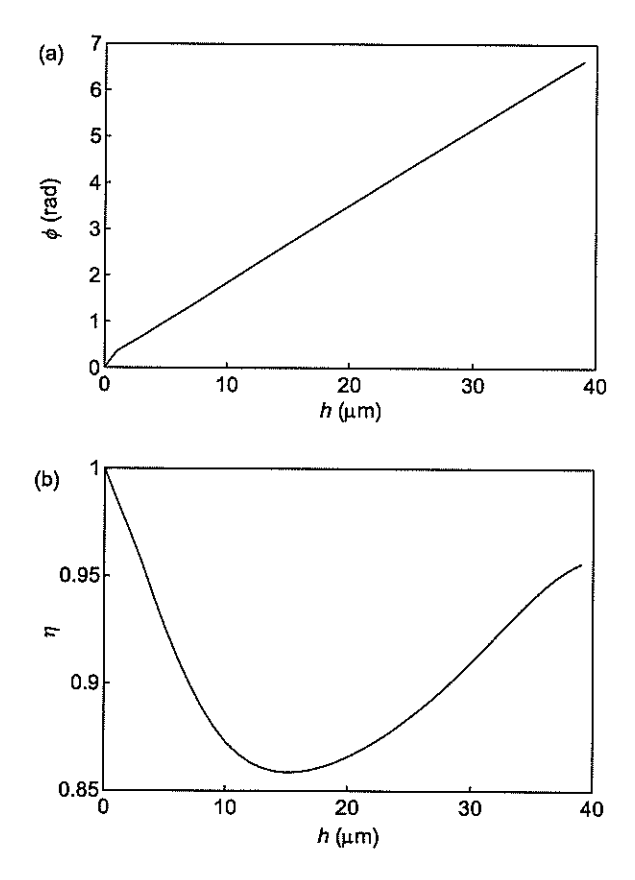


Fig. 12.9: Index-modulated waveguide structure.

In Fig. 12.10 the ion-exchanged modulated structure of Fig. 12.9 is analyzed. The wavelength is  $\lambda=0.6328~\mu\mathrm{m}$ . Again, the convergence was checked by increasing  $d_s$  and  $d_c$ . Values as low as  $d_s\approx d_c\approx 5~\mu\mathrm{m}$  were found to be sufficient.

It was seen that with the ion-exchanged index-modulated waveguide (Fig. 12.10) it is possible to obtain better efficiency than with a cover layer modulated waveguide (Fig.12.8). This is easily understood since with ion-exchanged index-modulated waveguides the change on the refractive index is smoother, eliminating reflections from the boundaries z=0 and z=h. The mathematical analysis of index-modulated waveguides is more complicated numerically. In our example, the element was divided into  $\sim 100$  layers in the z direction, while only three layers were needed with the cover layer modulated waveguide.



 $\textbf{Fig. 12.10:} \ \ \textbf{The output of an ion-exchanged index-modulated waveguide.} \ \ \textbf{(a) The phase difference and (b) the efficiency as a function of the slit width.}$ 

### Outlook

The work presented in this thesis has already led to many further studies.

We have started to design and analyze also 3D multilevel diffractive elements. Such elements, as well as many of those presented in this thesis will be fabricated using electron-beam lithography.

Recently, we have analyzed diffractive lenses using the quasi-rigorous analysis method introduced in Section 10.3.1. This work will be carried out in co-operation with University

of Bergen (Norway).

We also have plans to analyze more complicated waveguide structures, such as Bragg gratings in waveguides, using 3D grating diffraction theory. Experimental investigations of waveguides will be carried out together with Helsinki University of Technology (Finland) and Universidade de Santiago de Compostela (Spain).

It is also planned to continue the work on optical coherence theory in co-operation with University of Rome (Italy).

# Bibliography

- [1] M. Hutley, Diffraction Gratings (Academic Press, London, 1982).
- [2] R. Petit, ed., Electromagnetic Theory of Gratings (Springer-Verlag, Berlin, 1980).
- [3] J. W. Goodman, Introduction to Fourier Optics (McGraw-Hill, New York, 1968).
- [4] T. Stone and N. George, "Hybrid diffractive-refractive lenses and achromats," Appl. Opt. 27, 2960–2971 (1988).
- [5] A. P. Wood, "Design of infrared hybrid refractive-diffractive lenses," Appl. Opt. 31, 2253–2258 (1992).
- [6] N. Davidson, A. A. Friesem, and E. Hasman, "Analytic design of hybrid diffractive-refractive achromats," Appl. Opt. 32, 4770–4774 (1993).
- [7] D. Gabor, "A new microscopic principle," Nature 161, 777-778 (1948).
- [8] E. N. Leith and J. Upatnieks, "Reconstructed wavefronts and communication theory," J. Opt. Soc. Am. 52, 1123–1130 (1962).
- [9] E. N. Leith and J. Upatnieks, "Wavefront reconstruction with diffused illumination and three-dimensional objects," J. Opt. Soc. Am. 54, 1295–1301 (1964).
- [10] E. N. Leith, A. Kozma, J. Upatnieks, J. Marks, and N. Massey, "Holographic data storage in three-dimensional media," Appl. Opt. 5, 1303–1311 (1966).
- [11] H. Nishihara and T. Suhara, "Micro fresnel lenses," in *Progress in Optics*, Vol. XXIV, E. Wolf, ed. (Elsevier, Amsterdam, 1987), pp. 1–37.
- [12] K. Miyamoto, "The phase Fresnel lens," J. Opt. Soc. Am. 51, 17-20 (1961).
- [13] M. H. Horman and H. H. M. Chau, "Zone plate theory based on holography," Appl. Opt. 6, 317–322 (1967).
- [14] M. H. Horman, "Efficiences of zone plates and phase zone plates," Appl. Opt. 6, 2011–2013 (1967).
- [15] B. R. Brown and A. W. Lohmann, "Complex spatial filtering with binary masks," Appl. Opt. 5, 967-969 (1966).

- [16] A. W. Lohmann and D. P. Paris, "Binary Fraunhofer holograms, generated by computer," Appl. Opt. 6, 1739-1748 (1967).
- [17] A. W. Lohmann and D. P. Paris, "Computer generated spatial filters for coherent optical data processing," Appl. Opt. 7, 651-655 (1968).
- [18] H. Dammann, "Computer generated quaternary phase-only holograms," *Phys. Lett.* **29A**, 301–302 (1969).
- [19] H. Dammann, "Phase holograms of diffuse objects," J. Opt. Soc. Am. 60, 1635–1639 (1970).
- [20] H. Dammann, "Blazed synthetic phase-only holograms," Optik 31, 95-104 (1970).
- [21] H. Dammann and K. Görtler, "High-efficiency in-line multiple imaging by means of multiple phase holograms," Opt. Commun. 3, 312–315 (1971).
- [22] L. B. Lesem, P. M. Hirsch, and J. A. Jordan, Jr., "The kinoform: A new wavefront reconstruction device," IBM J. Res. Develop. 13, 150-155 (1969).
- [23] J. A. Jordan, Jr., P. M. Hirsch, L. B. Lesem, and D. L. Van Rooy, "Kinoform lenses," Appl. Opt. 9, 1883–1887 (1970).
- [24] J. P. Kirk and A. L. Jones, "Phase-only complex-valued spatial filter," J. Opt. Soc. Am. 61, 1023–1028 (1971).
- [25] D. Kermisch, "Image reconstruction from phase information only," J. Opt. Soc. Am. 60, 15-17 (1970).
- [26] O. Bryngdahl, "Computer-generated holograms as generalized optical components," Opt. Eng. 14, 426–435 (1975).
- [27] J. Turunen and F. Wyrowski, "Diffractive optics: from promise to fruition," in Trends in Optics: Research, Developments and Applications, Vol. 3, A. Consortini, ed. (Academic Press, San Diego, 1996), pp. 111-123.
- [28] S. P. McGrew, "Hologram counterfeiting: Problems and solutions," Proc. SPIE 1210, 66-76 (1990).
- [29] N. J. Phillips, "Optical security making life expensive for the counterfeiter," Proc. SPIE 1210, 2-13 (1990).
- [30] J. Rolfe, "Optically variable devices for use on bank notes," Proc. SPIE 1210, 14–19 (1990).
- [31] T. Wada, "Applications of computergraphics-image hologram for anticounterfeiting labels," Proc. SPIE 1210, 42–46 (1990).
- [32] M. T. Gale, K. Knop, and R. Morf, "Zero-order diffractive microstructures for security applications," Proc. SPIE 1210, 83-89 (1990).

- [33] C. E. Chesak, "Holographic counterfeit protection," Opt. Commun. 115, 429–436 (1995).
- [34] R. L. van Renesse, ed., Optical Document Security (Artech House, London, 1994).
- [35] J. R. Leger, D. Chen, and Z. Wang, "Diffractive optical element for mode shaping of a Nd:YAG laser," Opt. Lett. 19, 108-110 (1994).
- [36] J. R. Leger, D. Chen, and G. Mowry, "Design and performance of diffractive optics for custom laser resonators," Appl. Opt. 34, 2498-2509 (1995).
- [37] F. Wyrowski and R. Zuidema, "Diffractive interconnection between a high-power Nd:YAG laser and a fiber bundle," Appl. Opt. 33, 6732-6740 (1994).
- [38] S. Heinemann, "Computer generated beam shaping and focusing optical elements for laser material processing," Opt. Commun. 119, 613-622 (1995).
- [39] C. Heine and R. H. Morf, "Submicrometer gratings for solar energy applications," Appl. Opt. 34, 2476–2482 (1995).
- [40] J. Ojeda-Castañeda and G. Ramirez, "Zone plates for zero axial irradiance," Opt. Lett. 18, 87-89 (1993).
- [41] H. P. Herzig, P. Ehbets, J. M. Teijido, K. J. Weible, and H. J. Heimbeck, "Diffractive optical elements for space communication terminals," *Proc. SPIE* 2210, 104-111 (1994).
- [42] P. Blattner, H. P. Herzig, K. J. Weible, J. M. Teijido, H. J. Heimbeck, E. Landenbach, and J. Rogers, "Diffractive optics for compact space communication terminals," J. Mod. Opt. 43, 1473-1484 (1996).
- [43] J. N. Lee and A. Vanderlugt, "Acoustooptic signal processing and computing," Proc. IEEE 77, 1528-1557 (1989).
- [44] C. DeCusatis, P. Das, and D. M. Litynski, "Acousto-electro-optic phase gratings for optical signal processing applications," Appl. Opt. 30, 583-596 (1991).
- [45] Z. He and S. Sato, "Generation of optical Haar wavelets by zone plates," Opt. Lett. 19, 686-688 (1994).
- [46] Ph. Lalanne and P. Chavel, eds., Perspectives for Parallel Optical Interconnects (Springer-Verlag, Berlin, 1993).
- [47] N. Streibl, "Multiple beamsplitters," in Optical Computing Hardware, J. Jahns and S. H. Lee, eds. (Academic Press, Boston, 1994), pp. 227–248.
- [48] T. H. Barnes, T. Eiju, K. Matsuda, H. Ichikawa, M. R. Taghizadeh, and J. Turunen, "Reconfigurable free-space optical interconnections with a phase-only liquid-crystal spatial light modulator," Appl. Opt. 31, 5527-5535 (1992).

- [49] J. Jahns, "Planar packaging of free-space optical interconnections," Proc. IEEE 82, 1623–1631 (1994).
- [50] K. Iga, M. Oikawa, S. Misawa, J. Banno, and Y. Kokubun, "Stacked planar optics: An application of the planar microlens," Appl. Opt. 21, 3456-3460 (1982).
- [51] J. Jahns and A. Huang, "Planar integration of free-space optical components," Appl. Opt. 28, 1602–1607 (1989).
- [52] S. J. Walker, J. Jahns, L. Li, W. M. Mansfield, P. Mulgrew, D. M. Tennart, C. W. Roberts, L. C. West, and N. K. Aitawadi, "Design and fabrication of high-efficiency beam splitters and beam deflectors for integrated planar micro-optic systems," Appl. Opt. 32, 2494–2501 (1993).
- [53] M. G. Moharam and L. Young, "Hologram writing by the photorefractive effect," J. Appl. Phys. 48, 3230-3236 (1977).
- [54] J. Amako, H. Miura, and T. Sonehara, "Wave-front control using liquid-crystal devices," Appl. Opt. 32, 4323-4329 (1993).
- [55] J. Amako, H. Miura, and T. Sonehara, "Speckle-noise reduction on kinoform reconstruction using a phase-only spatial light modulator," Appl. Opt. 34, 3165–3171 (1995).
- [56] M. Kuittinen, P. Vahimaa, M. Honkanen, and J. Turunen, "Beam shaping in the non-paraxial domain of diffractive optics," Appl. Opt. (in press).
- [57] P. Vahimaa and J. Turunen, "Bragg diffraction of spatially partially coherent fields," J. Opt. Soc. Am. A (in press).
- [58] E. von Lau, "Beugungserscheinungen an Doppelrastern," Ann. Phys. 6, 418–423 (1948).
- [59] P. Vahimaa and J. Turunen, "Lau effect: non-paraxial analysis," J. Mod. Opt 43, 1361–1369 (1996).
- [60] J. Turunen, P. Vahimaa, M. Honkanen, O. Salminen, and E. Noponen, "Zeroth-order complex-amplitude modulation with dielectric Fourier-type diffractive elements," J. Mod. Opt. 43, 1389-1398 (1996).
- [61] V. Kettunen, P. Vahimaa, J. Turunen, and E. Noponen, "Zeroth-order coding of complex-amplitude in two dimensions," J. Opt. Soc. Am. A (in press).
- [62] M. Born and E. Wolf, Principles of Optics (Pergamon, Oxford, 1980).
- [63] L. Mandel and E. Wolf, Optical Coherence and Quantum Optics (Cambridge University Press, Cambridge, 1995).
- [64] A. J. Devaney and G. C. Sherman, "Plane-wave representations for scalar wave fields," SIAM Rev. 15, 765-787 (1973).

- [65] A. Roberts and J. E. Murphy, "Evanescent fields with subwavelength features: their behaviour and application to atom optics," Opt. Commun. 128, 41-47 (1996).
- [66] J. J. Stamnes, Waves in Focal Regions (Adam Hilger, Bristol, 1986).
- [67] A. T. Friberg and E. Wolf, "Relationships between the complex degrees of coherence in the space-time and in the space-frequency domains," Opt. Lett. 20, 623-625 (1995).
- [68] E. W. Marchand and E. Wolf, "Radiometry with sources of any state of coherence," J. Opt. Soc. Am. 64, 1219-1226 (1974).
- [69] A. T. Friberg, "On the existence of a radiance function for finite planar sources of arbitrary states of coherence," J. Opt. Soc. Am. 69, 192-198 (1979).
- [70] F. Gori and C. Palma, "Partially coherent sources which give rise to highly directional light beams," Opt. Commun. 27, 185-188 (1978).
- [71] F. Gori, "Directionality and spatial coherence," Opt. Acta 27, 1025-1034 (1980).
- [72] F. Gori, "Collett-wolf sources and multimode lasers," Opt. Commun. 34, 301–305 (1980).
- [73] A. Starikov and E. Wolf, "Coherent-mode representation of Gaussian Schell-model sources and of their radiation fields," J. Opt. Soc. Am. 72, 923-928 (1982).
- [74] S. T. Peng, "Rigorous formulation of scattering and guidance by dielectric grating waveguides: General case of oblique incidence," J. Opt. Soc. Am. A 6, 1869–1883 (1989).
- [75] L. Li, "A modal analysis of lamellar diffraction gratings in conical mountings," J. Mod. Opt. 40, 553-573 (1993).
- [76] L. Li, "Multilayer modal method for diffraction gratings of arbitrary profile, depth, and permittivity," J. Opt. Soc. Am. A 10, 2581-2591 (1993).
- [77] M. G. Moharam, E. B. Grann, D. A. Pommet, and T. K. Gaylord, "Formulation for stable and efficient implementation of the rigorous coupled-wave analysis of binary gratings," J. Opt. Soc. Am. A 12, 1067-1076 (1995).
- [78] P. Vincent, "Differential methods," in *Electromagnetic Theory of Gratings*, R. Petit, ed. (Springer-Verlag, Berlin, 1980), pp. 101–121.
- [79] M. G. Moharam and T. K. Gaylord, "Three-dimensional vector coupled-wave analysis of planar-grating diffraction," J. Opt. Soc. Am. 73, 1105-1112 (1983).
- [80] E. N. Glytsis and T. K. Gaylord, "Rigorous three-dimensional coupled-wave diffraction analysis of single and cascaded anisotropic gratings," J. Opt. Soc. Am. A 4, 2061–2080 (1987).

- [81] R. Bräuer and O. Bryngdahl, "Electromagnetic diffraction analysis of twodimensional gratings," Opt. Commun. 100, 1-5 (1993).
- [82] E. Noponen and J. Turunen, "Eigenmode method for electromagnetic synthesis of diffractive elements with three-dimensional profiles," J. Opt. Soc. Am. A 11, 2494– 2502 (1994).
- [83] D. Maystre, "Rigorous vector theories of diffraction gratings," in Progress in Optics, Vol. XXI, E. Wolf, ed. (North-Holland, Amsterdam, 1984), pp. 1-67.
- [84] T. K. Gaylord and M. G. Moharam, "Analysis and applications of optical diffraction by gratings," Proc. IEEE 73, 894-937 (1985).
- [85] J. J. Hanak and J. P. Russell, "Permanent holograms in glass by RF sputter etching," RCA Rev. 32, 319–325 (1971).
- [86] H. W. Lehmann, "Profile control by reactive ion etching," J. Vac. Sci. Technol. 15, 319–326 (1978).
- [87] J. S. Chang, "Selective reactive ion etching of silican dioxide," Solid State Technol. 4, 214-218 (1984).
- [88] M. Haruna, M. Takahashi, K. Wakahayashi, and H. Nishihara, "Laser beam lithographed micro-fresnel lenses," Appl. Opt. 29, 5120-5126 (1990).
- [89] M. T. Gale, G. K. Lang, J. M. Raynor, H. Schütz, and D. Prongué, "Fabrication of kinoform structures for optical computing," Appl. Opt. 31, 5712-5714 (1993).
- [90] H. Nishihara, Y. Handa, T. Suhara, and J. Koyama, "Direct writing of optical gratings using a scanning electron microscope," Appl. Opt. 17, 2342-2345 (1978).
- [91] S. M. Arnold, "Electron beam fabrication of computer-generated holograms," Opt. Eng. 24, 803-807 (1985).
- [92] P. B. Fischer and S. Y. Chou, "Sub-50 nm high aspect-ratio silicon pillars, ridges, and trenches fabricated using ultrahigh resolution electron beam lithography and reactive ion etching," *Appl. Phys. Lett.* **62**, 1414–1416 (1993).
- [93] M. T. Gale, M. Rossi, H. Schütz, P. Ehbets, H. P. Herzig, and D. Prongué, "Continuous-relief diffractive optical elements for two-dimensional array generation," Appl. Opt. 32, 2526-2533 (1993).
- [94] M. Ekberg, M. Larsson, S. Hård, and B Nilsson, "Multilevel phase holograms manufactured by electron beam lithography," Opt. Lett. 15, 568-569 (1990).
- [95] J. M. Stauffer, Y. Oppliger, P. Regnault, L. Baraldi, and M. T. Gale, "Electron beam writing of continuous resist profiles for optical applications," J. Vac. Sci. Technol. B 10, 2526-2529 (1992).

- [96] R. Waldhäusl, P. Dannberg, E. B. Kley, A. Bräuer, and W. Karthe, "Highly efficient blazed grating couplers in planar polymer waveguides," Int. J. Optoel. 8, 529–536 (1993).
- [97] M. Ekberg, F. Nikolajeff, M. Larsson, and S. Hård, "Proximity-compensated blazed transmission grating manufacture with direct-writing, electron-beam lithography," Appl. Opt. 33, 103-107 (1994).
- [98] R. J. Collier, C. B. Burckhardt, and L. H. Lin, Optical Holography (Academic Press, New York, 1971).
- [99] L. Solymar and D. J. Cooke, Volume Holography and Volume Gratings (Academic Press, London, 1981).
- [100] P. Hariharan, Optical Holography (Cambridge University Press, Cambridge, 1984).
- [101] D. Maystre, "Integral methods," in *Electromagnetic Theory of Gratings*, R. Petit, ed. (Springer-Verlag, Berlin, 1980), pp. 63–100.
- [102] D. Nyyssonen and C. P. Kirk, "Optical microscope imaging of lines patterned in thick layers with variable edge geometry: Theory," J. Opt. Soc. Am. A 5, 1270–1280 (1988).
- [103] D. Maystre and R. Petit, "Diffraction par un reseau lamellaire infiniment conducteur," Opt. Commun. 5, 90-93 (1972).
- [104] L. C. Botten, M. S. Craig, and R. C. McPhedran, "Highly conducting lamellar diffraction gratings," Opt. Acta 28, 1103-1106 (1981).
- [105] L. C. Botten, M. S. Craig, R. C. McPhedran, J. L. Adams, and J. R. Andrewartha, "The finitely conducting lamellar diffraction grating," Opt. Acta 28, 1087-1102 (1981).
- [106] L. C. Botten, M. S. Craig, R. C. McPhedran, J. L. Adams, and J. R. Andrewartha, "The dielectric lamellar diffraction grating," Opt. Acta 28, 413-428 (1981).
- [107] J. M. Miller, J. Turunen, E. Noponen, A. Vasara, and M. R. Taghizadeh, "Rigorous modal theory for multiply grooved lamellar gratings," Opt. Commun. 111, 526-535 (1994).
- [108] H. P. Herzig, M. T. Gale, H. W. Lehmann, and R. Morf, "Diffractive components: computer-generated elements," in *Perspectives for Parallel Optical Interconnects*, Ph. Lalanne and P. Chavel, eds. (Springer-Verlag, Berlin, 1993), pp. 71-107.
- [109] R. H. Morf, "Exponentially convergent and numerically efficient solution of Maxwell's equations for lamellar gratings," J. Opt. Soc. Am. A 12, 1043–1056 (1995).
- [110] G. Arfken, Mathematical Methods for Physicists (Academic Press, San Diego, 1985).

[111] C. B. Burckhardt, "Diffraction of a plane wave at a sinusoidally stratified dielectric grating," J. Opt. Soc. Am. 56, 1502–1509 (1966).

98

- [112] C. B. Burckhardt, "Efficiency of a dielectric grating," J. Opt. Soc. Am. 57, 601–603 (1967).
- [113] F.G. Kaspar, "Diffraction by thick, periodically stratified gratings with complex dielectric constant," J. Opt. Soc. Am. 63, 37-45 (1973).
- [114] K. Knop, "Rigorous diffraction theory for transmission phase gratings with deep rectangular grooves," J. Opt. Soc. Am. 68, 1206-1210 (1978).
- [115] T. Tamir and H. C. Wang, "Scattering of electromagnetic waves by a sinusoidally stratified half-space. I. Formal solution and analytic approximations," Can. J. Phys. 44, 2073–2094 (1966).
- [116] T. Tamir, "Scattering of electromagnetic waves by a sinusoidally stratified half-space. II. Diffraction aspects at the Rayleigh and Bragg wavelengths," Can. J. Phys. 44, 2461–2494 (1966).
- [117] L. Li and C. W. Haggans, "Convergence of the coupled-wave method for metallic lamellar diffraction gratings," J. Opt. Soc. Am. A 10, 1184–1189 (1993).
- [118] G. Granet and B. Guizal, "Efficient implementation of the coupled-wave method for metallic lamellar gratings in TM polarization," J. Opt. Soc. Am. A 13, 1019–1023 (1996).
- [119] P. Lalanne and G. M. Morris, "Highly improved convergence of the coupled-wave method for TM polarization," J. Opt. Soc. Am. A 13, 779-784 (1996).
- [120] L. Li, "Use of Fourier series in the analysis of discontinuous periodic structures," J. Opt. Soc. Am. A 13, 1870-1876 (1996).
- [121] M. G. Moharam, D. A. Pommet, E. B. Grann, and T. K. Gaylord, "Stable implementation of the rigorous coupled-wave analysis for surface-relief gratings: enhanced transmittance matrix approach," J. Opt. Soc. Am. A 12, 1077-1086 (1995).
- [122] G. Tayeb and R. Petit, "On the numerical study of deep conducting lamellar diffraction gratings," Opt. Acta 31, 1361-1365 (1984).
- [123] M. G. Moharam and T. K. Gaylord, "Rigorous coupled-wave analysis of planar-grating diffraction," J. Opt. Soc. Am. 71, 811-818 (1981).
- [124] M. G. Moharam and T. K. Gaylord, "Diffraction analysis of dielectric surface-relief gratings," J. Opt. Soc. Am. 72, 1385–1392 (1982).
- [125] K. Rokushima and J. Yamakita, "Analysis of anisotropic dielectric gratings," J. Opt. Soc. Am. 73, 901–908 (1983).

- [126] T. Delort and D. Maystre, "Finite-element method for gratings," J. Opt. Soc. Am. A 10, 2592-2601 (1993).
- [127] M. S. Miratznik, D. W. Prather, and J. N. Mait, "A hybrid finite element-boundary element method for the analysis of diffractive elements," J. Mod. Opt. 43, 1309–1321 (1996).
- [128] B. H. Kleeman, A. Mitreiter, and F. Wyrowski, "Integral equation method with parametrization of grating profile: Theory and experiments," J. Mod. Opt 43, 1323– 1349 (1996).
- [129] J. J. Greffet, "Scattering of s-polarized electromagnetic waves by a 2D obstacle near an interface," Opt. Commun. 72, 274–278 (1989).
- [130] A. Sentenac and J. J. Greffet, "Scattering by deep inhomogeneous gratings," J. Opt. Soc. Am. A 9, 996-1006 (1992).
- [131] A. Roberts, "Electromagnetic theory of diffraction by a circular aperture in a thick, perfectly conducting screen," J. Opt. Soc. Am. A 4, 1970–1983 (1987).
- [132] Y. L. Kok, "Boundary-value solution to electromagnetic scattering by a rectangular groove in a ground plane," J. Opt. Soc. Am. A 9, 302-311 (1992).
- [133] M. Kuittinen and J. Turunen, "Exact eigenmode model for index-modulated apertures," J. Opt. Soc. Am. A 13, 2014-2020 (1996).
- [134] J. Huttunen and J. Turunen, "Scattering of partially coherent electromagnetic fields by microstructured media," Phys. Rev. E. 52, 3081-3092 (1995).
- [135] C. V. Raman and N. S. N. Nath, "The diffraction of light by high frequency sound waves: Part I," Proc. Ind. Acad. Sci. A 2, 406-412 (1935).
- [136] C. V. Raman and N. S. N. Nath, "The diffraction of light by high frequency sound waves: Part II," Proc. Ind. Acad. Sci. A 2, 413-420 (1935).
- [137] C. V. Raman and N. S. N. Nath, "The diffraction of light by high frequency sound waves: Part III," Proc. Ind. Acad. Sci. A 3, 75-84 (1936).
- [138] C. V. Raman and N. S. N. Nath, "The diffraction of light by high frequency sound waves: Part IV," Proc. Ind. Acad. Sci. A 3, 119-125 (1936).
- [139] S. M. Rytov, "Electromagnetic properties of a finely stratified medium," Sov. Phys. JETP 2, 466-475 (1956).
- [140] H. Kikuta, H. Yoshida, and K. Iwata, "Ability and limitation of effective medium theory for subwavelength gratings," Opt. Rev. 2, 92–99 (1995).
- [141] E. Noponen, J. Turunen, and A. Vasara, "Parametric optimization of multilevel diffractive optical elements by electromagnetic theory," Appl. Opt. 31, 5910-5912 (1992).

- [142] D. A. Pommet, M. G. Moharam, and E. B. Grann, "Limits of scalar diffraction theory for diffractive phase elements," J. Opt. Soc. Am. A 11, 1827–1834 (1994).
- [143] N. Rajkumar and J. N. McMullin, "V-groove gratings on silicon for infrared beam splitting," Appl. Opt. 34, 2556–2559 (1995).
- [144] J. Turunen and E. Noponen, "V-groove gratings on silicon for infrared beam splitting: comment," Appl. Opt. 35, 807–808 (1996).
- [145] H. Kogelnik, "Coupled wave theory for thick hologram gratings," Bell Syst. Techn. J. 48, 2909–2947 (1969).
- [146] W. R. Klein and B. D. Cook, "Unified approach to ultrasonic light diffraction," IEEE Trans. Sonics Ultrason. SU-14, 123-134 (1967).
- [147] A. Korpel, Acousto-optics (Marcel Dekker, Inc., New York, 1988).
- [148] F. Wyrowski and O. Bryngdahl, "Digital holography as part of diffractive optics," Rep. Prog. Phys. 54, 1481-1571 (1991).
- [149] F. Wyrowski, "Upper bound of the diffraction efficiency of diffractive phase elements," Opt. Lett. 16, 1915–1917 (1991).
- [150] F. Wyrowski, "Design theory of diffractive elements in the paraxial domain," J. Opt. Soc. Am. A 10, 1553-1561 (1993).
- [151] H. Lüpken, T. Peter, F. Wyrowski, and O. Bryngdahl, "Phase synthesis for array illuminator," Opt. Commun. 91, 163-167 (1992).
- [152] U. Krackhardt, J. N. Mait, and N. Streibl, "Upper bound on the diffraction efficiency of phase-only fan-out elements," Appl. Opt. 31, 27-37 (1992).
- [153] J. Cederquist and A. M. Tai, "Computer-generated holograms for geometric transformations," Appl. Opt. 23, 3099-3104 (1984).
- [154] O. Bryngdahl, "Geometrical transformations in optics," J. Opt. Soc. Am. 64, 1092– 1098 (1974).
- [155] O. Bryngdahl, "Optical map transformations," Opt. Commun. 10, 164-168 (1974).
- [156] N. Davidson, A. A. Friesem, and E. Hasman, "Optical coordinate transformations," Appl. Opt. 31, 1067–1073 (1992).
- [157] I. Powell, "Ray tracing through systems containing holographic optical elements," Appl. Opt. 31, 2259-2264 (1992).
- [158] M. A. Seldowitz, J. P. Allebach, and D. W. Sweeney, "Synthesis of digital holograms by direct binary search," Appl. Opt. 26, 2788–2798 (1987).
- [159] S. Kirkpatrick, C. D. Gelatt, Jr., and M. P. Vecchi, "Optimization by simulated annealing," Science 220, 671-680 (1983).

- [160] K. A. Winick and J. R. Fienup, "Optimum holographic elements recorded with nonspherical wave fronts," J. Opt. Soc. Am. 73, 208-217 (1983).
- [161] J. N. Cederquist and J. R. Fienup, "Analytic design of optimum holographic optical elements," J. Opt. Soc. Am. A 4, 699-705 (1987).
- [162] R. W. Gerchberg and W. O. Saxton, "A practical algorithm for the determination of phase from image and diffraction plane pictures," Optik 35, 237-246 (1972).
- [163] N. C. Gallagher and B. Liu, "Method for computing kinoforms that reduces image reconstruction error," Appl. Opt. 12, 2328-2335 (1973).
- [164] H. Akahori, "Spectrum leveling by an iterative algorithm with a dummy area for synthesizing the kinoform," Appl. Opt. 25, 802-811 (1986).
- [165] J. R. Fienup, "Phase retrieval algorithms: A comparison," Appl. Opt. 21, 2758–2769 (1982).
- [166] F. Wyrowski and O. Bryngdahl, "Iterative Fourier-transform algorithm applied to computer holography," J. Opt. Soc. Am. A 5, 1058–1065 (1988).
- [167] M. W. Farn, "New iterative algorithm for the design of phase-only gratings," Proc. SPIE 1555, 34-42 (1991).
- [168] G. Z. Yang, B. Z. Dong, B. Y. Gu, J. Y. Zhuang, and O. K. Ersoy, "Gerchberg-Saxton and Yang-Gu algorithms for phase retrieval in a nonunitary transform system: A comparison," Appl. Opt. 33, 209-218 (1994).
- [169] X. Tan, B. Y. Gu, G. Z. Yang, and B. Z. Dong, "Diffractive phase elements for beam shaping: A new design method," Appl. Opt. 34, 1314-1320 (1995).
- [170] R. G. Dorsch, A. W. Lohmann, and S. Sinzinger, "Fresnel ping-pong algorithm for two-plane computer-generated hologram display," Appl. Opt. 33, 869-875 (1994).
- [171] E. Noponen, A. Vasara, J. Turunen, J. M. Miller, and M. R. Taghizadeh, "Synthetic diffractive optics in the resonance domain," J. Opt. Soc. Am. A 9, 1206-1213 (1992).
- [172] F. Wyrowski, "Iterative quantization of digital amplitude holograms," Appl. Opt. 28, 3864–3870 (1989).
- [173] F. Wyrowski and O. Bryngdahl, "Speckle-free reconstruction in digital holography," J. Opt. Soc. Am. A 6, 1171–1174 (1989).
- [174] P. DeSantis, F. Gori, G. Guattari, and C. Palma, "An example of a Collett-Wolf source," Opt. Commun. 29, 256–260 (1979).
- [175] J. D. Farina, L. M. Narducci, and E. Collett, "Generation of highly directional beams from a globally incoherent source," Opt. Commun. 32, 203-208 (1980).

- [176] Q. He, J. Turunen, and A. T. Friberg, "Propagation and imaging experiments with Gaussian Schell-model beams," Opt. Commun. 67, 245-250 (1988).
- [177] Y. Ohtsuka, "Modulation effects of a sound wave on the mutual coherence function of light," Opt. Commun. 17, 234-237 (1976).
- [178] Y. Ohtsuka, "Partial coherence of light modified by a frequency-modulated ultrasonic wave," Opt. Commun. 35, 4–8 (1980).
- [179] Y. Ohtsuka and Y. Nozoe, "Two-dimensional control of optical spatial coherence by acoustooptic interactions," Appl. Opt. 22, 3630-3636 (1983).
- [180] Y. Ohtsuka, Y. Arima, and Y. Imai, "Acoustooptic 2-D profile shaping of a Gaussian laser beam," Appl. Opt. 24, 2813–2819 (1985).
- [181] Y. Imai and Y. Ohtsuka, "Source of light with spatially periodic coherence and its uses in image addition or subtraction," J. Opt. Soc. Am. A 3, 1263-1267 (1986).
- [182] Y. Ohtsuka, "Modulation of optical coherence by ultrasonic waves," J. Opt. Soc. Am. A 3, 1247–1257 (1986).
- [183] D. Courjon, J. Bulabois, and W. H. Carter, "Use of a holographic filter to modify the coherence of a light field," J. Opt. Soc. Am. 71, 469-473 (1981).
- [184] E. Noponen and J. Turunen, "Binary high-frequency-carrier diffractive optical elements: Electromagnetic theory," J. Opt. Soc. Am. A 11, 1097-1109 (1994).
- [185] H. F. Talbot, "Facts relating to optical sciense," Phil. Mag. 9, 3B, 402-407 (1836).
- [186] J. Durnin, J. J. Miceli, Jr., and J. H. Eberly, "Diffraction-free beams," Phys. Rev. Lett. 58, 1499-1501 (1987).
- [187] J. Durnin, "Exact solutions for nondiffracting beams. I. The scalar theory," J. Opt. Soc. Am. A 4, 651–654 (1987).
- [188] J. Turunen, A. Vasara, and A. T. Friberg, "Holographic generation of diffraction-free beams," Appl. Opt. 27, 3959-3962 (1988).
- [189] K. Patorski, "The self-imaging phenomenon and its applications," in Progress in Optics, Vol. XXVII, E. Wolf, ed. (Elsevier, Amsterdam, 1989), pp. 1–108.
- [190] A. W. Lohmann, "An array illuminator based on the Talbot effect.," Optik 79, 41–45 (1988).
- [191] A. W. Lohmann and J. A. Thomas, "Making an array illuminator based on the Talbot effect," Appl. Opt. 29, 4337-4340 (1990).
- [192] P. Szwaykowski and V. Arrizón, "Talbot array illuminator with multilevel phase gratings," Appl. Opt. 32, 1109–1113 (1993).

- [193] J. R. Leger and G. J. Swanson, "Efficient array illuminator using binary-optics phase plates at fractional-Talbot planes," Opt. Lett. 15, 288-290 (1990).
- [194] V. Arrizón and J. Ojeda-Castañeda, "Talbot array illuminators with binary phase gratings," Opt. Lett. 18, 1–3 (1993).
- [195] J. Ibarra and J. Ojeda-Castañeda, "Talbot interferometry: A new geometry," Opt. Commun. 96, 294–301 (1993).
- [196] P. M. Mejías and R. M. Herrero, "Diffraction by one-dimensional Ronchi grids: On the validity of the Talbot effect," J. Opt. Soc. Am. A 8, 266-269 (1991).
- [197] E. Noponen and J. Turunen, "Electromagnetic theory of Talbot imaging," Opt. Commun. 98, 132-140 (1993).
- [198] F. Gori, "Lau effect and coherence theory," Opt. Commun. 31, 4-8 (1979).
- [199] R. Sudol and B. J. Thompson, "An explanation of the Lau effect based on coherence theory," Opt. Commun. 31, 105-110 (1979).
- [200] J. Jahns and A. W. Lohmann, "The Lau effect (A diffraction experiment with incoherent illumination)," Opt. Commun. 28, 263-267 (1979).
- [201] R. Sudol and B. J. Thompson, "Lau effect: Theory and experiment," Appl. Opt. 20, 1107-1116 (1981).
- [202] G. J. Swanson and E. N. Leith, "Lau effect and grating imaging," J. Opt. Soc. Am. 72, 552-555 (1982).
- [203] C. Colautti, L. M. Zerbino, E. E. Sicre, and M. Garavaglia, "Lau effect using circular gratings," Appl. Opt. 26, 2061–2062 (1987).
- [204] K. Hane, S. Hattori, and C. P. Grover, "Lau effect in reflection," J. Mod. Opt. 34, 1481–1490 (1987).
- [205] F. Yu, Y. Liang, Z. Li, and L. Liu, "Lau effect of a skew-periodic object: Theoretical and experimental investigation," J. Opt. Soc. Am. A 9, 2013-2020 (1992).
- [206] H. O. Bartelt and Y. Li, "Lau interferometry with cross gratings," Opt. Commun. 48, 1-6 (1983).
- [207] H. O. Bartelt and J. Jahns, "Interferometry based on the Lau effect," Opt. Commun. 30, 268-274 (1979).
- [208] N. Bolognini, J. Ojeda-Castañeda, and E. E. Sicre, "Interferometry based on the Lau effect a quasi-ray description," Opt. Acta 32, 409-422 (1985).
- [209] J. Jahns, A. W. Lohmann, and J. Ojeda-Castañeda, "Talbot and Lau effects, a parageometrical approach," Opt. Acta 31, 313–324 (1984).

- [210] L. Liu, "Partially coherent diffraction effect between Lau and Talbot effects," J. Opt. Soc. Am. A 5, 1709–1716 (1988).
- [211] L. Liu, "Talbot and Lau effects on incident beams of arbitrary wavefront, and their use," Appl. Opt. 28, 4668-4678 (1989).
- [212] J. Turunen, A. Vasara, and A. T. Friberg, "Propagation invariance and self-imaging in variable-coherence optics," J. Opt. Soc. Am. A 8, 282–289 (1991).
- [213] A. T. Friberg, A. Vasara, and J. Turunen, "Partially coherent propagation-invariant beams: Passage through paraxial optical systems," *Phys. Rev. A*. 43, 7079-7082 (1991).
- [214] G. Indebetouw, "Nondiffracting optical fields: some remarks on their analysis and synthesis," J. Opt. Soc. Am. A 6, 150–152 (1989).
- [215] J. H. McLeod, "The axicon: A new type of optical element," J. Opt. Soc. Am. 44, 592-597 (1954).
- [216] J. H. McLeod, "Axicons and their uses," J. Opt. Soc. Am. 50, 166-169 (1960).
- [217] H. Haidner, P. Kipfer, W. Stork, and N. Streibl, "Zero-order gratings used as an artificial distributed index medium," Optik 89, 107–112 (1992).
- [218] H. Haidner, P. Kipfer, and N. Streibl, "Optimization and reconstruction of high-frequency surface relief gratings," Optik 90, 32-36 (1992).
- [219] H. Haidner, J. T. Sheridan, J. Schwider, and N. Streibl, "Design of a blazed grating consisting of metallic subwavelength binary grooves," Opt. Commun. 98, 5-10 (1993).
- [220] H. Haidner, P. Kipfer, J. T. Sheridan, J. Schwider, N. Streibl, M. Collishon, J. Hut-fless, and M. März, "Diffraction grating with rectangular grooves exceeding 80% diffraction efficiency," *Infrared Phys.* 34, 467-475 (1993).
- [221] H. Haidner, J. T. Sheridan, and N. Streibl, "Dielectric binary blazed gratings," Appl. Opt. 32, 4276-4278 (1993).
- [222] M. W. Farn, "Binary gratings with increased efficiency," Appl. Opt. 31, 4453-4458 (1992).
- [223] W. Stork, N. Streibl, H. Haidner, and P. Kipfer, "Artificial distributed-index media fabricated by zero-order gratings," Opt. Lett. 16, 1921–1923 (1991).
- [224] I. Richter, P. C. Sun, F. Xu, and Y. Fainman, "Design considerations of form birefringent microstructures," Appl. Opt. 34, 2421-2429 (1995).
- [225] F. Xu, J. E. Ford, and Y. Fainman, "Polarization-selective computer-generated holograms: Design, fabrication, and applications," Appl. Opt. 34, 256-266 (1995).

- [226] J. E. Ford, F. Xu, K. Urquhart, and Y. Fainman, "Polarization-selective computer-generated holograms," Opt. Lett. 18, 456–458 (1993).
- [227] E. N. Glytsis and T. K. Gaylord, "High-spatial-frequency binary and multilevel stairstep gratings: Polarization-selective mirrors and broadband antireflection surfaces," Appl. Opt. 31, 4459-4470 (1992).
- [228] S. S. Wang, R. Magnusson, J. S. Bagby, and M. G. Moharam, "Guided-mode resonances in planar dielectric-layer diffraction gratings," J. Opt. Soc. Am. A 7, 1470–1474 (1990).
- [229] S. S. Wang and R. Magnusson, "Theory and applications of quided-mode resonance filters," Appl. Opt. 32, 2606–2613 (1993).
- [230] R. Magnusson and S. S. Wang, "Transmission bandpass guided-mode resonance filters," Appl. Opt. 34, 8106-8109 (1995).
- [231] S. S. Wang and R. Magnusson, "Multilayer waveguide-grating filters," Appl. Opt. 34, 2414–2420 (1995).
- [232] J. Saarinen, E. Noponen, and J. Turunen, "Guided-mode resonance filters of finite aperture," Opt. Eng. 34, 2560-2566 (1995).
- [233] D. C. Chu, J. R. Fienup, and J. W. Goodman, "Multiemulsion on-axis computer generated hologram," Appl. Opt. 12, 1386-1388 (1973).
- [234] T. Tamir, Integrated Optics (Springer-Verlag, Berlin, 1979).
- [235] T. Hosono, T. Hinata, and A. Inoue, "Numerical analysis of the discontinuities in slab dielectric waveguides," *Radio Science* 17, 75–83 (1982).
- [236] C. N. Capsalis, J. G. Fikioris, and N. K. Uzunoglu, "Scattering from an abruptly terminated dielectic-slab waveguide," J. Lightwave Technol. LT-3, 408-415 (1985).
- [237] P. Gelin, M. Petenzi, and J. Citerne, "Rigorous analysis of the scattering of surface waves in an abruptly ended slab dielectric waveguide," *IEEE Trans. Microwave Theory Tech.* MTT-29, 107-113 (1981).
- [238] J.-P. Weber, L. Thylén, and S. Wang, "Crosstalk and switching characteristics in directional couplers," *IEEE J. Quantum Electron.* QE-24, 537-548 (1988).
- [239] J. Čtyroký and L. Thylén, "Analysis of a directional coupler by coupled modes of a single waveguide," Opt. Lett. 19, 1621–1623 (1994).
- [240] Y. Shama, A. A. Hardy, and E. Marom, "Multimode coupling of unidentical waveguides," J. Lightwave Technol. LT-7, 420-425 (1989).
- [241] N. Schulz, K. Bierwirth, F. Arndt, and U. Koster, "Rigorous finite-difference analysis of coupled channel waveguides with arbitrarily varying index profile," J. Lightwave Technol. LT-9, 1244-1253 (1991).

- [242] B. E. Little, "A variational coupled-mode theory including radiation loss for grating-assisted couplers," J. Lightwave Technol. LT-14, 188-195 (1996).
- [243] H. Nishihara, M. Haruna, and T. Suhara, Optical Integrated Circuits (McGraw-Hill, New-York, 1985).
- [244] K. Iga, Fundamentals of Laser Optics (Plenum Press, New-York, 1994).
- [245] J. Chilwell and I. Hodgkinson, "Thin-film field-transfer matrix theory of planar multilayer waveguides and reflection from prism-loaded waveguides," J. Opt. Soc. Am. A 1, 724-753 (1984).
- [246] R. E. Smith, S. N. Houde-Walter, and G. W. Forbes, "Numerical determination of planar waveguide modes using the analyticity of the dispersion relation," Opt. Lett. 16, 1316-1318 (1991).
- [247] L. M. Walpita, "Solutions for planar optical waveguide equations by selecting zero elements in a characteristic matrix," J. Opt. Soc. Am. A 2, 595-602 (1985).
- [248] A. K. Ghatak, K. Thyagarajan, and M. R. Shenoy, "Numerical analysis of planar optical waveguides using matrix approach," J. Lightwave Technol. LT-5, 660-667 (1987).
- [249] X. Wang, Z.-H. Wang, and Z.-M. Huang, "Propagation constant of a planar dielectric waveguide with arbitrary refractive-index variation," Opt. Lett. 18, 805–807 (1993).
- [250] A. T. Galick, T. Kerkhoven, and U. Ravaioli, "Iterative solution of the eigenvalue problem for a dielectric waveguide," *IEEE Trans. Microwave Theory Tech.* MTT-40, 699-705 (1992).
- [251] B. E. A. Saleh and M. C. Teich, Fundamentals of Photonics (John Wiley & Sons, Inc., New York, 1991).
- [252] K. Hirayama and M. Koshiba, "Analysis of discontinuities in an open dielectric slab waveguide by combination of finite and boundary elements," *IEEE Trans. Mi*crowave Theory Tech. MTT-37, 761-768 (1989).
- [253] K. Hirayama and M. Koshiba, "Numerical analysis of arbitrarily shaped discontinuities between planar dielectric waveguides with different thicknesses," IEEE Trans. Microwave Theory Tech. MTT-38, 260-264 (1990).
- [254] K. Hirayama and M. Koshiba, "Analysis of discontinuities in an asymmetric dielectric slab waveguide by combination of finite and boundary elements," IEEE Trans. Microwave Theory Tech. MTT-40, 686-691 (1992).
- [255] K. Hirayama and M. Koshiba, "Rigorous analysis of coupling between laser and passive waveguide in multilayer slab waveguide," J. Lightwave Technol. LT-11, 1353-1359 (1993).

**BIBLIOGRAPHY** 

- [256] P. G. Cottis and N. K. Uzunoglu, "Analysis of longitudinal discontinuities in dielectric slab waveguides," J. Opt. Soc. Am. A 1, 206-215 (1984).
- [257] T. G. Livernois and D. P. Nyquist, "Integral-equation formulation for scattering by dielectric discontinuities along open-boundary dielectric waveguides," J. Opt. Soc. Am. A 4, 1289–1295 (1987).
- [258] U. Rogge and R. Pregla, "Method of lines for the analysis of strip-loaded optical waveguides," J. Opt. Soc. Am. B 8, 459-463 (1991).
- [259] S. I. Najafi, ed., Introduction to Glass Integrated Optics (Artech House, London, 1992).
- [260] R. V. Ramaswamy and R. Srivastava, "Ion-exchanged glass waveguides: a review," J. Lightwave Technol. LT-6, 986-1002 (1988).
- [261] T. Findakly, "Glass waveguides by ion exchange: a review," Opt. Eng. 24, 244-250 (1985).
- [262] J. Saarinen, S. Honkanen, S. I. Najafi, and J. Huttunen, "Double-ion-exchange process in glass for the fabrication of computer generated waveguide holograms," Appl. Opt. 33, 3353-3359 (1994).
- [263] X. Prieto, C. Montero, and J. Liñanes, "Three-step diffused surface waveguides for fabricating and designing integrated optical components," J. Mod. Opt. 42, 2159– 2163 (1995).